UNIVERSITÀ
DEGLI STUDI
DI BRESCIA

DIPARTAMENTO DI INGEGNERIA CIVILE, ARCHITETTURA,
TERRITORIO, AMBIENTE E DI MATEMATICA

DOTTORATO DI RICERCA IN
Ingegneria Civile, Ambientale, della Cooperazione Internazionale e di Matematica

SETTORE SCIENTIFICO DISCIPLINARE
ICAR09

CICLO
XXXVII

# ANALYSING CORROSION OF REINFORCED CONCRETE ELEMENTS IN CRACKED STAGE UNDER SUSTAINED LOADS

Dottorando:
Muhammad Bilal

Relatore:
Prof. Antonio Conforti

Co-Relatori:
Prof. Giovanni A. Plizzari

***Muhammad Bilal***
*Ph.D. in Civil Engineering*

Università degli Studi di Brescia
Via Branze 43, 25123
Brescia (Italy)

m.bilal@unibs.it
bilalmandokhail@outlook.com

*For the quite nights, the sleepless hours,*
*and the dreams that refused to let me rest.*
*And to those who stood by me through it all*
*this is for you*

## ACKNOWLEDGMENTS

Firstly, I would like to extend my heartfelt gratitude to Professor Antonio Conforti, whose guidance and support were fundamental throughout my three years of PhD research. His constant encouragement and constructive feedback have played a crucial role in shaping this thesis, and I am truly thankful for the invaluable mentorship he provided during this journey.

I would also like to express my deep gratitude to Professor Giovanni Plizzari for his unwavering support and for creating the opportunity to carry out this research. His valuable guidance and encouragement have been instrumental in the successful completion of this work, and I am truly thankful for his contributions to this journey.

I would also like to extend my heartfelt thanks to HEC Pakistan for providing me with the scholarship opportunity that enabled me to carry out my research in Italy. Their generous support was crucial in making this research possible, and I am deeply grateful for their role in helping me pursue my academic goals abroad.

I would like to express my sincere thanks to Alan Piemonti and Giovanni Bosetti for their invaluable assistance with the laboratory experimental work. Their expertise, support, and collaboration were essential to the successful completion of my research, and I am truly grateful for their help during this process.

Thanks to Collegio Luigi Lucchini for providing me with the opportunity to stay here during my PhD. I truly consider it my second home, and it has been a place of great comfort and inspiration. I would also like to thank my wonderful colleagues from the Collegio: Antonio Campana, Michele Fioroni, Oleksii, Bruno, Nicholas Vargas, Leti Bertola, Giaele, Marcos, Camilla Carraro, Gaia Antolini, Alice, Elisabetta Trapletti, Jozef Lazri, Federico Tailo, Alessandro Rigamonti, Linda Anelli, Giada Barucca, Hajar Lagha, Iman Ettaqy, Aurora Montini, Martina, Sofia Barezzani, Sofia Cicca, Daniele, and Ivan. Their friendship and support have made my time here even more memorable.

I would like to extend my heartfelt thanks to my Colleagues who have been incredibly supportive throughout my PhD journey. Usman, Waqas Ali, Raheel Shahzad, Salman Jan, Adnan Khan, Raja Muhammad Awais, Imran, Suryia, Syed Sohail, Imdad Ullah, and Tahir have been a constant source of encouragement and help, and I am deeply grateful for their unwavering support during this time.

Last but not least, I would like to give special thanks to my family for their unwavering support throughout this journey. Their love, patience, and encouragement have been a constant source of strength. I am truly grateful to each one of them for their belief in me during this time

## ABSTRACT

The corrosion of reinforcement bars (rebars) in reinforced concrete (RC) structures is a critical factor affecting the long-term durability and service life, particularly in aggressive environments such as marine environments or areas exposed to de-icing salts. These conditions facilitate chloride ion ingress, which accelerates the corrosion process by providing a direct pathway for chloride penetration to reinforcement. Corrosion weakens the load-bearing capacity of reinforcement and compromises structural integrity. While significant research has been conducted on corrosion in RC structures, the influence of cracks on corrosion initiation and propagation, particularly in chloride-induced environments, remains poorly understood. This thesis addresses this gap by investigating the effect of crack width on corrosion behaviour, focusing on corrosion kinetics and the mechanical performance of reinforcement in RC elements exposed to accelerated corrosion conditions. For this purpose, A 31 tension tie specimens (90 x 90 x 830 mm) were cast using grade C30/37 concrete and reinforced with Ø12 mm hot-rolled ribbed bars. The specimens were pre-cracked to induce varying crack widths and subjected to accelerated corrosion testing under wet and dry cycles, with exposure to a chloride solution (35 g/l) simulating real-world exposure conditions. The results showed corrosion initiation occurred in all specimens from the first cycle, with no delay in corrosion start regardless of crack width. During the corrosion propagation phase, there was no clear linear relationship between crack width and pitting depth, with wide variability observed. However, both maximum pit depth and mean pit depth tend to increase as crack width increases. The deepest pits and highest average pit depths were observed in specimens with yielded rebar. The mechanical testing of corroded rebars revealed that the ultimate strength was only marginally affected, but ductility was significantly reduced, especially in specimens with wider cracks and those subjected to higher strain levels. In specimens with 5‰ strain, ductility loss reached up to 74%, highlighting a serious risk of brittle failure under service loads.

## SOMMARIO

La corrosione delle barre di armatura (ferri) nelle strutture in calcestruzzo armato (CA) è un fattore critico che influisce sulla durabilità a lungo termine e sulla vita utile, in particolare in ambienti aggressivi come gli ambienti marini o le aree esposte a sali de-iceranti. Queste condizioni facilitano l'ingresso di ioni cloruro, che accelerano il processo di corrosione fornendo un percorso diretto per la penetrazione del cloruro nell'armatura. La corrosione indebolisce la capacità portante dell'armatura e compromette l'integrità strutturale. Sebbene siano state condotte ricerche significative sulla corrosione nelle strutture in CA, l'influenza delle fessure sull'iniziazione e sulla propagazione della corrosione, in particolare negli ambienti indotti dal cloruro, è ancora poco compresa. Questa tesi affronta questa lacuna investigando l'effetto della larghezza della fessura sul comportamento della corrosione, concentrandosi sulla cinetica della corrosione e sulle prestazioni meccaniche dell'armatura in elementi in CA esposti a condizioni di corrosione accelerate. A tale scopo, sono stati realizzati 31 provini a trazione (90 x 90 x 830 mm) in calcestruzzo di classe C30/37, armati con barre nervate Ø12 mm in acciaio laminato a caldo. I provini sono stati pre-fessurati per indurre diverse larghezze di fessura e sottoposti a test di corrosione accelerata sotto cicli umido-secco, con esposizione a una soluzione di cloruro (35 g/l) simulante le condizioni di esposizione reali. I risultati hanno mostrato che l'iniziazione della corrosione è avvenuta in tutti i provini già dal primo ciclo, senza ritardi nell'inizio della corrosione indipendentemente dalla larghezza della fessura. Durante la fase di propagazione della corrosione, non è emersa una relazione lineare chiara tra la larghezza della fessura e la profondità delle pitting, con una variabilità osservata. Tuttavia, sia la profondità massima della pitting che la profondità media della pitting tendono ad aumentare con l'aumento della larghezza della fessura. Le pitting più profonde e le maggiori profondità medie delle pitting sono state osservate nei provini con barre di armatura cedute. I test meccanici sulle barre di armatura corrose hanno rivelato che la resistenza ultima è stata solo marginalmente influenzata, ma la duttilità è stata significativamente ridotta, specialmente nei provini con fessure più larghe e quelli sottoposti a livelli di deformazione più elevati. Nei provini con deformazione del 5‰, la perdita di duttilità ha raggiunto il 74%, evidenziando un serio rischio di rottura fragile sotto carichi di servizio.

# CONTENTS

## LIST OF FIGURES

## LIST OF TABLES

# ANALYSING CORROSION OF REINFORCED CONCRETE ELEMENTS IN CRACKED STAGE UNDER SUSTAINED LOADS

# 1 INTRODUCTION

## *1.1 Statement of problems and aim of the research*

Corrosion of reinforcement bars (rebars) in reinforced concrete (RC) structures significantly affects their service life and durability, especially in aggressive environments such as marine or areas where de-icing salts are applied. These conditions promote chloride ion penetration, which accelerates the corrosion process. Cracks in the concrete provide an additional pathway for chloride ingress, further intensifying the corrosion. Despite substantial research on corrosion in RC structures, the effect of crack width on the initiation and propagation of corrosion – particularly under chloride-induced conditions remains poorly understood. This research aims to investigate the impact of crack width on the corrosion behavior of reinforcement bars, with a focus on both corrosion initiation and propagation and the effect on the mechanical properties of the reinforcement. By analyzing these factors, the study seeks to contribute to a deeper understanding of how corrosion progresses in RC structures and its influence on their structural integrity and durability in aggressive environments.

To investigate this, 31 tension tie specimens (830 x 90 x 90 mm) were cast and exposed to accelerated corrosion testing under controlled laboratory conditions. The specimens were immersed in a chloride solution with a concentration of 35 g/L and underwent a series of wet and dry cycles, consisting of 3 days of wet exposure followed by 4 days of drying, simulating real-world environmental conditions. The duration of these wet and dry cycles lasted for 40 weeks. The study aimed to evaluate how variations in crack width influence corrosion kinetics, propagation, and the mechanical performance of the reinforcement bars in RC elements exposed to accelerated corrosion conditions.

The research was conducted over three years at the University of Brescia, within the Department of Civil Engineering, Architecture, Territory, Environment, and Mathematics (DICATAM). During this time, in addition to conducting my research, I also participated in a variety of academic activities, including one summer school, two courses, seven seminars, and one international conference, all of which significantly contributed to my academic and professional growth.

## 1.2 *Thesis Organization*

This PhD thesis is organized into five chapters as follows:

**Chapter 1** introduces the problem statement and outlines the research objective This chapter provides an overview of the study's motivation and the specific aims of the research.

**Chapter 2** presented a comprehensive literature review on corrosion initiation and propagation in reinforced concrete and fiber-reinforced concrete (FRC). The review focuses primarily on studies published from 1990 onward, discussing key parameters such as chloride concentration, observed crack widths, and types of cracks induced during corrosion. Additionally, it examines the types of loads applied during testing and various acceleration techniques used to simulate corrosion. The chapter also addresses the incorporation of findings from past experiments, this chapter provides a solid foundation for understanding the methodologies and outcomes relevant to this study.

**Chapter 3** outlines the experimental campaign conducted to study chloride-induced corrosion in tension tie specimens. These specimens were subjected to wet and dry cycles over a 40-week period to accelerate the corrosion process.

**Chapter 4** presents the experimental results, focusing on corrosion initiation and propagation in the specimens. This chapter also explores the influence of different crack widths on corrosion behaviour and examines the mechanical properties of corroded reinforced bars, assessing the impact of corrosion on the structural performance of reinforcement.

**Chapter 5** summarizes the main conclusions drawn from this research, highlighting the key findings and their implications for the field of corrosion in reinforced concrete structures.

# 2. LITERATURE SURVEY

## *2.1 Introduction*

A major factor affecting the durability of reinforced concrete (RC) structures is the corrosion of the reinforcement, particularly in structures exposed to the marine environment and de-icing salts [1]. Corrosion not only leads to the degradation of reinforcement but also accelerates cracking in the concrete. primary cracking, such as flexural and shear cracks, occurs due to external loads acting on the RC structures and can significantly expedite the corrosion process. Secondary cracks, known as longitudinal cracks, result from the formation of iron oxide products on the rebar, which generate internal stresses in the concrete, leading to crack propagation. [2]. In the early stages, the concrete has a moisture content that evaporates due to the heat of hydration, which causes an increase in temperature and subsequent shrinkage cracks A. W. Beeby, (1983).

The service life of reinforced concrete structures is divided into two phases: the initiation phase and the propagation phase (Figure 1). During the initiation phase, aggressive agents such as chloride and $CO_2$ penetrate the concrete surface reach the reinforcement. If the concentration of chlorides in contact with the rebar reaches a critical threshold, the passive layer, a thin protective layer of hydrated iron oxides that forms on the rebar during the hydration of concrete, becomes compromised[3]. Once the passive layer is damaged, it can no longer protect the rebar, marking the end of the initiation phase [4] [5], [6].

The initiation phase of corrosion depends on several factors: the concrete cover over the reinforcement, the concentration of aggressive agents, and the rate at which these agents penetrate the concrete. The concrete cover to reinforcement is defined in construction codes, while the penetration rate is influenced by the concrete's porosity. Higher-quality concrete tends to be denser and less porous compared to low-quality concrete, thus providing better resistance to chloride ingress [7]. Once the aggressive agents break through the passive layer, the corrosion process enters the propagation phase, which is driven by factors such as temperature and humidity. The corrosion of the reinforcement can be controlled in two distinct phases: before initiation and after initiation, through to the end of the structure's service life. For better durability of the structures, generally preferable to extend the initiation phase; once corrosion is initiated, it is difficult to halt Sahmaran et al., (2008).

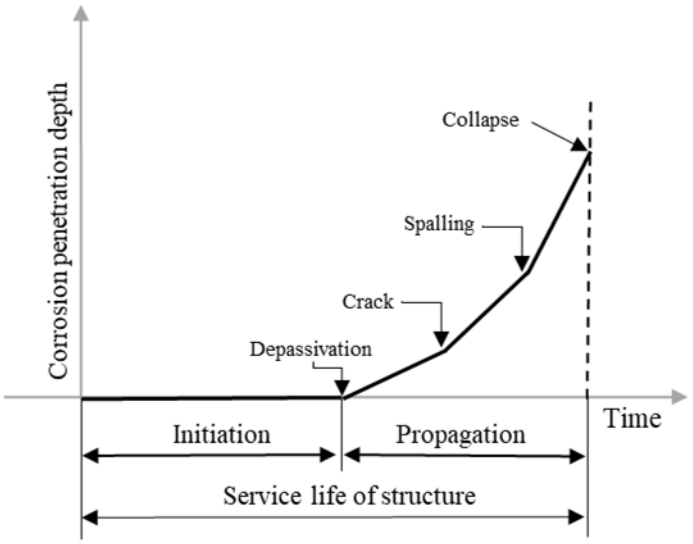


*Figure 2.1-1. Initiation and propagation period of corrosion in reinforced concrete structures [6].*

Rebar corrosion can be classified into two types: uniform corrosion and localized corrosion. Carbonation of concrete leads to uniform corrosion by destroying the entire passive layer on rebar, whereas chloride-induced corrosion typically causes localized breakdown, resulting in pitting corrosion [8]. The corrosion rate can be calculated in μm/year, and in laboratory conditions, it can be calculated in μA/cm2 or mA/m2. Corrosion is considered negligible if the corrosion rate is below 2 μm/year. Moderate corrosion rate ranges from 5 to 10 μm/year, while intermediate rate are between range from 10 to 50 μm/year. Rates between 50 to 100 μm/year are classified as high, and anything above 100 μm/year is considered very high. For reference, a corrosion rate of 1 mA/m2 (or 0.1 μA/cm$^2$) corresponds to a steel mass loss of approximately 9 g/m$^2$, which results in a penetration rate of about 1.17 μm/year.
One of the main factors affecting both initiation and corrosion rate is the crack width. According to past research, no significant correlation has been found between crack width and corrosion rate as long as the crack width remains below 0.5 mm [9], [10], [11], [12], [13], [14]. The corrosion process is also affected by environmental factors, such as moisture content in concrete. Saturated concrete tends to have a lower oxygen level, while dry concrete has higher resistivity, which both influence the corrosion rate. In addition to environmental conditions, factors such as concrete permeability, clear cover to rebar, and crack width play crucial roles in the initiation of corrosion. Increasing the clear cover to rebar is considered as a barrier to aggressive agents, thus

delaying the corrosion initiation. However, the concrete cover must be within certain limits [15]. A the concrete cover decreases, the corrosion rate typically increases [16], Additionally, corrosion initiation is influenced by the width of cracks; as the crack decreases, the depassivation time (the time taken for the passive layer to be damaged) increases [17]. When the crack width is below 0.3 - 0.5 mm, the corrosion rate can be low. In very thin cracks (< 0.1mm), the corrosion product can seal the cracks, enabling the regeneration of the passive layer [6]. In such case, self-healing of the cracks could delay or even prevent corrosion initiation [18].

Reinforcement bars can also be protected by applying coating such as epoxy, zinc, or red oxide. Among these, epoxy coating shows better performance [19]. These coatings can be applied either as a liquid or in the form of powder. However, due to handling, the epoxy coating applied to the rebar can be damaged even before casting at the time of placement, which can compromise its performance [20]. Furthermore, the bond between concrete and epoxy-coated rebar is typically weaker than that of conventional rebar, reducing the overall effectiveness of the protective coating.

### *2.1.1 Scope of literature survey*

This literature review focuses on the corrosion of reinforced concrete (RC) structures, particularly those exposed to aggressive environments such as marine conditions and de-icing salts. It includes studies published from 1990 to the present, offering an up-to-date examination of recent findings. This review covers the mechanism of corrosion, including chloride-induced corrosion, carbonation, and formation of iron oxide products on the reinforcement. Special attention is given to the initiation and propagation phases of corrosion, which focus on how aggressive agents penetrate the concrete and reach the reinforcement.

The review analyses various factors influencing corrosion, including environmental factors, crack topology, and different crack widths. The environmental condition in this study shows the amount of chloride used and the duration of exposure conditions. Many studies have utilized small-scale specimens, which may not represent real-world conditions; such studies are not included in this literature. The review further explores the effects of crack formation on specimens. A detailed analysis of the crack widths used in the previous studies, along with the type of cracks (e.g., flexural, shear, longitudinal), is provided. Studies that focus on a maximum crack width of 0.5 mm are particularly emphasized, as this is the maximum allowable crack width according to Eurocode 2 [21]. Additionally, the relationship between crack formation and corrosion acceleration is explored, with a focus on how crack propagation influences the corrosion rate during both the initiation and propagation phases.

The review also included different kinds of loading conditions applied to the specimens, both during the pre-cracking phase and the corrosion phase. These

Loading conditions, such as flexural, shear, or tensile loads, play a significant role in inducing cracks, which helps to accelerate the corrosion process.
Furthermore, the review addresses various corrosion acceleration techniques used in the literature, such as accelerated chloride exposure, cyclic wet-dry cycles, and the application of electrical current. These techniques are commonly used to speed the corrosion process in experimental processes, and their effectiveness and relevance to real-world conditions are critically evaluated.
To better understand trends in the research, findings are summarized in a pie chart representing key variables, such as the amount of chloride used, types of corrosion acceleration techniques, the crack width, and loading condition applied during corrosion initiation and propagation phase. Additionally, review also explores the types of fibres used in the studies and the amount and types of fibres used in concrete mix. This analysis provides insight into how different fibre types, such as steel, glass, and synthetic fibres, affect the corrosion resistance and cracking behaviour of reinforced concrete structures.
By studying the various experimental conditions and variables, the review offers a comprehensive overview of how these factors influence the corrosion process in RC structures. Additionally, this study highlights the limitations of the existing research, particularly regarding the specimen size and the findings derived from small-scale studies, which may not fully replicate real-world conditions.

### *2.1.2 Types of corrosion in reinforced concrete*

Corrosion in reinforced concrete is characterised according to the mechanism that leads to the depassivation of reinforcement bars (rebars). Two primary types of corrosion are chloride-induced corrosion and carbonation-induced corrosion. Chloride-induced corrosion occurs when aggressive agents, such as chloride from de-icing salts or marine environments, penetrate the concrete and reach the reinforcement, disrupting the protective passive layer on the rebar. In contrast, carbonation-induced corrosion is caused by the diffusion of carbon dioxide ($CO_2$) from the atmosphere into the concrete. This process lowers the pH of the concrete, leading to the breakdown of the protective layer around the rebar. Both types of corrosion will be discussed in more detail in the following sections.

#### *2.1.2.1 Chloride-induced corrosion*

Chloride-induced corrosion is one of the most destructive forms of corrosion in reinforced concrete structures, especially those exposed to chloride-rich environments, such as marine structures or areas where de-icing salts are applied [22]. The presence of chloride ions is a major factor influencing the durability of reinforced concrete. When chloride ions penetrate the concrete and reach the reinforcement bars, they break down the passive oxide layer that normally protects the rebar in the alkaline environment of concrete, initiating the corrosion [23].

The passive film that surrounds the rebar is a protective layer formed due to the high pH (alkalinity) of concrete. However, once chloride ions come into contact with the rebar, they disrupt the protective layer in a process known as depassivation [24], [25]. As a result, the rebar is exposed to surrounding aggressive agents such as oxygen, moisture, and additional chloride ions. This exposure initiates an electrochemical reaction that leads to corrosion.

The point where aggressive agents come in encounters rebar is known as anode (where the corrosion begins), whereas the surrounding areas remain protected and are referred as cathode region [26]. The corrosion process begins when iron (Fe) in the rebar becomes unstable due to the presence of chloride ions. In this unstable state, iron releases two electrons ($2e^-$) to the nearby cathodic region. This process is called oxidation, and during this process, iron (Fe) loses two electrons it becomes a ferrous ion ($Fe^{2+}$), which dissolves into the surrounding concrete, causing pitting corrosion.

$$Fe \longrightarrow Fe^{2+} + 2e^-$$

In the cathodic region, the electron released by the anode combine with oxygen and water to form a hydroxide ion ($OH^-$) in a process known as reduction:

$$O_2 + 2H_2O + 2e^- \longrightarrow 4OH^-$$

The hydroxide ions ($OH^-$) produced at the cathode then combine with ferrous ions ($Fe^{2+}$) released from the anode to form iron hydroxide ($Fe(OH)_2$).

$$Fe^{2+} + 2OH^- \longrightarrow Fe(OH)_2$$

Iron hydroxide is unstable, and over time, it further undergoes oxidation to form hydrated iron oxide. Which is generally known as rust.

$$4Fe(OH)_2 + O_2 + 2H_2O \longrightarrow 2Fe_2O_3.2H_2O$$

As the corrosion progresses, the volume of rust (iron oxides and hydroxides) increases significantly, with the volume of corrosion products becoming 2 to 6 times greater than the original volume of rebar [27], [28]. This increase in volume exerts internal pressure on the surrounding concrete, causing cracks and spall. The continuous formation of corrosion products further exposes the rebar to aggressive agents, accelerates the degradation of the concrete. Over time, the cumulative effects of corrosion, cracking, and spalling can lead to structural failure if the process is not mitigated.

Apart from cracks, several other factors influence the rate of chloride-induced corrosion in reinforced concrete structures. These include the concentration of chlorides, the amount of moisture present, the quantity and porosity of the concrete, and the thickness of the concrete cover. In reinforced concrete, the embedded steel reinforcement is initially protected by a passive film formed in the high alkalinity environment of the concrete. However, this passive layer can be disrupted once the

concentration of chloride ions at the reinforcement surface exceeds a critical threshold, commonly referred to as critical chloride content or chloride threshold [29].

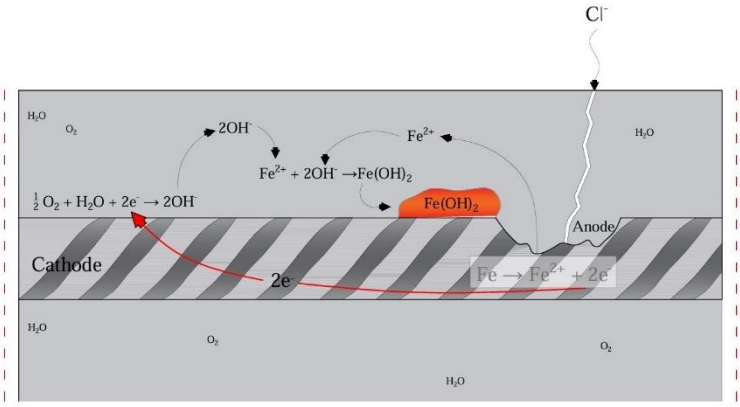


*Figure 2.1-2. Schematic sketch of chloride-induced corrosion in reinforced concrete structure.*

It's difficult to determine the exact amount of critical chloride content concentration, as it depends on various factors such as concrete quality, surrounding environment, type of rebar, and presence of aggressive agents. Some studies suggested a threshold value ranging between 0.1% to 3.1% by weight of cement, while other studies suggested a mean value of 0.48% [30], [31].

To summarise, chloride-induced corrosion remains one of the most critical durability concerns for reinforced concrete structures, particularly in marine or chloride-rich environments. Once chloride concentration exceeds the threshold and initiates corrosion, it often manifests as localized pitting corrosion. Over time, the formation of corrosion products (rust), which occupy 2 to 6 times the volume of the original steel, generates expansive internal stress. This leads to cracking and spalling of the concrete cover, further exposing the reinforcement to moisture and chlorides, thus accelerating the deterioration process.

#### *2.1.2.2 Corrosion due to carbonation*

Carbonation occurs when calcium hydroxide ($Ca(OH)_2$) in concrete reacts with carbon dioxide ($CO_2$) from the atmosphere, resulting in the formation of calcium carbonate ($Ca(CO)_3$) [32]. This chemical process is not pronounced in the presence of moisture and can significantly affect the durability of reinforced concrete structures [33]. When the carbonation reaches the rebar, it lowers the pH value of the concrete surrounding the reinforcement, typically reducing it from a range of 12 - 13 to about 9 or lower, thereby damaging the passive protective layer surrounding the rebar [34]. The breakdown of the passive film exposes the reinforcement to the aggressive environment, initiating corrosion. Initially, this results in a uniform reduction in the

cross-sectional area of the rebar, weakening its load-carrying capacity. With the passage of time, corrosion products, such as iron oxides and hydroxides, accumulate around the rebar with their volume increasing 2 to 6 times that of the original steel [27]. This creates internal stresses, which lead to the formation of cracks and concrete spalling.

As corrosion progresses, these cracks may get deeper and widen, further exposing the reinforcement to moisture and $CO_2$. The combination of uniform reduction of rebar along with concrete spalling can significantly weaken the structural integrity and durability of the entire RC element, eventually leading to structural failure.

Several factors affect the pace of carbonation and, consequently, the corrosion process. The amount of $CO_2$ in the air, temperature, humidity, and concrete quality all significantly affect carbonation [35]. The environment with higher $CO_2$ concentration, such as densely populated urban areas or regions with warm, humid climates, carbonation occurs more rapidly [36]. Additionally, poorly compacted or porous concrete allows $CO_2$ to penetrate more easily, accelerating the carbonation process [37]. The thickness of the concrete cover is another critical factor: RC structures with thin concrete cover are more vulnerable to carbonation-induced corrosion, as carbonation can reach the rebar more quickly [38].

To summarise, corrosion induced by carbonation significantly threatens the durability of reinforced concrete structures. To minimize the damage caused by carbonation, it is essential to ensure adequate concrete cover over the reinforcement, use dense concrete, and implement effective monitoring and maintenance strategies to detect and address cracks early.

#### *2.1.2.3 Corrosion due to sulphate attack*

A sulphate attack occurs when sulphate ions ($SO_4^{2-}$), originating from external sources such as soil, groundwater, or seawater, come in contact with concrete. This leads to a chemical degradation process in the concrete, where the sulphate ions react with the cement's hydration products, particularly calcium hydroxide ($Ca(OH)_2$) and calcium aluminate ($C_3A$), to form expansive product like gypsum ($CaSO_4.\ 2H_2O$) and compound ($3CaO.Al_2O_3.3CaSO_4.32H_2O$). these expansive minerals increase in volume and generate internal pressure within concrete, causing cracking, surface scaling, and ultimately weakening the concrete structure [39], [40].

Sulphate attacks can be classified into two types: internal or external. External sulphate occurs when sulphate ions from an external source, such as sulphate-rich soil or water, penetrate the concrete and degrade its surface and internal structure. Conversely, an internal sulphate attack occurs when sulphate-rich aggregates or a high concentration of tricalcium aluminate ($C_3A$) are added to the cement used in the mix. In such circumstances, the sulphate originates within the concrete itself, interacting with the cement during the hydration, leading to internal damage.

The intensity and rate of sulphate attack are influenced by a number of factors. The major factor is the concentration of sulphate ions present in the surrounding environment. Higher concentrations of sulphates, such as those in saltwater or industrial waste, can result in more severe attacks. Another key consideration is the porosity of the concrete. More porous concrete makes it easier for sulphate ions to penetrate, increasing the risk of attack [41]. Concrete with a higher water-to-cement ratio produces more porous concrete and, therefore, is more susceptible to sulphate penetration. Additionally, sulphate attack can be accelerated by environmental exposure conditions such as varying moisture levels. The composition of the cement mix is also critical; cement with a higher concentration of tricalcium aluminate ($C_3A$) is more prone to sulphate attack, which is why sulphate-resisting Portland cement is highly recommended for use in sulphate-rich environments [42].
Sulphate attack causes noticeable surface cracking, scaling, and discoloration of the concrete, as well as the development of internal cracks that may damage the reinforcement. The concrete matrix is primarily affected by this attack, as it alters the pH and moisture content of the concrete, which in turn may lead to corrosion of embedded rebar.

#### *2.1.2.4 Corrosion due to alkali-silica reaction*

The alkali-silica reaction (ASR) is a harmful chemical reaction that occurs between certain types of reactive silica found in concrete aggregates and the alkalis (potassium and sodium) present in cement [43]. This reaction produces an alkali-silica gel that swells, absorbs water, and generates internal pressure within the concrete, leading to cracking, loss of strength, and ultimately structural damage due to the expansion of the gel. ASR is a significant durability issue for concrete structures exposed to specific climatic conditions, especially in areas with high humidity or where concrete is exposed to moisture.
The ASR process begins when weak crystalline silica in the aggregate reacts with the alkalis, primarily sodium (Na) and potassium (K), from the cement. This reactive silica is commonly found in natural aggregates such as granite, basalt, and sandstone, which contain silicate minerals that can penetrate ASR. When concrete is exposed to moisture, the alkalis in the cement dissolve into the pore water and interact with the reactive silica in the aggregates to form an alkali silica gel. This gel has a strong water affinity and expands as it absorbs moisture [44].
The concrete experiences internal pressure as the gel expands. This pressure causes cracks to develop over time, potentially extending deep into the structure [45]. These cracks provide pathways for further moisture infiltration, which accelerates the deterioration process. The surface of the concrete often displays a characteristic map-like cracking pattern, and the concrete may lose strength as the expansion continues. In extreme cases, the expansion can lead to severe spalling and structural failure.

Several factors influence the severity of ASR, including the alkali content of cement, the type and quantity of reactive silica in the aggregates, and the availability of moisture [46]. ASR is more likely to occur in concrete with a high alkali content, which is typically associated with the use of Portland cement. Moisture availability is also a critical factor, as ASR generally occurs in areas with high humidity or where concrete is exposed to water, such as in wet climates, groundwater, or structures exposed to rainfall [47].

The sign of ASR damage includes surface map cracking, discoloration (often a yellowish or greyish hue due to the alkali-silica gel), and concrete expansion. These symptoms frequently emerge in concrete that is exposed to moisture, such as the surface of concrete, joints, or in water-bearing structures. As the reaction progress, internal cracking may spread further, leading to significant structural damage.

To summarise, a chemical reaction between alkalis in the cement and the reactive silica in the aggregates causes an alkali-silica reaction (ASR), which causes serious durability problems in reinforced concrete. The reaction from gel that absorbs water expands and generates internal cracking and structural damage. ASR can be effectively mitigated by using low-alkali cement, non-reactive aggregates, and supplementary materials. Furthermore, the risk of ASR can be reduced by controlling exposure and applying sealants to concrete.

#### *2.1.2.5 Corrosion due to freeze and thaw*

Freeze-thaw is a physical deterioration that occurs when concrete is subjected to cyclic freeze and thaws in the presence of moisture. This form of corrosion is problematic, especially in regions where temperature fluctuates around the freezing point. In such conditions, water that has penetrated the concrete freezes, expands, and then thaws, leading to repeated cycles of internal stress. Over time, these cycles can cause surface scaling, microcracking, and, eventually, significant deterioration of the concrete structure [48], [49].

The process of freeze-thaw begins when water infiltrates into concrete pores. Upon freezing, the volume of water increases by approximately 9%, generating internal pressure within the concrete matrix. The pressure is released as the ice thaws and the temperature rises, but the initial freezing expansion may have damaged the concrete [50]. Frequent cycles of freezing and thawing worsen the damage, resulting in progressive cracking, surface delamination, and, in severe cases, structural failure.

Numerous factors influence the severity of freeze-thaw damage. One of the most critical factors is the porosity of the concrete. Highly porous or low-density concrete is more likely to absorb water, increasing its vulnerability to freeze-thaw damage. The water to cement (w/c) ratio also plays a crucial role – higher w/c ratios produce more porous concrete, which can absorb greater amounts of moisture. Additionally,

structures exposed to frequent wetting and drying cycles are more vulnerable, as water within the pores is more likely to freeze during colder temperatures [51].
In summary, freeze-thaw damage is a prevalent type of concrete degradation that occurs in areas that see frequent cycles of freezing and thawing. The expansion of water during freezing induces internal stresses that lead to cracking and surface degradation. Implementing preventive measures such as air entrainment, reduced porosity, and regular maintenance is essential to enhance the freeze-thaw resistance and prolong the service life of concrete.

#### *2.1.2.6 Galvanic corrosion*

Galvanic corrosion is a form of electrochemical degradation that occurs when two dissimilar metals come into electrical in the presence of an electrolyte, such as moisture within concrete. In reinforced concrete structures, this phenomenon arises when carbon steel reinforcement comes into contact with other metals such as copper, aluminium, or stainless steel, either embedded within the structure or introduced through external connections. This contact forms a galvanic cell, initiating an electrochemical reaction [52].
Within this cell, the metal with the lower electrochemical potential acts as the anode and undergoes accelerated corrosion, while the metal with the higher potential serves as the cathode and remains protected. The flow of electrons from the anode to the cathode through the metallic connection, combined with iconic movement through the electrolyte (i.e., the moist concrete), facilitates the corrosion process. The severity of galvanic corrosion depends on factors such as the electrochemical potential difference between the metals, the conductivity of the electrolyte, and the surface area ratio between the anode and cathode.
In concrete environments, moisture and the presence of chloride ions common in marine or coastal regions further intensify the galvanic activity by increasing iconic conductivity.
Tom mitigates galvanic corrosion; it is essential to avoid direct contact between dissimilar metals or to use insulating materials at the point of contact. Additionally, selecting compatible materials, applying protective coating, or using a sacrificial anode can help manage the electrochemical interactions that lead to this form of corrosion.
In summary, galvanic corrosion is a serious durability concern in reinforced concrete structures where dissimilar metals are present. The resulting electrochemical reaction can significantly accelerate corrosion of the steel reinforcement, especially under moist or chloride rich conditions. Proper material selection, detailing, and isolation techniques are critical to preventing this form of degradation.

#### 2.1.2.7 *Crevice corrosion*

Crevice corrosion is a type of localized corrosion that occurs in small voids or gaps with limited access to oxygen and other chemicals. In the case of reinforced concrete, crevice corrosion typically occurs where the reinforcing steel and concrete encounter or where metal components are positioned near the concrete but protected from the elements [53]. These confined areas can create favourable conditions for the electrochemical process that leads to metal corrosion.

Crevice corrosion is caused by a difference in the concentration of oxygen and other ions within the crevice compared to the surrounding areas. The cathodic reaction consumes oxygen in the narrow gap, creating an oxygen-deprived zone. As a result, the electrochemical potential shifts in favour of anodic reactions, or corrosion, which speeds up the process [54]. In the meantime, corrosion is less severe in the surrounding areas, where oxygen is more readily available. Due to its localized nature, crevice corrosion can spread quickly in small areas and frequently goes undetected until extensive damage has occurred.

The availability of oxygen is a key factor in crevice corrosion. The corrosion process is self-replicating; once it begins in a crack, it uses all the oxygen in a small area, leading to more corrosion. As a result, only a small portion of the metal experiences severe corrosion, while the surrounding metal remains unaffected. The corrosion cycle can be accelerated by the corrosive byproduct, such as iron oxide, which obstructs the flow of oxygen into the cracks.

In general, crevice corrosion in reinforced concrete is a very confined yet potentially damaging form of corrosion. Because it occurs in small cracks or gaps, it underscores the importance of high-quality construction practice and addressing any flaws in the concrete structures that might create restricted areas where corrosive conditions can develop.

## 2.2 *Experimental methodology in literature*

Cracks play a crucial role in reinforced concrete structures by providing a path for chloride to penetrate through the protective surface and reach reinforcement. To induce cracks in laboratory conditions that replicate real-world conditions, researchers have used a variety of experimental procedures. This section will provide an overview of different methods used in past studies to produce cracks in concrete, with the aim of simulating real-world conditions.

### 2.2.1 *Pre-cracking by mechanical loading*

One of the most common methods used to induce cracks in concrete specimens is mechanical loadings. This technique closely reflects the structural conditions found in real world, where applied loads and seismic forces cause cracks in concrete. Through this method, researchers can precisely control the width, depth, and direction of

cracks by applying mechanical loadings such as flexural, tensile, or splitting forces. These artificial cracks mimic the real-life damage to structures, allowing chlorides to penetrate the concrete and corrode the rebar during experimental campaigns.

#### *2.2.1.1 Flexural loading*

In studies of chloride-induced corrosion, it is essential to induce cracks that resemble the conditions present in real-world situations. Flexural loading creates bending stresses, resulting in compressive stresses at the top and tensile stress at the bottom of the concrete specimen. Cracks appear when tensile stress exceeds the tensile strength of the concrete [55], [56], [57], which may serve as an entry point for chlorides.
Researchers can control the width and depth of cracks to investigate the influence of chloride penetration and corrosion of rebar. To perform flexural loading, the most common tests are three-point or four-point bending tests, which allow precise control over crack formation.
In a three-point bending test, the beam is supported at both ends, with a concentrated load applied at the centre. This method generates a single crack in the

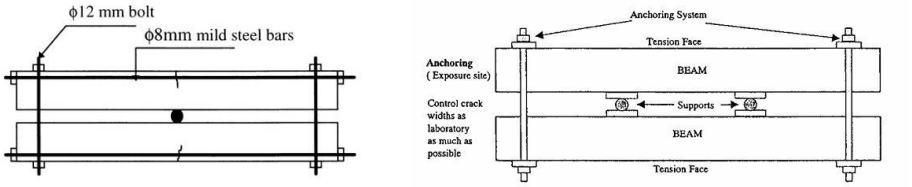


(a) (b)

*Figure 2.2-1. a) Schematic sketch of three point load* [58], *b) Schematic sketch of four point load* [59].

middle, making it ideal for investigating the direct influence of a single crack on chloride ingress. In contrast, a four-point bending test applies two symmetrically loads to the beams, creating a constant bending moment region between the load points. This method results in multiple cracks, allowing researchers to assess the effect of different crack widths on chloride penetration.
To summarise, flexural loading is an effective method for inducing controlled cracks in laboratory conditions. It provides researchers with the ability to simulate real-life cracking scenarios, enabling studies on chloride ingress and corrosion mechanisms.

#### *2.2.1.2 Direct tensile loading*

Another reliable method to induce cracks in reinforced concrete specimens is through the application of direct tensile loads by subjecting the specimen to uniaxial tensile stresses until failure occurs. This approach closely replicates tensile stresses found in structure elements such as walls, slabs, and pre-stressed members, making it highly relevant for studying chloride-induced corrosion [14].

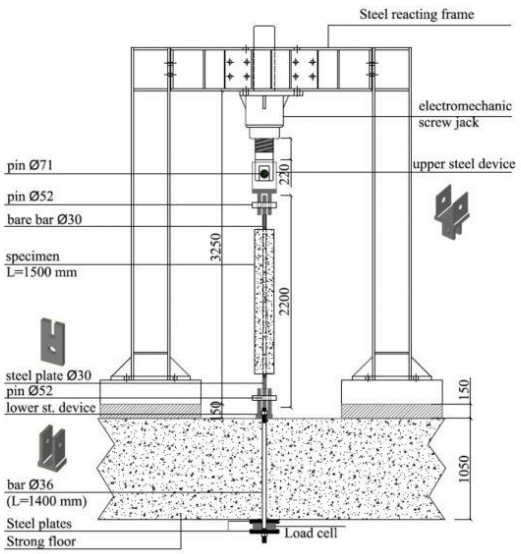


*Figure 2.2-2.Schematic sketch of direct tensile loading load* [60].

During the test, a crack is induced along a plane perpendicular to the direction of the applied load, resulting in cracks with precise width and depth. These cracks act as pathways for aggressive agents such as chloride, moisture, and oxygen to penetrate the concrete and initiate corrosion in the reinforcing steel. Following cracking, the specimens are typically exposed to chloride-rich environments such as wet-dry cycles to simulate the exposure conditions commonly experienced by reinforced concrete structures in marine environments.

Direct tensile loading offers several advantages in replicating real-world scenarios. The uniform distribution of tensile stress across the specimen cross-section ensures that cracking generated during the tensile test is purely caused by tensile force [61], [62], leading to consistent and uniform cracking patterns. This contrasts with flexural loading, which generally results in localized cracking at the region of maximum tensile stress.

In addition, direct tensile testing can be applied to various specimen to various specimen geometries, such as dog-bone shaped specimen. Since tensile failure often plays a significant role in the deterioration of concrete in practical applications, this method offers valuable insights into the tensile behaviour, cracking pattern, and overall durability of reinforced concrete. As such, it serves as a vital complement to flexural loading in corrosion-related studies. By enabling controlled and uniform crack formation, direct tensile loading enhances the ability of researchers to systematically study the influence of crack geometry on chloride ingress and corrosion propagation, providing a clearer understanding of structural durability in a chloride-exposed environment.

### 2.2.2 *Pre-cracking by artificial techniques*

One common method in laboratory conditions to produce cracks in reinforced concrete specimens for analysis is the application of artificial notches [59]. In contrast to mechanical loading techniques, which depend on applying external forces, artificial methods use non-mechanical means to introduce controlled cracks. Since crack width, depth, and orientation are critical factors in investigating chloride ingress, artificial notching ensures consistency and repeatability in crack characteristics, allowing the researcher to focus on how environmental exposure and crack effect corrosion behaviour.

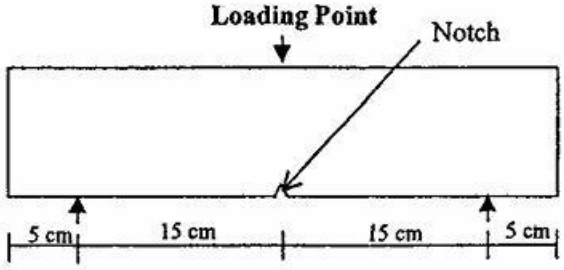


*Figure 2.2-3. Schematic sketch of crack produced by notch* [59].

One of the most widely used methods involves the using pre-made notches [63] either embedded into the concrete during casting or integrated into mold design. After the casting of concrete, those inserts to produce notches are taken out, leaving cracks and voids in their place. This method allows for precise crack placement at specific locations to facilitate chloride penetration rate.

Another common method is the use of saw-cutting, where concrete is mechanically sliced to create artificial cracks with controlled width and depth. These types of artificial cracks offer high reproducibility for the study of cracks on chloride ingress. However, they do not fully replicate the complex, irregular cracking patterns typically observed in real structures.

Overall, artificial pre-cracking techniques offer greater control over crack geometry, which is essential for evaluating the effect of crack width on chloride penetration. Compared to mechanical loading, the artificial crack approach frequently requires fewer setups and takes less time [63]. Despite their limitations in simulating real-world crack behaviour, these techniques remain valuable tools in academic research focused on the influence of cracking on corrosion in reinforced concrete structures.

## 2.3 *Corrosion acceleration techniques in literature*

Accelerated corrosion techniques have been widely used to analyse the behaviour of reinforced concrete structures under aggressive environments within a manageable

time frame. Under natural conditions, steel corrosion in concrete often takes several years to occur, making long-term studies difficult and time-consuming. To address this constraint, researchers have developed a range of methods to accelerate the corrosion process in the laboratory under a controlled environment. These techniques are designed to simulate real-world deterioration mechanisms, allowing for a better understanding of corrosion progress and the effectiveness of various strategies aimed at improving the durability of reinforced concrete structures.

### *2.3.1 Accelerated laboratory condition*

The idea behind accelerated laboratory tests is to speed up the natural process that causes corrosion, allowing researchers to systematically investigate the impact of various factors on corrosion rates, including crack width, concrete mix design, curing conditions, and environmental exposures. Accelerated laboratory methods are essential for improving our understanding of corrosion behaviour and for evaluating the long-term performance of concrete structures.

#### *2.3.1.1 Wet and dry cycles*

Wet and dry cycles are one of the most effective accelerated techniques used in laboratory [64], [65] to understand the impact of environmental exposure on reinforced concrete structures. This technique replicates the conditions experienced by reinforced concrete structures exposed to marine, coastal, or de-icing salt environments. Alternate wet and dry cycles speed up the entry of chloride ions, producing corrosion in a shorter period compared to the natural process [66]. as
During wet and dry cycles, concrete specimens are subjected to chloride-rich environments, such as sodium chloride solutions, at regular intervals. This process allows chloride ions to diffuse through concrete during the wet phase. During the drying phase, oxygen infiltrates the concrete, which is essential for maintaining the corrosion process. With the help of wet and dry cycles, researchers can replicate the years of exposure conditions in a few months [67].

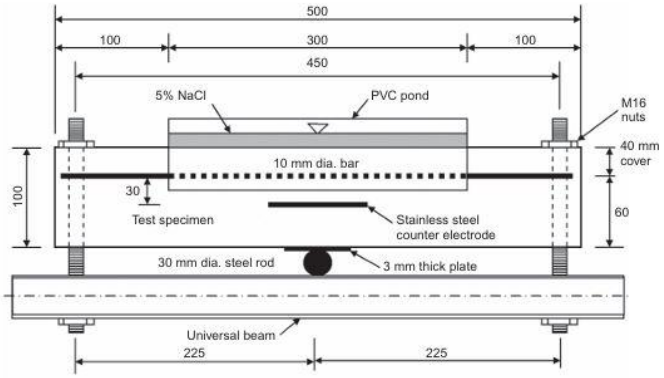


*Figure 2.3-1. Schematic sketch of wet and dry cycle ponding* [17].

One of the significant benefits of wet and dry cycles is their ability to simulate real-world aggressive conditions in a controlled laboratory environment. Numerous reinforced concrete structures, such as bridge piers and decks, as well as structures in marine environments, reflect the condition experienced in wet and dry cycles. With the help of this technique, researchers can investigate the effect of concrete mix design, crack width, and concrete clear depth to rebar on chloride ingress and rebar corrosion [68], [69].

However, Certain limitations of this method should be acknowledged, such as temperature, humidity, the duration of wet and dry cycles, and concentration of chloride solutions, all of which can lead to different results. Despite these limitations, wet and dry cycles remain an effective acceleration technique for inducing corrosion and assessing materials' durability under aggressive environmental conditions.

Advantage:

- Effectively simulate real-world exposure conditions, such as marine and coastal environments.
- Can replicate years of chloride ingress and corrosion in a few months.
- Allow control over variables like concrete mix, crack width, and cover depth.
- Useful for studying the impact of environmental cycling on corrosion behavior.

Limitations:

- Results may vary based on test parameters such as temperature, humidity, duration of each cycle, and chloride concentration.
- Cannot perfectly replicate natural exposure complexity.
- Require careful calibration to ensure consistency across experiments.

#### *2.3.1.2 Imposed current technique*

Another popular laboratory approach for accelerating the corrosion of rebar in concrete is the imposed current technique [70], [71], sometimes referred to as impressed current or electrochemical acceleration. This method simulates the anodic and cathodic process that occurs during the natural corrosion process by applying an external electrical current. This technique significantly reduces the time required to induce corrosion in rebar, making it an essential tool for investigating chloride-induced corrosion. The rebar is connected to an external power source, a direct current (DC), and an external electrode. As the current flows through the rebar, the corrosion process is accelerated. The rate of corrosion can be controlled by varying the magnitude of the applied current, allowing the simulation of natural corrosion over a few weeks.

The accelerated corrosion process allows researchers to investigate the important aspects of chloride-induced corrosion, such as crack formation caused by steel

expansion and the effect of corrosion on the bond strength between rebar and concrete. Researchers can also evaluate the durability of coatings, corrosion-resistant materials, and other strategies to enhance durability strategies by using this technique.

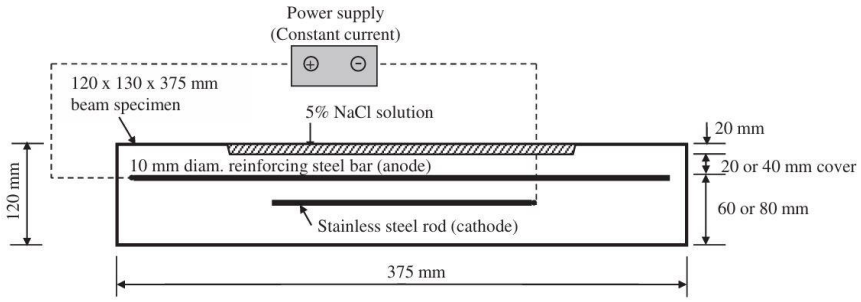


*Figure 2.3-2. Schematic sketch of accelerated imposed current corrosion* [16].

The imposed current technique offers a high level of control over the corrosion process, making it advantageous for experimental studies. This method allows for precise regulation of current density [72], [73], which is directly linked to the corrosion rate. Furthermore, the imposed current technique is cost-effective and time efficient, enabling accelerated corrosion testing without prolonged exposure to aggressive environmental conditions.

However, the imposed current technique has certain limitations. The electrochemical environment created during imposed current testing may differ significantly from that of natural exposure, potentially leading to the formation of corrosion products that are not representative of those occurring under real-world conditions. Moreover, applying excessively high current densities can result in unrealistic corrosion patterns and damage. Therefore, the researcher must carefully calibrate the applied current to strike a balance between acceleration and realism.

Despite these limitations, the imposed current technique remains a widely used and effective method for inducing chloride-related corrosion in reinforced concrete under controlled laboratory conditions.

Advantage:

- Allows precise control over the corrosion rate by adjusting current density.
- Highly time-efficient corrosion can be induced in days or weeks instead of years.
- Useful for studying crack development, bond strength degradation, and evaluating anti-corrosion measures.
- Ideal for comparative studies under standardized conditions.

Limitations

- Electrochemical conditions may not reflect those in the natural environment, affecting the type and distribution of corrosion products.

- Excessive current can lead to unrealistic or exaggerated damage patterns.
- Requires careful setup and calibration to avoid over-acceleration.

### *2.3.2 Natural exposure studies*

Natural exposure investigates the long-term behaviour of corrosion by exposing reinforced concrete structures to actual environmental conditions. Unlike accelerated techniques, this method focuses on natural chloride infiltration under typical exposure conditions [74], [75], such as marine environments, coastal regions, or areas where de-icing salts are commonly used.

Concrete specimens are typically placed in environments that simulate specific exposure conditions. For example, specimens may be immersed in seawater, exposed to tidal zones, or exposed to cyclic wet-dry cycles. Over time, chloride ions from the environment penetrate the concrete and reach the reinforcement, leading to the initiation and propagation of corrosion [16]. These studies are also valuable for understanding how environmental factors like humidity, temperature, and duration of exposure influence the rate of corrosion.

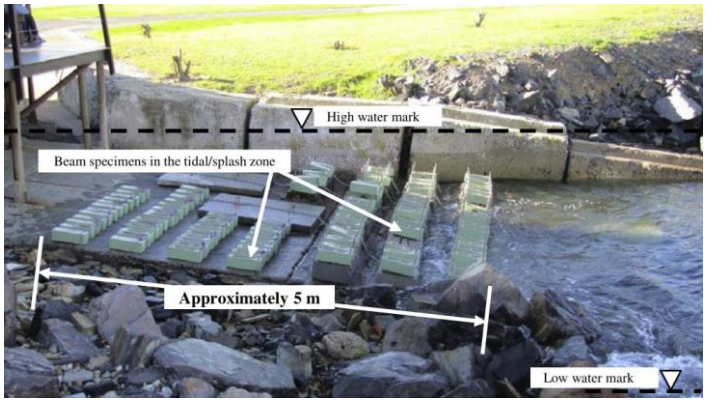


*Figure 2.3-3 Beams specimens exposed to natural exposure conditions* [16].

However, the main drawback of natural exposure studies is the long duration required to obtain significant results. These tests are often not suitable for quick assessment due to the slow rate of reinforcement corrosion and chloride ingress. Additionally, the variability of environmental factors, such as fluctuations in chloride concentration or weather patterns, can make it challenging to ensure that results are consistent and repeatable.

Advantages:

- Provide a realistic and comprehensive understanding of corrosion behavior under actual environmental conditions.

- Capture the full impact of climatic factors, including humidity, rainfall, and temperature.
- Essential for validating laboratory-based accelerated tests and for long-term performance assessment.

Limitations

- Requires long duration, often years, to observe significant corrosion.
- Environmental variables are difficult to control, leading to possible inconsistency in results.
- Not suitable for rapid material screening or early-stage experimental testing.

### *2.3.3 Chloride penetration and diffusion studies*

Chloride penetration and diffusion studies focus on the movement of chloride ions through the concrete to the reinforcement, aiming to understand the corrosion mechanism. Chloride ingress is the primary cause of corrosion in reinforced concrete structures, especially in marine environments.

Researchers can evaluate the durability of durability of reinforcement by examining the penetration and diffusion of chlorides within the concrete. In the laboratory, concrete specimens are submerged in a chloride-rich solution [76] for a predetermined period to accelerate the chloride ingress. Concrete samples from various depths are then extracted and analysed to determine the extent of chloride penetration. This method provides clear insights into the degree of chloride ingress and the protective capability of the concrete cover.

The diffusion studies aim to understand the long-term movement of chloride ions through the concrete's pores. The diffusion coefficient of concrete is measured using a steady state diffusion test and the rapid chloride migration test (RCMT). By applying Fick's law of diffusion [77], researchers can use this data to estimate the chloride ingress and estimate how long it will take for chloride to reach reinforcement.

Studies on the chloride penetration and diffusion are also important to assess how different factors such as water-cement ratio, aggregate type, cement composition, and curing conditions affect the concrete durability. A key advantage of these tests is their ability to evaluate a material's resistance to chloride ingress [78], which is crucial for the long-term durability and service life of structures. However, chloride penetration and diffusion tests required extended periods to simulate natural chloride transport accurately.

## *2.4 Influence of crack width on corrosion of reinforcement*

A significant amount of research has been conducted to investigate the durability of RC exposed to aggressive environments, as summarized in Table 1. The table includes data from the 1990s onward and categorizes specimens based on various factors.

- The "Environmental Conditions" column details the exposure conditions and the amount of chloride used in research. According to Figure 2, crack width influences the behaviour of RC elements. Sixty percent of the authors used NaCl concentration ranging from 2% to 4%, which is close to the NaCl concentration in seawater. The exposure conditions are further subdivided into laboratory conditions and field exposure. In the laboratory, 58% of the authors used wet and dry cycles, and 34% used current to accelerate corrosion, as shown in Figure 2.
- The "Loading Condition" section presents the loads applied during both the pre-cracking and the corrosion phases. According to Figure 2, 52% of researchers used three-point bending, 35% used four-point bending, and only 13% of authors used tensile loads.
- The last column provides data on crack width and crack topology, with the majority of cracks being flexural.

Francois and Arliguie [79] conducted an experiment on a 3-meter-long beam over 12 years under loading conditions exposed to salt fog spray of (35 g/l of NaCl). According to their findings, crack width (less than 0.5 mm) does not influence the development of corrosion; instead, tensile micro-cracking, caused by sustained loads, allows aggressive agents to penetrate the concrete, playing a more critical role in corrosion. Research by [59], [80] found that a plain bar corrodes less than deformed bars, as deformed bars have large gaps underneath, contributing to an increased corrosion rate. In the same research, the author concluded that, besides crack width, water-cement ratio plays an important role in affecting reinforcement durability.

Jaffer and Hansson [81] used high-performance concrete (HPC) and normal concrete (NC) beams subjected to both static and dynamic loading. Their study concluded that loading conditions had minimal impact on beam performance compared to the quality of concrete. In their research, HPC exhibited better resistance than NC. Maaddawy et al [74] conducted experiments on loaded and unloaded beams exposed to corrosion. They found that, under sustained loads, the time from corrosion initiation to corrosion cracking was reduced by 44%, and cracks due to corrosion increased by 22% in the first 50 days. The reduction in the load-carrying capacity of the corroded beams was directly proportional to the cross-sectional area of the rebar. Otieno et al., [17] studied the influence of crack width, crack reopening, and water-cement ratio on corex slag and ordinary Portland cement (OPC) beams. Their findings indicated that a crack width below 0.4 mm affected the corrosion rate of ordinary concrete but not blended concrete (corex slag). The corrosion rate of OPC concrete increased by 210%, whereas corrosion in blended concrete increased by 40%, which is considered an acceptable rate for a concrete structure in marine environment.

Wang et al., [82] compared the results of ground granulated blast-furnace slag (GGBS) and Portland cement containing at least 95% Portland cement clinker (CEMI) under three different loading conditions. According to their results, GGBS delays corrosion

initiation compared to CEMI, which is beneficial for structures exposed to aggressive environments. Otieno et al., [16] conducted parallel research on 210 beams in the laboratory and natural corrosion in the marine tidal zone. Their results showed that blended cement concrete outperformed standard concrete in both cracked and uncracked beams. A significant reduction in corrosion was observed with the partial replacement of Portland cement (PC) with fly ash (FA) at 30% and ground granulated blast-furnace slag (GCBS) at 50%. The corrosion rate increased with the reduction in cover depth and crack width.

*Table 2.4-1. Loading condition, environmental condition and type of loadings of experimental campaigns on RC elements.*

| Reference | Specimen Shape and Size | Environmental condition | Loading condition | | Corrosion Acceleration Technique | Crack width and typology |
|---|---|---|---|---|---|---|
| | | | Pre-Cracking Phase | Corrosion Phase | | |
| [83] | 24 beams with 1000 mm length and cross-section of 150 mm x 150 mm | - | Four-point loading<br><br>- | Four-point loading<br><br>Static load | Current | 0.3875 (Average)<br><br>NA |
| [84] | 28 beams with length 1360 mm and cross section of 135 mm x 100 mm | 3% NaCl spray used for 12 months | No load applied | No load applied | Wet and dry cycle | 0.3 mm (max) Flexural cracks |
| [85] | 7 beams with length 384 mm and cross section of 125 mm x 160 mm | Partially immersed in 5% NaCl solution | Four-point bending | No load applied | Current | NA |
| [79] | 4 beams with length 3000 mm and 150 and cross section of mm x 280 mm | Salt fog spray 35 g/l of NaCl for 12 years | Three-point bending test. | Sustained load.<br><br>Static load. | Wet and dry cycles | 0.1, 0.2, 0.3, 0.4, 0.5 mm<br><br>Flexural cracks |
| [80] | Concrete specimen with length | Salt fog spray 3.5 % NaCl | No load applied | No load applied | Wet and dry cycles | 0.3 mm |

| | | | | | | |
|---|---|---|---|---|---|---|
| | 100 mm and cross section of 230 mm x 290 mm | | | | | Flexural cracks |
| [58] | 2 beams having length 650 mm and cross section of 100 mm x 90 mm | Immersed in 3 % NaCl for 300 days | Three-point bending test. | Sustained load.<br><br>Static load. | Immersed in NaCl solution | 0.3 mm (max)<br>Flexural cracks |
| [86] | 2 beams having length of 3000 mm and cross section of 150 mm x 280 mm | Salt fog spray 35 g/l of NaCl for 13 years | Three-point bending | Sustained load<br><br>Static load | Wet and dry cycles | NA<br><br>Flexural cracks |
| [59] | Beams having length 1250 mm and cross section of 150 mm x 150 mm | Salt spray of 3.5 % NaCl once a week for 16 months | Four-point bending | Sustained load<br><br>Static load | Wet and dry cycles | 0.1, 0.3 and 0.7 mm<br>Flexural cracks |
| [87] | 2 beams having length 3000 mm and cross section of 150 mm x 280 mm | Salt fog spray of 35 g/l of NaCl for 14 and 17 years | Three-point bending test. | Sustained load.<br><br>Static load. | Wet and dry cycles | NA<br><br>Flexural cracks |
| [88] | 16 beams having length of 400 mm and cross section of 100 mm x 100 mm | Immersed in NaCl solution for 7 days and one month | Three-point/ Four-point bending test.<br><br>Static load. | No load applied. | - | 0.1 - 0.5 mm |
| [74] | 9 beams having length of 3200 mm and cross | 2.25 % $Cl^-$ ions (by weight of concrete) added to concrete mix | Four-point bending test. | Sustained load on 4 beams.<br><br>Static load. | Current | 0.15 mm (Average)<br>Flexural cracks |

| | | | | | | |
|---|---|---|---|---|---|---|
| | section of 152 and 254 | | | | | |
| [81] | 36 beam 1200 mm long and cross section of 120 mm x 70 mm | Immersed in 3% NaCl solution for 18 months | Three-point bending test. | Sustained load.<br><br>Static/dynamic load. | Wet and dry cycles | NA<br><br>Flexural cracks |
| [89] | 9 prestressed beams with length 3000 mm and cross section of 200 x 300 mm and | 5 % NaCl pounding at the top of the beam for 2 days | No load applied | Four-point bending test<br><br>Static load | Current | NA<br><br>Flexural cracks |
| [90] | 1 beams 400 mm long and cross section of 100 mm x 100 mm | Immersed in 3.% NaCl for one year. | No load applied | No load applied | Wet and dry cycles | No cracks |
| [17] | 48 beams 500 mm long and cross section of 100 x 100 mm | Immersed in 5% NaCl for 31 weeks | Three-point bending test. | Sustained load.<br><br>Static load. | Wet and dry cycles | 0.4 mm and 0.7 mm Flexural cracks |
| [82] | 24 beams 1200 mm long and cross section of 250 x 200 mm. | Immersed in 10% NaCl for 60 weeks | Four-point bending test | Sustained load.<br><br>Static load. | Wet and dry cycles | mm Flexural crack |
| [16] | 105 beams 375 mm long and cross section of 120 x 130 mm | 5 % NaCl pounding for 122 weeks | Three-point bending test.<br><br>Static load. | No load applied | Current/ wet and dry cycles | Incipient crack, 0.4 and 0.7 mm Flexural cracks |
| [16] | 105 beams 375 mm long and cross | Expose to marine tidal environment for 122 weeks | Three-point bending test. | No load applied | Current/ Marine environment | Incipient crack, 0.4 and 0.7 mm |

| | | | | | | |
|---|---|---|---|---|---|---|
| | section of 120 x 130 mm | | Static load. | | | Flexural cracks |
| [12] | 11 concrete prism 500 mm long and having cross section of 150 mm x 150 mm | $CaCl_2.2H_2O$ added to concrete mix to get 3% mass ratio of $Cl^-$ to cement. | No load applied | No load applied | Current | NA |
| [91] | 3 beams having length of 3000 mm and cross section of 150 mm x 150 mm | Immersed in 3% NaCl for 10 days | Static tensile load.<br><br>Static load. | No load applied | Current | 0.05 - 10 mm Flexural cracks |
| [92] | 57 beam 813 mm long and cross section of 235 x 76 mm | 3% of NaCl pound for 550 days | Tensile load. | Sustained load.<br><br>Static load. | Wet and dry cycle | 0.1 mm, 0.3 mm and 0.7 mm. Flexural crack |
| [93] | 48 Concrete prisms having dimension 120 x 90 x 50 mm | 10% NaCl and 0.3 M NaOH | Three-point bending test.<br><br>Static load. | No load applied | Current | 5-70 μm Flexural crack |
| [13] | 54 beam 1100 mm long and cross section of 180 x 100 mm. | Beams Partially (three quarter) immersed in 16.5% NaCl solution for 3 years | Three-point bending test | Sustained load.<br><br>Static load. | Wet and dry cycles | 0.1, 0.2, 0.3- and 0.4-mm flexural crack |
| [94] | Prestressed reinforced concrete beam 3000 mm long and cross section of 200 x 300 mm | Partially immersed in 3% NaCl solution for one month | Four-point bending | No load applied | Current | NA |

| | | | | | | |
|---|---|---|---|---|---|---|
| [95] | 4 Tension ties 600 mm long and cross section of 90 x 90 mm | Immersed in 3% of NaCl solution for 615 days | Uniaxial tensile loads | No load applied | Wet and dry cycles | 0.2, 0.3, 0.5 and 0.7 mm Flexural cracks |
| [95] | 10 Prismatic specimen 120 mm long and cross section of 90 x 50 mm | Immersed in 3.5 % NaCl solution for 800 days | Three-point bending | No load applied Static load | Wet and dry cycles | - |
| [14] | 42 tension ties 830 mm long and cross section of 90 x 90 mm | Immersed in 5% NaCl for 280 days | Tensile test applied.<br><br>Static loads | Static tensile loading | Wet and dry cycles | 0.175 (mean) and 0.336 (mean) Tensile cracks |

Alarab et al., [92] conducted research on beams with three different crack widths. They observed that the top part of the bar, just below the cracks, was more corroded than the bottom. The rate of corrosion was directly proportional to the crack width. Chen et al., [13] studied plain concrete beams alongside beams with three types of fibers (hybrid, synthetic, and steel) exposed to sustained loads, with crack widths ranging from 0.1 to 0.4mm. The beams were partially immersed in sodium chloride solution (16.5% NaCl) for a two-week wet and two-week dry cycle over three years. It was noted that beams with fibers exhibited less corrosion than plain concrete.

However, beams with synthetic fiber show a larger standard deviation due to uneven fiber distributions. No relationship between local corrosion and flexural cracks was found.

Experimental work carried out by Leporace-Guimil et al., [14] on RC tension ties, revealing high variation in pitting depth in relation to crack width (ranging from 0.06 and 0.24 mm). In some cracks, no corrosion was observed (most likely due to crack sealing), while some other cracks showed severe corrosion. There is no agreement on the influence of the crack width on both initiation time and corrosion rate.

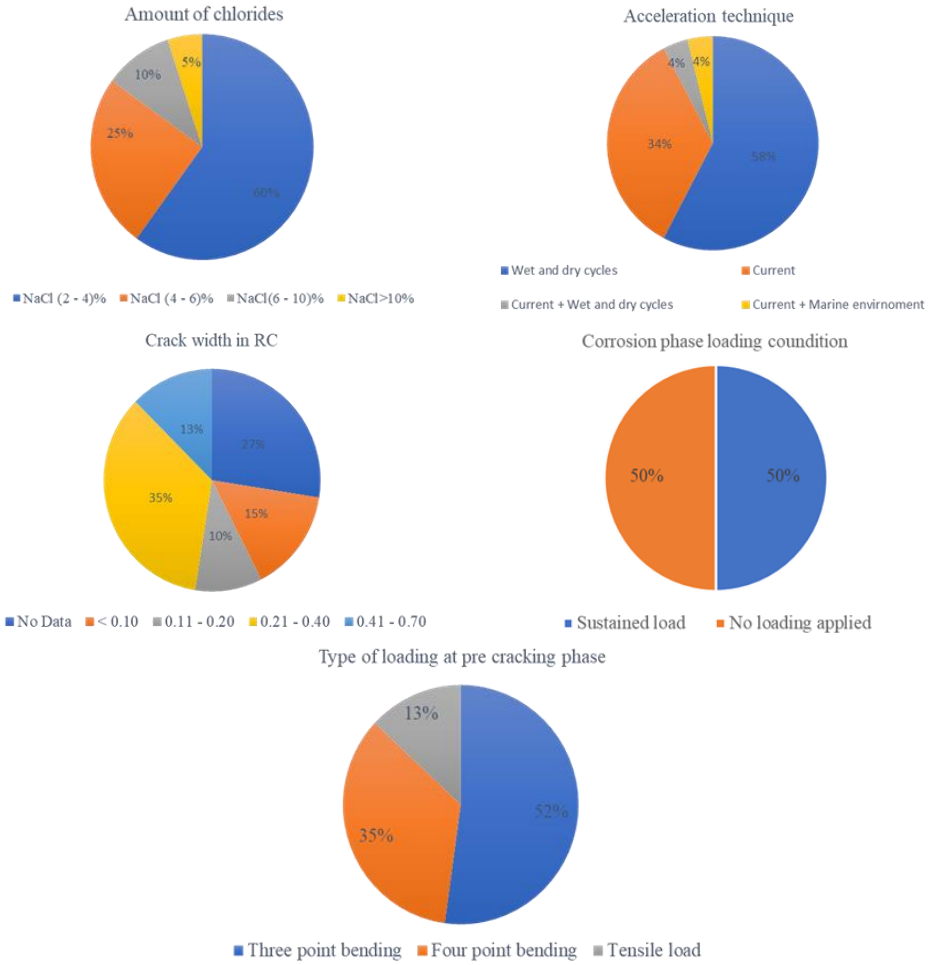


*Figure 2.4-1. Main parameters varied during corrosion tests on RC elements.*

### *2.4.1 Influence of other parameters*

Apart from crack width, several other factors influence the corrosion process. These factors include materials and environmental parameters, such as temperature, exposure condition, moisture content, and concrete cover to rebar. These factors affect the rate of corrosion elements, including carbon dioxide and chloride, penetration to reach rebar in concrete. To evaluate the durability and lifespan of concrete, it is essential to consider the impact of these parameters

#### *2.4.1.1 Concrete cover thickness*

Concrete cover is the distance between the concrete surface and the reinforcement inside the concrete. Since concrete acts as a barrier between the steel reinforcement

and the surrounding environment, this parameter is crucial for ensuring the lifespan and durability of concrete by preventing the ingress of aggressive agents like moisture, chloride, and carbon dioxide, which are major causes of corrosion. An adequate concrete cover can delay the ingress of external aggressive agents, thus delaying the onset of corrosion.

According to past research, a thick concrete cover can protect the rebar surface for an extended period, particularly in areas with carbonation and high chloride levels. For example, a thick concrete cover is essential in marine environments, where concrete is exposed to high humidity and seawater, in order to prevent chloride penetration, which is the main cause of corrosion in such conditions.

Concrete cover not only serves as a barrier but also affects how cracks appear and develop. Early cracking due to insufficient cover thickness can expose the reinforcement to aggressive conditions and promote corrosion. On the other hand, an adequate cover can absorb environmental pressure, reducing the possibility of early crack formation and prolonging the protection of reinforcement.

The American Concrete Institute (ACI) and Eurocode provide guidelines for the minimum concrete cover thickness based on environmental exposure classes and the diameter of rebar. By following these recommendations, the concrete structures will be protected from corrosion for the duration of their expected lifespan.

#### *2.4.1.2 Moisture levels and exposure conditions*

In reinforced concrete structures, moisture content and exposure conditions have a significant impact on the development of corrosion. Moisture availability is critical to the corrosion process because corrosion is an electrochemical reaction, which involves the formation of an anode and cathode, through which ions travel from anode to cathode with the help of electrolytes. Moisture content acts as the electrolyte by facilitating the electrochemical process at the rebar surface.

Another significant factor in corrosion is the nature of exposure conditions surrounding reinforced concrete structures. Marine environments, with their high chloride content and high humidity level, are particularly vulnerable to the corrosion process, as chloride ions can initiate the corrosion process by either penetrating through cracks or tiny pores in concrete. The alkaline environment that typically shields the rebar is also neutralized by the presence of carbonation in dry environments.

Furthermore, the durability of the reinforced concrete structure can be negatively impacted by wet and dry cycles. The localized concentration of chloride ions, resulting from repeated wet and dry cycles, accelerates the development of corrosion. It is crucial to use an appropriate mix design and implement strategies to protect rebar from chloride ingress. Concrete resistance to corrosion can be increased by ensuring

it is properly concealed and shielded from excessive moisture content during the early curing stage.

#### *2.4.1.3 Temperature*

Another important factor influencing the rate of corrosion in reinforced concrete is temperature. Both the physical properties and chemical reactions that cause corrosion are affected by temperature. Lower temperatures can slow down the corrosion process, while higher temperatures generally accelerate it. This occurs because temperature changes the mobility of ions and increases the ductility of concrete, which in turn speeds up the corrosion process. In warmer climates, a rise in temperature may also cause chloride ions to diffuse into the concrete more quickly, further accelerating the corrosion process. Additionally, high temperatures tend to make concrete more porous and brittle, which makes it easier for aggressive agents to reach the reinforcement.

The physical properties of concrete are also significantly impacted by temperature. Abrupt temperature changes can lead to thermal expansion and contraction, which can create pressure and produce cracks. These cracks can provide pathways for moisture and chloride ions, accelerating the corrosion process.

Repeated freeze-thaw cycles in colder climates can cause internal pressure that leads to cracking in concrete structures. This makes it easier for water and chloride ions to enter the concrete, increasing the risk of corrosion. Furthermore, de-icing salt, when used in winter to lower the freezing temperature of snow, can accelerate corrosion in areas where they are applied.

In order to reduce the effect of temperature, strategies such as thermal insulation, appropriate concrete mix design, and protective coating are effective in reducing temperature-related impact.

## *2.5 Influence of crack width on corrosion of fiber-reinforced concrete*

An overview of studies on fiber-reinforced concrete (FRC) exposed to aggressive environments is presented in Table 2. The studies are categorized as follows:

- Specimen shape and size: The length range between 350 mm and 1100 mm, and the number of specimens used in each experiment.
- Environmental conditions: describe the chloride concentration, duration, and exposure conditions. Sodium chloride (NaCl) was used by 70% of the authors, with concentrations ranging from 2% to 4%.
- Type of loading: The loading conditions applied to the specimen are further divided into pre-cracking and corrosion phases. According to Figure 3, the authors were evenly split between those who applied a sustained load and

those who did not apply a load. 56% of authors used three-point bending, 22% used tensile loading, and 11% used four-point loading.

- Crack width: Specimen were mostly subjected to flexural cracks. About 40% of authors used a crack width in the range of 0.21 - 0.40 mm, whereas 33% of authors used a crack width of 0.11 – 0.20 mm.
- Types of fibers: The studies utilized different types and amounts of fibers. 64% of the research focused on steel fibers, whereas 22% used polyvinyl (PVA) alcohol fibers.

One way to reduce cracking in concrete is by adding fibers, which reduce the cracks in concrete through fiber bridging [13]. It has been observed that the FRC with 1.5% fiber content shows a longer corrosion initiation period. However, corrosion can affect the crack-bridging capacity of fibers by reducing their cross-sectional area due to the corrosion of fibers. Despite this, according to Marcos-Meson et al., [96], stainless steel fiber provides complete protection against chloride-induced corrosion, both in cracked and uncracked stages. Berrocal et al., [97] concluded that the presence of fibers, which reduces crack width, can extend the corrosion initiation time.

Several studies have demonstrated the advantages of using fiber in structural elements. for example, Granju and Ullah Balouch, [98] conducted an experiment on cracked steel fiber-reinforced concrete (SFRC) with a crack width of up to 0.5mm. After one year of exposure to the marine environment, no corrosion was found in a crack width of less than 0.1mm. Fiber located within 2 to 3 mm from the concrete surface was severely corroded, while those further from the surface exhibited only minor corrosion with no significant reduction in their cross-sectional area. Surprisingly, the strength of the sample exposed to the aggressive environment increased as a result of corrosion. The external surface of the fiber became rougher, which made it more difficult for fibers to slip, ultimately leading to an increase in the sample's strength.

Mihashi et al., [90] conducted research on RC beams made of plain mortar, fiber-reinforced cementitious composites (FRCC) containing polyethylene (PE) fiber, and hybrid fiber-reinforced cementitious composites (HFRCC) consisting of both PE and hybrid steel cord (SC). According to the results, the sample made of plain mortar was the first to initiate the corrosion, followed by FRCC and HFRCC. The amount of steel reduction in FRCC was 60% less than in plain mortar, attributed to the bridging effect and self-healing capacity. Among the three types, the HFRCC exhibited the least corrosion. The result from the three samples was compared with the amount of corrosion calculated using Faraday's law, where both mortar and FRCC showed close results. However, the experimentally measured corrosion for the HFRCC was much greater than the amount calculated theoretically.

*Table 2.5-1. Loading conditions, environmental conditions, and types of loadings in experimental campaigns on FRC elements.*

| Reference | Specimen Shape and Size | Environmental condition | Loading condition | | Corrosion Acceleration Technique | Crack width | Type of Fibre |
|---|---|---|---|---|---|---|---|
| | | | Pre-Cracking Phase | Corrosion Phase | | | |
| [98] | 2 concrete prism 500 mm long and cross section of 100 mm x 100 mm | Immersed in 3.5% NaCl for one year. | Three-point bending test.<br><br>Static loads | No load applied. | Wet and dry cycles | 0.5 mm Flexural crack | Hooked steel fibres 0.5 %, Flexural cracks |
| [90] | 2 beams 400 mm long and cross section of 100 mm x 100 mm | Immersed in 3. % NaCl for one year. | No load applied | No load applied | Wet and dry cycles | No cracks | (1.5%) Polyethylene fibers for fiber reinforced cementitious composites, (0.75%) polyethylene and (0.75%) hybrid steel cord for fiber reinforced cementitious composites. |
| [99] | 15 beams 350 mm long and cross section of 100 mm x 100 mm | Immersed in 3.5% NaCl solution for 56 weeks | Four-point bending test.<br><br>Static load | Flexural load applied. | Wet and dry cycles | 0.25 to 0.30 mm (mean), 0.6 to 0.8 mm (mean) | Cellulose and polypropylene fibres 0.1 % and 0.3 % |
| [100] | 12 beams 608 mm long and cross section of 152 mm | 3% of NaCl pound for 9 months | Cyclic loading<br><br>Static load | No load applied | Wet and dry cycles | Flexural cracks 300 µm – | Polyvinyl alcohol fibres 0.2 % and |

| | | | | | | | |
|---|---|---|---|---|---|---|---|
| | x 152 mm | | | | | 400 µm | steel fibres 0.5 %, 0.8 % |
| [97] | 54 Beam having length of 1100 mm and having cross section of 100 mm x 180 mm | Immersed in 16.5 % NaCl for max 22 weeks. | Three-point bending test.<br><br>Static loads | Sustained load. | Wet and dry cycles | 0.1, 0.2, 0.3 and 0.4 mm (Target ) | Low carbon steel fibres (0.5%), Polyvinyl alcohol fibres (0.35% ,0.15% ) for hybrid series, Polyvinyl alcohol (0.75% ) for synthetic series,<br><br>Flexural cracks |
| [101] | 54 beams 1100 mm long and having cross section of 180 mm x 100 mm | Partially immersed in 3.5 NaCl solution | Three-point bending<br><br>Static load | Sustained load. | Wet and dry cycles | 0.2 mm - 0.6 mm | End-hooked steel fibres, polyvinyl Alcohol fibres and steel fibres < 1 Vol % |
| [13] | 15 beam 1100 mm long and cross section of 180 x 100 mm. | Beams Partially (three quarter) immersed in 16.5% NaCl solution for 3 years | Three-point bending test | Sustained load.<br><br>Static load. | Wet and dry cycles | 0.1, 0.2, 0.3- and 0.4-mm flexural crack | (0.5%) 35 mm end hooked Steel fibers, (0.75% ) 30 mm straight polyvinyl alcohol and combination of steel |

| | | | | | | | |
|---|---|---|---|---|---|---|---|
| | | | | | | | (0.35%) and 18mm long polyvinyl alcohol (0.15%) for hybrid series. |
| [102] | 1 Dog-bone shape specimen having length 330 mm and having cross section of 30 mm x 13 mm | Immersion in 3.5 % Immersed in NaCl for 7 weeks | Direct tensile test, Static Direct tensile test at post cracking phase | No load applied, Static loads | Wet and dry cycle | NA | 2% straight steel fibres |
| [95] | 4 Tension ties 600 mm long and cross section of 90 mm x 90 mm | Immersed in 3% of NaCl solution for 615 days | Three-point bending Static load | unloaded | Wet and dry cycles | 0.2 mm (max) Flexural cracks | 0.64 % hooked end steel fibres |
| [14] | 42 Tension ties 830 mm long and cross section of 90 mm x 90 mm | Immersed in 5% NaCl for 280 days | Tensile test applied. Static loads | Axial tensile load | Wet and dry cycles | 0.110, 0.213 (mean), Tensile cracks | Hooked Steel fibres 0.64 % |

Mitchell et al., [99] used cellulose and polypropylene fiber to investigate the effect of chloride diffusion reduction in reinforced concrete. They found that chloride ions diffuse through the concrete and interact with fibers, which reduces the amount of chloride available to reach and affect the reinforcement. Among the two types of fiber used, cellulose fibers demonstrated better performance in mitigating chloride ions.

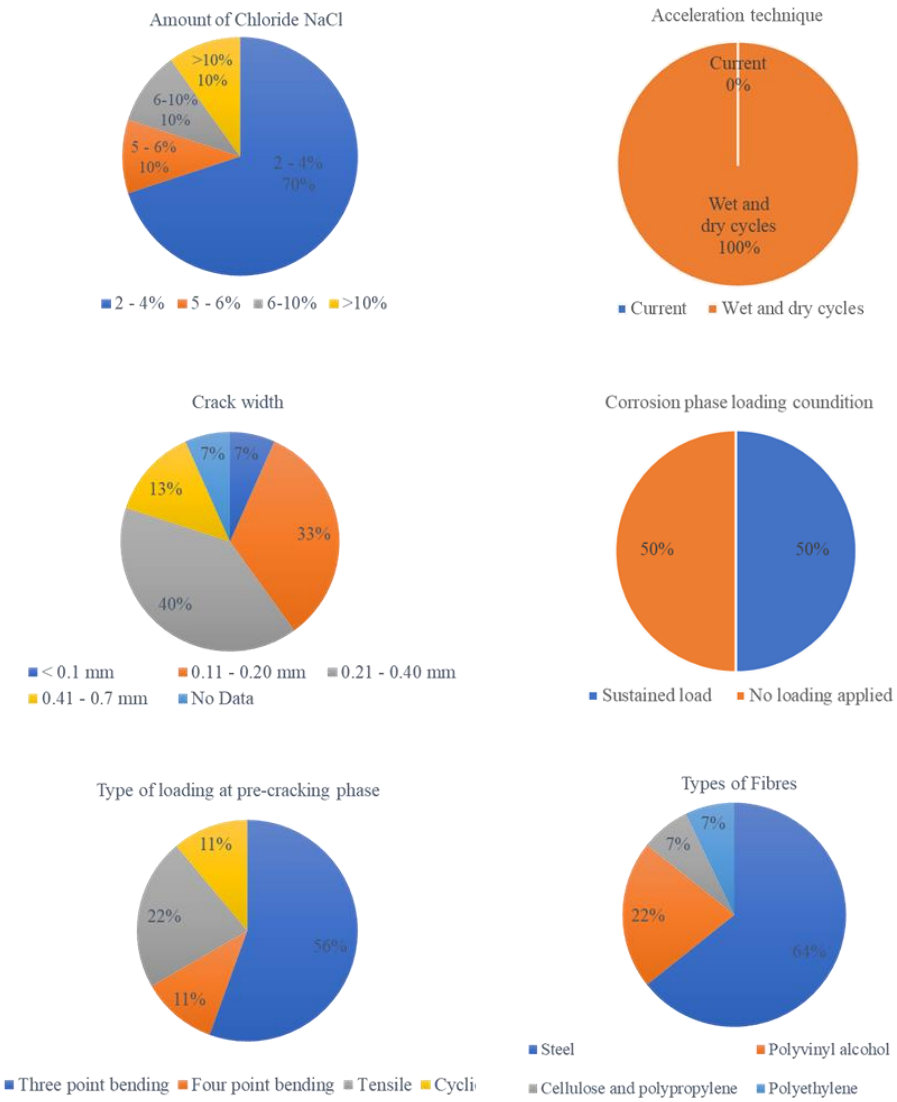


*Figure 2.5-1. Main parameters varied during corrosion tests on FRC elements.*

Similar findings were reported by Blunt et al., [100], who studied the effect of hybrid fiber on reducing the corrosion rate of rebar in concrete. When comparing the results of the hybrid fiber-reinforced (HyFRC) with normal concrete (NC), HyFRC effectively delayed the corrosion compared to NC after being subjected to the same cyclic flexural loading.

Berrocal et al., [97] investigated the use of plain, steel, hybrid, and synthetic fibers in concrete elements subjected to different loading conditions and exposed to aggressive environments. The results indicated that the addition of fiber at a low dosage had no significant effect on the flexural capacity of concrete. However, steel fibers produce the best results among all fibers. There was no sign of corrosion in the uncracked specimen by the end of the experiment, whereas the cracked specimens exhibited corrosion after 17 weeks.

Leporace-Guimil et al., [14] adopted an innovative testing method to accelerate the corrosion process while applying sustained loads. They used tension ties made of plain and fiber-reinforced concrete (FRC), exposed to a wetting and drying cycle (three days wet and four days dry) for a duration of 40 weeks. Fibers positively influence on corrosion resistance by reducing the crack spacing by 16% and the crack width by 35-40%. Despite these improvements, corrosion was still observed on the external surface and at cracked locations of FRC beams. No clear correlation between crack width and corrosion was observed.

Fiber contributes to the self-healing ability of concrete by controlling crack width, spacing, and propagation and providing bridging across cracks [103], [104], [105]. However, the influence of FRC on the durability of RC structures in the presence of cracks is under discussion, as it is still unclear whether the crack width influences corrosion initiation and propagation. Moreover, fibers can add in crack sealing, which significantly increases the corrosion initiation time [18]. Further research is yet required in this area.

## 2.6 *Limitation on crack width in international standards*

As previously discussed, one of the main factors affecting the durability of reinforced concrete structures is the crack width, which plays a critical role in the serviceability requirements of RC structures. From a code perspective, it is very important to control the crack width, especially for structures exposed to aggressive environments such as the marine environment, which is one of the most severe and aggressive environmental conditions that cause severe concrete degradation, reinforcement corrosion, and concrete cover spalling. According to different codes, the maximum allowable crack width for RC structures exposed to aggressive environments is 0.4 mm.

### *2.6.1* *Euro code*

According to Eurocode 2, [21], crack must be minimized to ensure they do not affect the structure's durability, proper functioning or make it look unattractive. Cracks have been divided according to different exposure conditions in Table 3, apart from cracks formed due to plastic shrinkage or any expansive reaction.

According to Table 3, exposure class X0 represents the concrete inside the buildings, with very low humidity and no risk of corrosion attack. Exposure classes (XC1, XC2, XC3, and XC4) carbonation-induced corrosion. XC1 represents dry conditions, such as concrete inside a building with low humidity, or permanently wet conditions, such as concrete submerged in water. XC2 represents wet or rarely dry concrete subjected to long-term water contact. Exposure class XC3 represents concrete inside a building with moderate or high relative humidity. Exposure class XC4 represents concrete structures exposed to wet and dry cycles.

*Table 2.6-1. Recommended value of maximum crack width according to Eurocode 2* [21].

| Exposure class | Maximum crack width (mm) |
|---|---|
| X0, XC1 | 0.4 |
| XC2, XC3, XC4<br>XD1, XD2, XS1, XS2, XS3 | 0.3 |

Exposure classes (XD1, XD2, and XD3) represent chloride-induced corrosion. XD1 shows moderate humidity exposed to airborne chlorides. Exposure class XD2 represents wet and rarely dry conditions, such as concrete components exposed to industrial waters containing chlorides. Exposure class XD3 represents the cyclic wet and dry cycles of pavement, parking slabs, and bridge parts exposed to continuous chloride spraying.
Exposure Classes XS1, XS2, and XS3 represent corrosion induced by chlorides from seawater. Where XS1 represents structures exposed to airborne salt but not in direct contact with seawater, like structures near the coast. Class XS2 presents permanently submerged structures, and XS3 represents structures exposed to tidal, splash, and spray zones.

### ***2.6.2*** *Model code*

According to Model Code 2010, 2012, [106] in order to fulfil the requirements for functionality, durability, and appearance, the crack width must satisfy the $w_d \leq w_{lim}$. Where $w_d$ is the design crack width and $w_{lim}$ is the nominal crack width value on the concrete surface.
(Table 4), shows that exposure class X0 is a very dry environment where there is no risk of corrosion. XC represents corrosion caused by carbonation. Exposure class XF represents corrosion due to the freeze and thaw cycle, whereas exposure classes XD and XS represent corrosion induced by chlorides other than seawater and corrosion due to seawater, respectively. According to ACI 318-19 (2019), the maximum permissible crack width for interior exposure conditions is 0.4 mm, and for external exposure conditions is 0.3 mm to ensure that crack width does not adversely affect the durability, serviceability, or safety of the structures. ACI 318-19, [107]addresses the

control of crack width described in section 10.6.3 to 10.6.7 indirectly through the limitation of the maximum bar spacing and bar cover for beams and one-way slabs.

*Table 2.6-2. Crack width limits according to Model Code 2010* [106].

| Exposure class | $w_{lim}$ |
|---|---|
| X0, XC | 0.3 |
| XD, XS, XF | 0.2 |

## 2.7 References


[1] S. W. Tang, Y. Yao, C. Andrade, and Z. J. Li, "Recent durability studies on concrete structure," *Cement and Concrete Research*, vol. 78, pp. 143–154, Dec. 2015, doi: 10.1016/j.cemconres.2015.05.021.

[2] F. Tamàs and G. L. Balázs, "Properties of concrete (fourth edition)," *Cement and Concrete Research*, vol. 26, no. 8, p. 1290, Aug. 1996, doi: 10.1016/0008-8846(96)82366-0.

[3] L. Veleva, M. A. Alpuche-Aviles, M. K. Graves-Brook, and D. O. Wipf, "Comparative cyclic voltammetry and surface analysis of passive films grown on stainless steel 316 in concrete pore model solutions," *Journal of Electroanalytical Chemistry*, vol. 537, no. 1–2, pp. 85–93, Nov. 2002, doi: 10.1016/S0022-0728(02)01253-6.

[4] A. Alhozaimy, R. R. Hussain, and A. Al-Negheimish, "Significance of oxygen concentration on the quality of passive film formation for steel reinforced concrete structures during the initial curing of concrete," *Cement and Concrete Composites*, vol. 65, pp. 171–176, Jan. 2016, doi: 10.1016/j.cemconcomp.2015.10.022.

[5] U. M. Angst, "Predicting the time to corrosion initiation in reinforced concrete structures exposed to chlorides," *Cement and Concrete Research*, vol. 115, pp. 559–567, Jan. 2019, doi: 10.1016/j.cemconres.2018.08.007.

[6] K. Tuutti, *Corrosion of steel in concrete*. Stockholm: Swedish Cement and Concrete Research Institute, 1982.

[7] M. Sahmaran, V. C. Li, and C. Andrade, "Corrosion Resistance Performance of Steel-Reinforced Engineered Cementitious Composite Beams," *MJ*, vol. 105, no. 3, 2008, doi: 10.14359/19820.

[8] U. Angst, B. Elsener, C. K. Larsen, and Ø. Vennesland, "Chloride induced reinforcement corrosion: Rate limiting step of early pitting corrosion," *Electrochimica Acta*, vol. 56, no. 17, pp. 5877–5889, Jul. 2011, doi: 10.1016/j.electacta.2011.04.124.

[9] C. Arya and F. K. Ofori-Darko, "Influence of crack frequency on reinforcement corrosion in concrete," *Cement and Concrete Research*, vol. 26, no. 3, pp. 345–353, Mar. 1996, doi: 10.1016/S0008-8846(96)85022-8.

[10] A. Bentur, S. Diamond, and Berke Neal Steven, *Steel corrosion in concrete: fundamentals and civil engineering practice*, 1st ed. London ; New York: E & FN Spon, 1997.

[11] C. Andrade, A. Cesetti, G. Mancini, and F. Tondolo, "Estimating corrosion attack in reinforced concrete by means of crack opening," *Structural Concrete*, vol. 17, no. 4, pp. 533–540, Dec. 2016, doi: 10.1002/suco.201500114.

[12] F. Pedrosa and C. Andrade, "Corrosion induced cracking: Effect of different corrosion rates on crack width evolution," *Construction and Building Materials*, vol. 133, pp. 525–533, Feb. 2017, doi: 10.1016/j.conbuildmat.2016.12.030.

[13] E. Chen, C. G. Berrocal, I. Löfgren, and K. Lundgren, "Correlation between concrete cracks and corrosion characteristics of steel reinforcement in pre-cracked plain and fibre-reinforced concrete beams," *Mater Struct*, vol. 53, no. 2, p. 33, Apr. 2020, doi: 10.1617/s11527-020-01466-z.

[14] B. Leporace-Guimil, A. Conforti, R. Zerbino, and G. A. Plizzari, "Chloride-induced corrosion in reinforced concrete and fiber reinforced concrete elements under tensile service loads," *Cement and Concrete Composites*, vol. 124, p. 104245, Nov. 2021, doi: 10.1016/j.cemconcomp.2021.104245.

[15] G. Nossoni and R. S. Harichandran, "Electrochemical-Mechanistic Model for Concrete Cover Cracking Due to Corrosion Initiated by Chloride Diffusion," *J. Mater. Civ. Eng.*, vol. 26, no. 6, p. 04014001, Jun. 2014, doi: 10.1061/(ASCE)MT.1943-5533.0000470.

[16] M. Otieno, H. Beushausen, and M. Alexander, "Chloride-induced corrosion of steel in cracked concrete – Part I: Experimental studies under accelerated and natural marine environments," *Cement and Concrete Research*, vol. 79, pp. 373–385, Jan. 2016, doi: 10.1016/j.cemconres.2015.08.009.

[17] M. B. Otieno, M. G. Alexander, and H.-D. Beushausen, "Corrosion in cracked and uncracked concrete – influence of crack width, concrete quality and crack reopening," *Magazine of Concrete Research*, vol. 62, no. 6, pp. 393–404, Jun. 2010, doi: 10.1680/macr.2010.62.6.393.

[18] E. Cuenca, A. Tejedor, and L. Ferrara, "A methodology to assess crack-sealing effectiveness of crystalline admixtures under repeated cracking-healing cycles," *Construction and Building Materials*, vol. 179, pp. 619–632, Aug. 2018, doi: 10.1016/j.conbuildmat.2018.05.261.

[19] M. M. H. Al-Tholaia, A. K. Azad, S. Ahmad, and M. H. Baluch, "A comparative study of corrosion resistance of different coatings for mortar–embedded steel plates," *Construction and Building Materials*, vol. 56, pp. 74–80, Apr. 2014, doi: 10.1016/j.conbuildmat.2014.01.059.

[20] H. Vakili, B. Ramezanzadeh, and R. Amini, "The corrosion performance and adhesion properties of the epoxy coating applied on the steel substrates treated by cerium-based conversion coatings," *Corrosion Science*, vol. 94, pp. 466–475, May 2015, doi: 10.1016/j.corsci.2015.02.028.

[21] *Eurocode 2: design of concrete structures : part 1-1: general rules and rules for buildings*. London: British Standards Institution, 2004.

[22] M. Ali *et al.*, "A review on chloride induced corrosion in reinforced concrete structures: lab and *in situ* investigation," *RSC Adv.*, vol. 14, no. 50, pp. 37252–37271, 2024, doi: 10.1039/D4RA05506C.

[23] B. H. Oh, S. Y. Jang, and Y. S. Shin, "Experimental investigation of the threshold chloride concentration for corrosion initiation in reinforced concrete structures," *Magazine of Concrete Research*, no. 2, 2003.
[24] H. DorMohammadi, Q. Pang, P. Murkute, L. Árnadóttir, and O. B. Isgor, "Investigation of chloride-induced depassivation of iron in alkaline media by reactive force field molecular dynamics," *npj Mater Degrad*, vol. 3, no. 1, p. 19, Apr. 2019, doi: 10.1038/s41529-019-0081-6.
[25] Q. Wang *et al.*, "Research Progress in Corrosion Behavior and Anti-Corrosion Methods of Steel Rebar in Concrete," *Metals*, vol. 14, no. 8, p. 862, Jul. 2024, doi: 10.3390/met14080862.
[26] C. Andrade, "Propagation of reinforcement corrosion: principles, testing and modelling," *Mater Struct*, vol. 52, no. 1, p. 2, Feb. 2019, doi: 10.1617/s11527-018-1301-1.
[27] H. Mohd Noh and Y. Sonoda, "Potential Effects of Corrosion Damage on the Performance of Reinforced Concrete Member," *MATEC Web of Conferences*, vol. 47, p. 02007, 2016, doi: 10.1051/matecconf/20164702007.
[28] S. Na and I. Paik, "Application of Thermal Image Data to Detect Rebar Corrosion in Concrete Structures," *Applied Sciences*, vol. 9, no. 21, p. 4700, Nov. 2019, doi: 10.3390/app9214700.
[29] S. Lv and K. Li, "Semiconducting Behaviour and Corrosion Resistance of Passive Film on Corrosion-Resistant Steel Rebars," *Materials*, vol. 15, no. 21, p. 7644, Oct. 2022, doi: 10.3390/ma15217644.
[30] U. Angst, B. Elsener, C. K. Larsen, and Ø. Vennesland, "Critical chloride content in reinforced concrete — A review," *Cement and Concrete Research*, vol. 39, no. 12, pp. 1122–1138, Dec. 2009, doi: 10.1016/j.cemconres.2009.08.006.
[31] J. S. Lawler, J. C. Kurth, S. M. Garrett, and P. D. Krauss, "Statistical Distributions for Chloride Thresholds of Reinforcing Bars," *MJ*, vol. 118, no. 2, Mar. 2021, doi: 10.14359/51730411.
[32] H. A. Y. Alshaeer *et al.*, "Review on Carbonation Study of Reinforcement Concrete Incorporating with Bacteria as Self-Healing Approach," *Materials*, vol. 15, no. 16, p. 5543, Aug. 2022, doi: 10.3390/ma15165543.
[33] M. Stefanoni, U. Angst, and B. Elsener, "Corrosion rate of carbon steel in carbonated concrete – A critical review," *Cement and Concrete Research*, vol. 103, pp. 35–48, Jan. 2018, doi: 10.1016/j.cemconres.2017.10.007.
[34] A. Belda Revert, K. De Weerdt, K. Hornbostel, and M. R. Geiker, "Carbonation-induced corrosion: Investigation of the corrosion onset," *Construction and Building Materials*, vol. 162, pp. 847–856, Feb. 2018, doi: 10.1016/j.conbuildmat.2017.12.066.
[35] A. F. A. Fuhaid and A. Niaz, "Carbonation and Corrosion Problems in Reinforced Concrete Structures," *Buildings*, vol. 12, no. 5, p. 586, May 2022, doi: 10.3390/buildings12050586.

[36] Y. Chen, P. Liu, and Z. Yu, "Effects of Environmental Factors on Concrete Carbonation Depth and Compressive Strength," *Materials*, vol. 11, no. 11, p. 2167, Nov. 2018, doi: 10.3390/ma11112167.

[37] A. Jabed, M. M. H. Tusher, Md. S. I. Shuvo, and A. Imam, "Corrosion of Steel Rebar in Concrete: A Review," *Corrosion Science and Technology*, vol. 22, no. 4, pp. 273–286, Aug. 2023, doi: 10.14773/CST.2023.22.4.273.

[38] M. Ghanooni-Bagha, M. R. YekeFallah, and M. A. Shayanfar, "Durability of RC Structures against Carbonation-Induced Corrosion under the Impact of Climate Change," *KSCE Journal of Civil Engineering*, vol. 24, no. 1, pp. 131–142, Jan. 2020, doi: 10.1007/s12205-020-0793-8.

[39] H. M. Nadir and A. Ahmed, "The Mechanisms of Sulphate Attack in Concrete – A Review," vol. 5, no. 2.

[40] W. Piasta, "Analysis of carbonate and sulphate attack on concrete structures," *Engineering Failure Analysis*, vol. 79, pp. 606–614, Sep. 2017, doi: 10.1016/j.engfailanal.2017.05.008.

[41] D. Sun, Z. Cao, C. Huang, K. Wu, G. De Schutter, and L. Zhang, "Degradation of concrete in marine environment under coupled chloride and sulfate attack: A numerical and experimental study," *Case Studies in Construction Materials*, vol. 17, p. e01218, Dec. 2022, doi: 10.1016/j.cscm.2022.e01218.

[42] K. Al Marri, F. Mir, S. David, and A. Aljuboori, Eds., *BUiD Doctoral Research Conference 2022: Multidisciplinary Studies*, vol. 320. in Lecture Notes in Civil Engineering, vol. 320. Cham: Springer Nature Switzerland, 2023. doi: 10.1007/978-3-031-27462-6.

[43] F. Rajabipour, E. Giannini, C. Dunant, J. H. Ideker, and M. D. A. Thomas, "Alkali–silica reaction: Current understanding of the reaction mechanisms and the knowledge gaps," *Cement and Concrete Research*, vol. 76, pp. 130–146, Oct. 2015, doi: 10.1016/j.cemconres.2015.05.024.

[44] R. B. Figueira *et al.*, "Alkali-silica reaction in concrete: Mechanisms, mitigation and test methods," *Construction and Building Materials*, vol. 222, pp. 903–931, Oct. 2019, doi: 10.1016/j.conbuildmat.2019.07.230.

[45] R. N. Swamy, "The Alkali-Silica Reaction in Concrete".

[46] I. Fernandes and M. A. T. M. Broekmans, "Alkali–Silica Reactions: An Overview. Part I," *Metallogr. Microstruct. Anal.*, vol. 2, no. 4, pp. 257–267, Aug. 2013, doi: 10.1007/s13632-013-0085-5.

[47] K. M. D. V. Moreira, P. V. G. Oliveira, Ê. P. De Deus, and A. E. B. Cabral, "Alkali-silica reaction: understanding the phenomenon," *J Build Rehabil*, vol. 6, no. 1, p. 5, Dec. 2021, doi: 10.1007/s41024-020-00100-3.

[48] P. Zhang *et al.*, "Steel reinforcement corrosion in concrete under combined actions: The role of freeze-thaw cycles, chloride ingress, and surface impregnation," *Construction and Building Materials*, vol. 148, pp. 113–121, Sep. 2017, doi: 10.1016/j.conbuildmat.2017.05.078.

[49] L. Chong, J. Yang, Z. Z. Xu, and X. Xu, "Freezing and thawing resistance of MKPC paste under different corrosion solutions," *Construction and Building Materials*, vol. 212, pp. 663–674, Jul. 2019, doi: 10.1016/j.conbuildmat.2019.03.269.
[50] S. Kim, Y. Jeong, M. Kwon, and J. Kim, "Combined deterioration effects of freeze–thaw and corrosion on the cyclic flexural behavior of RC beams," *Journal of Building Engineering*, vol. 84, p. 108564, May 2024, doi: 10.1016/j.jobe.2024.108564.
[51] S. Zhang, B. Tian, B. Chen, X. Lu, B. Xiong, and N. Shuang, "The Influence of Freeze–Thaw Cycles and Corrosion on Reinforced Concrete and the Relationship between the Evolutions of the Microstructure and Mechanical Properties," *Materials*, vol. 15, no. 18, p. 6215, Sep. 2022, doi: 10.3390/ma15186215.
[52] Symposium on Galvanic Corrosion, *Galvanic corrosion*, Online-Ausg. in ASTM STP 978. Philadelphia, Pa: American Society for Testing and Materials, 1988. doi: 10.1520/STP978-EB.
[53] N. J. Laycock, J. Stewart, and R. C. Newman, "The initiation of crevice corrosion in stainless steels," *Corrosion Science*, vol. 39, no. 10–11, pp. 1791–1809, Oct. 1997, doi: 10.1016/S0010-938X(97)00050-4.
[54] L. Yan, G.-L. Song, Z. Wang, and D. Zheng, "Crevice corrosion of steel rebar in chloride-contaminated concrete," *Construction and Building Materials*, vol. 296, p. 123587, Aug. 2021, doi: 10.1016/j.conbuildmat.2021.123587.
[55] A. Blagojevi, D. A. Koleva, and J. C. Walraven, "THE INFLUENCE OF CRACKS ON CHLORIDE- INDUCED CORROSION OF REINFORCED CONCRETE STRUCTURES – DEVELOPMENT OF THE EXPERIMENTAL SET-UP".
[56] J. Wang, P. A. M. Basheer, S. V. Nanukuttan, and Y. Bai, "Influence of Cracking Caused by Structural Loading on Chloride-Induced Corrosion Process in Reinforced Concrete Elements: A Review," in *Durability of Reinforced Concrete from Composition to Protection*, C. Andrade, J. Gulikers, and R. Polder, Eds., Cham: Springer International Publishing, 2015, pp. 99–113. doi: 10.1007/978-3-319-09921-7_10.
[57] S. M. S. M. K. Samarakoon, B. Piatek, and G. H. M. J. S. De Silva, "Investigation of the Flexural Behavior of Preloaded and Pre-Cracked Reinforced Concrete Beams Strengthened with CFRP Plates," *Materials*, vol. 16, no. 1, p. 22, Dec. 2022, doi: 10.3390/ma16010022.
[58] N. Gowripalan, V. Sirivivatnanon, and C. C. Lim, "Chloride diffusivity of concrete cracked in flexure," *Cement and Concrete Research*, vol. 30, no. 5, pp. 725–730, May 2000, doi: 10.1016/S0008-8846(00)00216-7.
[59] T. U. Mohammed, N. Otsuki, M. Hisada, and T. Shibata, "Effect of Crack Width and Bar Types on Corrosionof Steel in Concrete," *J. Mater. Civ. Eng.*, vol. 13, no. 3, pp. 194–201, Jun. 2001, doi: 10.1061/(ASCE)0899-1561(2001)13:3(194).
[60] G. Tiberti, F. Minelli, and G. Plizzari, "Cracking behavior in reinforced concrete members with steel fibers: A comprehensive experimental study," *Cement and Concrete Research*, vol. 68, pp. 24–34, Feb. 2015, doi: 10.1016/j.cemconres.2014.10.011.

[61] A. Soltani, K. A. Harries, and B. M. Shahrooz, "Crack Opening Behavior of Concrete Reinforced with High Strength Reinforcing Steel," *Int J Concr Struct Mater*, vol. 7, no. 4, pp. 253–264, Dec. 2013, doi: 10.1007/s40069-013-0054-z.

[62] G. P. A. G. Van Zijl *et al.*, "Durability of strain-hardening cement-based composites (SHCC)," *Mater Struct*, vol. 45, no. 10, pp. 1447–1463, Oct. 2012, doi: 10.1617/s11527-012-9845-y.

[63] B. Matthews, A. Palermo, and A. Scott, "Impact of Artificial Corrosion Technique under Variable Acceleration on Morphological Efficacy in Reinforced Concrete Elements," *J. Mater. Civ. Eng.*, vol. 37, no. 2, p. 04024520, Feb. 2025, doi: 10.1061/JMCEE7.MTENG-18819.

[64] J.-J. Guo, P.-Q. Liu, C.-L. Wu, and K. Wang, "Effect of Dry–Wet Cycle Periods on Properties of Concrete under Sulfate Attack," *Applied Sciences*, vol. 11, no. 2, p. 888, Jan. 2021, doi: 10.3390/app11020888.

[65] M. Sadiq Radhi, M. S. Hassan, and I. N. Gorgis, "Experimental Comparability Among Different Accelerated Reinforced Steel Concrete Corrosion Methods," *IJET*, vol. 7, no. 4.20, pp. 209–213, Nov. 2018, doi: 10.14419/ijet.v7i4.20.25928.

[66] M. S. Yusuf and X. Wen, "Chloride Resistance of Concrete under Complex Stress and Environment," *OJCE*, vol. 13, no. 01, pp. 171–180, 2023, doi: 10.4236/ojce.2023.131012.

[67] L. Wang *et al.*, "Chloride Corrosion Process of Concrete with Different Water–Binder Ratios under Variable Temperature Drying–Wetting Cycles," *Materials*, vol. 17, no. 10, p. 2263, May 2024, doi: 10.3390/ma17102263.

[68] A. Poursaee and B. Ross, "The Role of Cracks in Chloride-Induced Corrosion of Carbon Steel in Concrete—Review," *CMD*, vol. 3, no. 2, pp. 258–269, Jun. 2022, doi: 10.3390/cmd3020015.

[69] S. Robuschi, O. L. Ivanov, M. Geiker, I. Fernandez, and K. Lundgren, "Impact of cracks on distribution of chloride-induced reinforcement corrosion," *Mater Struct*, vol. 56, no. 1, p. 7, Feb. 2023, doi: 10.1617/s11527-022-02085-6.

[70] S. Ahmad, "TECHNIQUES FOR INDUCING ACCELERATED CORROSION OF STEEL IN CONCRETE," 2009.

[71] T. H. Y. Nguyen, V. H. L. Bui, V. M. Tran, N. T. Cao, W. Pansuk, and P. Jongvivatsakul, "Verifying the Reliability of Impressed Current Method to Simulate Natural Corrosion in Reinforced Concrete," *EJ*, vol. 25, no. 3, pp. 105–116, Mar. 2021, doi: 10.4186/ej.2021.25.3.105.

[72] S. Ahmad, M. A. A. Jibran, A. K. Azad, and M. Maslehuddin, "A Simple and Reliable Setup for Monitoring Corrosion Rate of Steel Rebars in Concrete," *The Scientific World Journal*, vol. 2014, pp. 1–10, 2014, doi: 10.1155/2014/525678.

[73] M. Nikoo, Ł. Sadowski, and M. Nikoo, "Prediction of the Corrosion Current Density in Reinforced Concrete Using a Self-Organizing Feature Map," *Coatings*, vol. 7, no. 10, p. 160, Sep. 2017, doi: 10.3390/coatings7100160.

[74] T. E. Maaddawy, K. Soudki, and T. Topper, "Long-Term Performance of Corrosion-Damaged Reinforced Concrete Beams," *SJ*, vol. 102, no. 5, 2005, doi: 10.14359/14660.
[75] O. Poupard, V. L'Hostis, S. Catinaud, and I. Petre-Lazar, "Corrosion damage diagnosis of a reinforced concrete beam after 40 years natural exposure in marine environment," *Cement and Concrete Research*, vol. 36, no. 3, pp. 504–520, Mar. 2006, doi: 10.1016/j.cemconres.2005.11.004.
[76] Z. Lv, M. Zhang, and Y. Sun, "Research on The Chloride Diffusion Modified Model for Marine Concretes with Nanoparticles under The Action of Multiple Environmental Factors," *JMSE*, vol. 10, no. 12, p. 1852, Dec. 2022, doi: 10.3390/jmse10121852.
[77] R. Zhao, C. Li, and X. Guan, "Advances in Modeling Surface Chloride Concentrations in Concrete Serving in the Marine Environment: A Mini Review," *Buildings*, vol. 14, no. 6, p. 1879, Jun. 2024, doi: 10.3390/buildings14061879.
[78] J. Pontes, J. A. Bogas, S. Real, and A. Silva, "The Rapid Chloride Migration Test in Assessing the Chloride Penetration Resistance of Normal and Lightweight Concrete," *Applied Sciences*, vol. 11, no. 16, p. 7251, Aug. 2021, doi: 10.3390/app11167251.
[79] R. François and G. Arliguie, "Influence of Service Cracking on Reinforcement Steel Corrosion," *J. Mater. Civ. Eng.*, vol. 10, no. 1, pp. 14–20, Feb. 1998, doi: 10.1061/(ASCE)0899-1561(1998)10:1(14).
[80] T. U. Mohammed, N. Otsuki, and M. Hisada, "Corrosion of Steel Bars with Respect to Orientation in Concrete," *MJ*, vol. 96, no. 2, 1999, doi: 10.14359/439.
[81] S. J. Jaffer and C. M. Hansson, "The influence of cracks on chloride-induced corrosion of steel in ordinary Portland cement and high performance concretes subjected to different loading conditions," *Corrosion Science*, vol. 50, no. 12, pp. 3343–3355, Dec. 2008, doi: 10.1016/j.corsci.2008.09.018.
[82] J. Wang, S. Nanukuttan, P. A. M. Basheer, and Y. Bai, "Influence of Micro and Macro Cracks Due to Sustained Loading on Chloride-Induced Corrosion of Reinforced Concrete Beams," in *Proceedings of the 4th International Conference on the Durability of Concrete Structures*, Purdue University Libraries Scholarly Publishing Services, Jul. 2014. doi: 10.5703/1288284315481.
[83] G. J. Al-Sulaimani, M. Kaleemullah, I. A. Basunbul, and Rasheeduzzafar, "Influence of Corrosion and Cracking on Bond Behavior and Strength of Reinforced Concrete Members," *SJ*, vol. 87, no. 2, 1990, doi: 10.14359/2732.
[84] C. Arya and F. K. Ofori-Darko, "Influence of crack frequency on reinforcement corrosion in concrete," *Cement and Concrete Research*, vol. 26, no. 3, pp. 345–353, Mar. 1996, doi: 10.1016/S0008-8846(96)85022-8.
[85] J. G. Cabrera, "Deterioration of concrete due to reinforcement steel corrosion," *Cement and Concrete Composites*, vol. 18, no. 1, pp. 47–59, Jan. 1996, doi: 10.1016/0958-9465(95)00043-7.

[86] A. Castel, R. François, and G. Arliguie, "Mechanical behaviour of corroded reinforced concrete beams—Part 1: Experimental study of corroded beams," *Mat. Struct.*, vol. 33, no. 9, pp. 539–544, Nov. 2000, doi: 10.1007/BF02480533.

[87] T. Vidal, A. Castel, and R. François, "Analyzing crack width to predict corrosion in reinforced concrete," *Cement and Concrete Research*, vol. 34, no. 1, pp. 165–174, Jan. 2004, doi: 10.1016/S0008-8846(03)00246-1.

[88] P. P. Win, M. Watanabe, and A. Machida, "Penetration profile of chloride ion in cracked reinforced concrete," *Cement and Concrete Research*, vol. 34, no. 7, pp. 1073–1079, Jul. 2004, doi: 10.1016/j.cemconres.2003.11.020.

[89] Z. Rinaldi, S. Imperatore, and C. Valente, "Experimental evaluation of the flexural behavior of corroded P/C beams," *Construction and Building Materials*, vol. 24, no. 11, pp. 2267–2278, Nov. 2010, doi: 10.1016/j.conbuildmat.2010.04.029.

[90] H. Mihashi, S. F. U. Ahmed, and A. Kobayakawa, "Corrosion of Reinforcing Steel in Fiber Reinforced Cementitious Composites," *ACT*, vol. 9, no. 2, pp. 159–167, Jun. 2011, doi: 10.3151/jact.9.159.

[91] S. Imperatore, Z. Rinaldi, and S. Spagnuolo, "Influence of corrosion on the experimental behaviour of R.C. ties," *Engineering Structures*, vol. 198, p. 109458, Nov. 2019, doi: 10.1016/j.engstruct.2019.109458.

[92] L. A. Alarab, B. E. Ross, and A. Poursaee, "Influence of Transverse Crack Opening Size on Chloride-Induced Corrosion of Steel Bars in Concrete," *J. Bridge Eng.*, vol. 25, no. 6, p. 04020027, Jun. 2020, doi: 10.1061/(ASCE)BE.1943-5592.0001555.

[93] N. Russo, M. Gastaldi, P. Marras, L. Schiavi, A. Strini, and F. Lollini, "Effects of load-induced micro-cracks on chloride penetration resistance in different types of concrete," *Mater Struct*, vol. 53, no. 6, p. 143, Dec. 2020, doi: 10.1617/s11527-020-01580-y.

[94] A. Benenato, B. Ferracuti, S. Imperatore, M. Kioumarsi, and S. Spagnuolo, "Behaviour of prestressed concrete beams damaged by corrosion," p. 8, Dec. 2020.

[95] E. Gomez, B. Leporace-Guimil, A. Conforti, G. Plizzari, G. Duffó, and R. Zerbino, "A practical approach for monitoring reinforcement corrosion in steel fiber reinforced concrete elements exposed to chloride rich environments," *Structural Concrete*, p. suco.202200302, Sep. 2022, doi: 10.1002/suco.202200302.

[96] V. Marcos-Meson, A. Michel, A. Solgaard, G. Fischer, C. Edvardsen, and T. L. Skovhus, "Corrosion resistance of steel fibre reinforced concrete - A literature review," *Cement and Concrete Research*, vol. 103, pp. 1–20, Jan. 2018, doi: 10.1016/j.cemconres.2017.05.016.

[97] C. G. Berrocal, I. Löfgren, K. Lundgren, and L. Tang, "Corrosion initiation in cracked fibre reinforced concrete: Influence of crack width, fibre type and loading conditions," *Corrosion Science*, vol. 98, pp. 128–139, Sep. 2015, doi: 10.1016/j.corsci.2015.05.021.

[98] J.-L. Granju and S. Ullah Balouch, "Corrosion of steel fibre reinforced concrete from the cracks," *Cement and Concrete Research*, vol. 35, no. 3, pp. 572–577, Mar. 2005, doi: 10.1016/j.cemconres.2004.06.032.
[99] M. R. Mitchell, R. E. Link, M. Sappakittipakorn, and N. Banthia, "Corrosion of Rebar and Role of Fiber Reinforced Concrete," *J. Test. Eval.*, vol. 40, no. 1, p. 103873, 2012, doi: 10.1520/JTE103873.
[100] J. Blunt, G. Jen, and C. P. Ostertag, "Enhancing corrosion resistance of reinforced concrete structures with hybrid fiber reinforced concrete," *Corrosion Science*, vol. 92, pp. 182–191, Mar. 2015, doi: 10.1016/j.corsci.2014.12.003.
[101] C. G. Berrocal, I. Löfgren, and K. Lundgren, "The effect of fibres on steel bar corrosion and flexural behaviour of corroded RC beams," *Engineering Structures*, vol. 163, pp. 409–425, May 2018, doi: 10.1016/j.engstruct.2018.02.068.
[102] D.-Y. Yoo, W. Shin, and B. Chun, "Corrosion effect on tensile behavior of ultra-high-performance concrete reinforced with straight steel fibers," *Cement and Concrete Composites*, vol. 109, p. 103566, May 2020, doi: 10.1016/j.cemconcomp.2020.103566.
[103] L. Ferrara, V. Krelani, and F. Moretti, "Autogenous healing on the recovery of mechanical performance of High Performance Fibre Reinforced Cementitious Composites (HPFRCCs): Part 2 – Correlation between healing of mechanical performance and crack sealing," *Cement and Concrete Composites*, vol. 73, pp. 299–315, Oct. 2016, doi: 10.1016/j.cemconcomp.2016.08.003.
[104] L. Ferrara, V. Krelani, F. Moretti, M. Roig Flores, and P. Serna Ros, "Effects of autogenous healing on the recovery of mechanical performance of High Performance Fibre Reinforced Cementitious Composites (HPFRCCs): Part 1," *Cement and Concrete Composites*, vol. 83, pp. 76–100, Oct. 2017, doi: 10.1016/j.cemconcomp.2017.07.010.
[105] K. Van Tittelboom, E. Gruyaert, H. Rahier, and N. De Belie, "Influence of mix composition on the extent of autogenous crack healing by continued hydration or calcium carbonate formation," *Construction and Building Materials*, vol. 37, pp. 349–359, Dec. 2012, doi: 10.1016/j.conbuildmat.2012.07.026.
[106] *Model Code 2010*. in Bulletin / Fédération Internationale du Béton, no. 66. Lausanne: International Federation for Structural Concrete (fib), 2012.
[107] *ACI 318-19*. American Concrete Institute, 2019. doi: 10.14359/51716937.

# 3. EXPERIMENTAL CAMPAIGN ON CHLORIDE INDUCED CORROSION

## *3.1 Introduction*

Corrosion of reinforced concrete elements, particularly due to chloride ingress, poses a significant challenge to the durability and sustainability of concrete structures. One of the main factors affecting both durability and long-term performance is the presence of cracks in concrete, which facilitates the penetration of chloride ions and their eventual interaction with embedded steel reinforcement [1], [2]. The effect of crack width on both corrosion initiation and propagation has been a focus of extensive research; however, a comprehensive understanding of this relationship remains limited in several contexts.

This chapter outlines the experimental campaign designed to investigate the influence of crack width on the initiation and propagation of corrosion under sustained loading conditions.

The main focus of this experimental work was to evaluate how varying crack width affects both the initiation phase and its subsequent propagation of corrosion. Cracks in concrete can result from shrinkage, thermal effects, and mechanical loading. Once formed, these cracks serve as pathways for chloride, which is one of the most aggressive agents to induce corrosion in steel reinforcement [3], [4]. The primary objective of this research was to explore the relation between the crack width, pitting depth, pit volume, and pit length.

To achieve this, 31 tension ties of 90 x 90 x 830 mm with Ø12 mm rebar were cast and induced with different crack widths. These specimens were exposed to a chloride-rich environment (35 g/L of NaCl) under accelerated laboratory conditions. A wet and dry cycle was applied to simulate typical exposure scenarios for RC structures in marine environments or regions where de-icing salts are commonly used.

The experimental campaign began with a pre-cracking phase, during which controlled tensile loading was applied to induce cracks in the tension ties. The influence of crack width on corrosion initiation was then monitored using the COR-MAP instrument, the working principle of which will be discussed in the following sections.

The following sections of this chapter will present the comprehensive overview of materials, specimen geometry, experimental setup, and wet-dry procedures used to accelerate chloride-induced corrosion. This study aims to enhance our understanding

of how crack width influences corrosion behaviour, offering insights that improve the service life prediction of reinforced concrete structures.

## 3.2 Materials and specimen geometry

This section provides an overview of the materials and specimen geometry used in the experimental setup. For this research, normal concrete was selected due to its representative properties and widespread use in structural application. The choice of material was essential as it directly impacted the results and validity of the study's conclusion.

when choosing the specimens, careful consideration was given to their shapes and sizes, taking into account several factors [5], [6] such as limitations of the testing equipment and the goal of optimizing available resources. For instance, the specimen geometry was selected to fit within the clear span of the Instron machine. Additionally, the specimens were designed to align with existing formworks and water tanks, which were necessary to apply tensile loads [7], thereby optimizing the use of available infrastructure while maintaining experimental consistency.

### 3.2.1 Materials

For this experimental setup, normal concrete with a specified grade of C30/37, as described in *Table 3.2-1* below was used as the primary material for casting the specimens. This grade of concrete was chosen due to its widespread use in structural engineering applications, ensuring that the results of this study would be applicable to typical construction practices.

*Table 3.2-1. Mix design and fresh properties of concrete.*

| | |
|---|---|
| Portland cement 42.5 R [kg/m$^3$] | 390 |
| Water/cement ratio | 0.48 |
| Fine aggregate sand [kg/m$^3$] | 889 |
| Medium gravel (4-10mm) [kg/m$^3$] | 332 |
| Coarse Gravel (10-20mm) [kg/m$^3$] | 583 |
| Water [kg/m$^3$] | 190 |
| Slump [mm] | 180 |

### 3.2.2 Mechanical properties of concrete

In this study, three separate batches of concrete were prepared, with 15 concrete cubes cast for each batch. These specimens were placed in a humidity chamber for curing over a period of 28 to 35 days to ensure optimal hydration conditions. After the curing period, the compressive strength of concrete cubes was tested, and the results are provided in *Table 3.2-2* below.

*Table 3.2-2.Compressive properties of concrete (CV in brackets)*

| Series | $f_{c,cube}$ [MPa] | $f_c$ [MPa] |
|---|---|---|
| Batch 1 | 45.33 (0.04) | 43.94 |
| Batch 2 | 43.93 (0.08) | 44.48 |
| Batch 3 | 44.48 (0.11) | 48.55 |

To assess the consistency of the concrete's performance, the coefficient of variation (CV) was calculated for each batch. Batch 1 exhibited the highest consistency in compressive strength, with a CV of 4.59%. Batch 2 showed moderate consistency, with a CV of 8.29%, while batch 3 exhibited the highest variability with a CV of 11.4%.
In conclusion, all three batches show satisfactory compressive strength values. However, the consistency of the concrete varied between batches.

### *3.2.3 Mechanical properties of steel*

Hot-rolled ribbed bars of steel class B500B were used in this study, classified as normal ductility steel in MC2010. This specific type of rebar was selected for its ability to withstand various loading conditions during both the pre-cracking phase in the Instron machine and the subsequent corrosion phase. The rebar also featured a threaded end, which allowed for the connection with supplementary rebar using sleeve nuts (female connector).

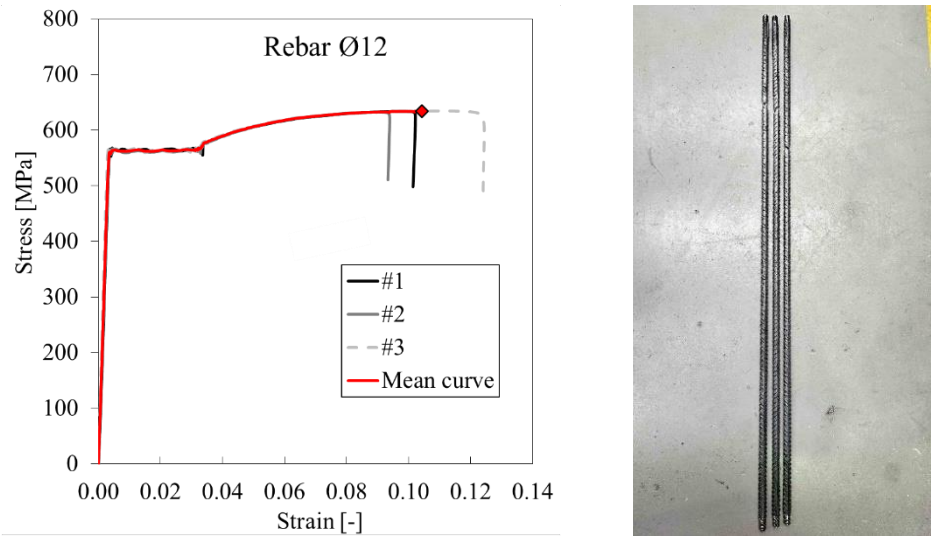


*(a)* *(b)*

*Figure 3.2-1.* Stress-strain relationship of rebars Ø12 adopted (EN 15630-1); *b) Rebar after tensile test.*

The yielding stress, maximum tensile strength, and maximum strain were determined through a tensile test. Three bars were tested without supplementary bars, yielding

the following average values of $f_y$ = 560 MPa, $f_u$ = 633, $\varepsilon_y$ = 0.003, and $\varepsilon_u$ = 0.104, as shown in *Table 3.2-3*. The stress strain-strain curve, along with the average of three bars, is presented in *Table 3.2-3a.*

The steel rebars in this study were accepted based on their verified mechanical characteristics, ensuring reliable results for structural integrity. Steel rebars were used as received, with no surface treatment prior to casting, thereby valuing their inherent properties rather than any external modification.

*Table 3.2-3. Tensile properties of rebar (CV in brackets)*

| | $f_y$ | $\varepsilon_y$ | $f_u$ | $\varepsilon_u$ |
|---|---|---|---|---|
| | [MPa] | [-] | [MPa] | [-] |
| Ø12 | 560 | 0.003 | 633 | 0.104 |
| | (0.01) | (0.06) | (0.01) | (0.13) |

### ***3.2.4*** *Specimen geometry*

The geometry of the specimens used in this study is shown in Figure 3.2-2. Each tension tie has a total length of 830 mm and a square cross-sectional area of 90 mm x 90 mm. The concrete clear cover is 39 mm, providing adequate protection to the embedded reinforcement. The ratio of the clear cover to the bar diameter is $C/Ø$ = 3.25, ensuring proper confinement and enhancing the durability of the steel reinforcement within the concrete.

A single steel rebar is centrally placed in each tension tie, with the ribbed side facing upward (see *Figure 3.2-3*), which promotes a strong bond with the surrounding concrete and facilitates the transfer of tensile stresses. The specimens were designed

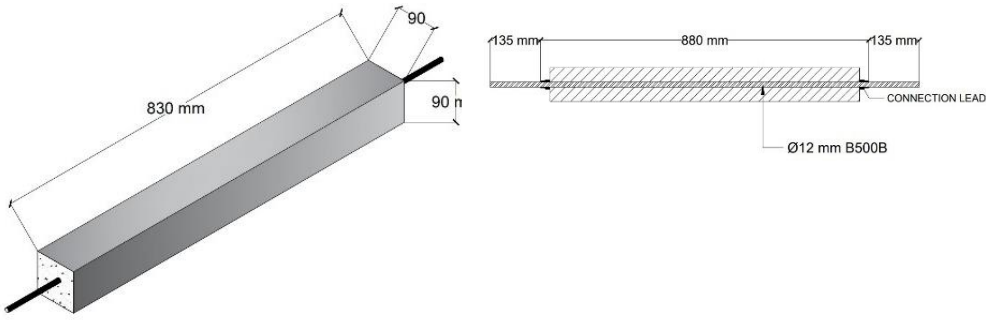


*(a)* *(b)*

*Figure 3.2-2. a) Tension ties Geometry; b) Iso metric view.*

with an effective reinforcement ratio $\rho_{eff}$ = 1.40% and an effective reinforcement length of 860 mm. The total length of the rebar is 1150 mm, extending beyond the length of the concrete specimen to accommodate adequate anchorage.

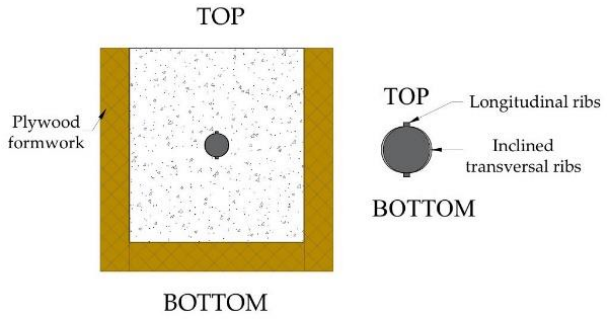


*Figure 3.2-3. Cross-section of tension tie placed in plywood formwork*

The length and geometry of the specimens were carefully selected to facilitate the formation of three to five cracks during the pre-cracking phase. This crack formation range is ideal for studying the effect of different crack widths on corrosion. The tension ties were pre-cracked using the Instron machine, which has a maximum clear span of 1200 mm for the tensile test. This span length was critical in determining the overall length of the specimens, ensuring that the tension ties were subjected to a controlled and uniform force within the testing equipment's capacity.

## 3.3 Experimental campaign

A total of 31 tension ties, 45 cubes, and 18 cylinders were cast, as shown in *Figure 3.3-3* and *Figure 3.3-2*. The casting process was organized into three distinct phases, each designed to minimize material variability and ensure a balanced experimental setup. This approach facilitated the effective monitoring of curing conditions and specimen handling while also allowing for the detection and control of potential discrepancies in material properties.

In phase 1, the initial set of specimens was cast, including 10 tension ties, 6 cylinders, and 15 cubes. These specimens, as depicted in *Figure 3.3-2* were carefully prepared and positioned to ensure uniformity during the curing process. The setup for phase 1 served as the baseline for the experiment, providing a solid foundation for the subsequent phases.

Phase 2 involved duplicating the casting process from phase 1. The same number of specimens were produced: 10 tension ties, 6 cylinders, and 15 cubes.

Phase 3 involved the casting of 11 tension ties, 6 cylinders, and 18 cubes. Which represents a slight increase in the number of tension ties and cubes compared to

previous phases. This increase in specimen numbers was aimed at providing more robust data for analysis. Throughout the entire process, each set of specimens was carefully monitored and managed to ensure that the material properties remained consistent across all phases.

(a) (b) (c)

*Figure 3.3-1. a) Rebar placed in plywood form work ready for casting; b) Casting of cubes and cylinders; c) Casting of tension ties.*

Once cured, all specimens were placed in a humidity chamber maintained at (T = 20 ±2 ◦C and R.H.>95%) to ensure optimal curing conditions. This step was essential for maintaining the required moisture content during the early stages of hydration, preventing the concrete from drying too quickly and allowing it to develop its full strength.

*Figure 3.3-2. All tension ties, cylinders, and cubes were placed in a humidity chamber to maintain optimal moisture conditions.*

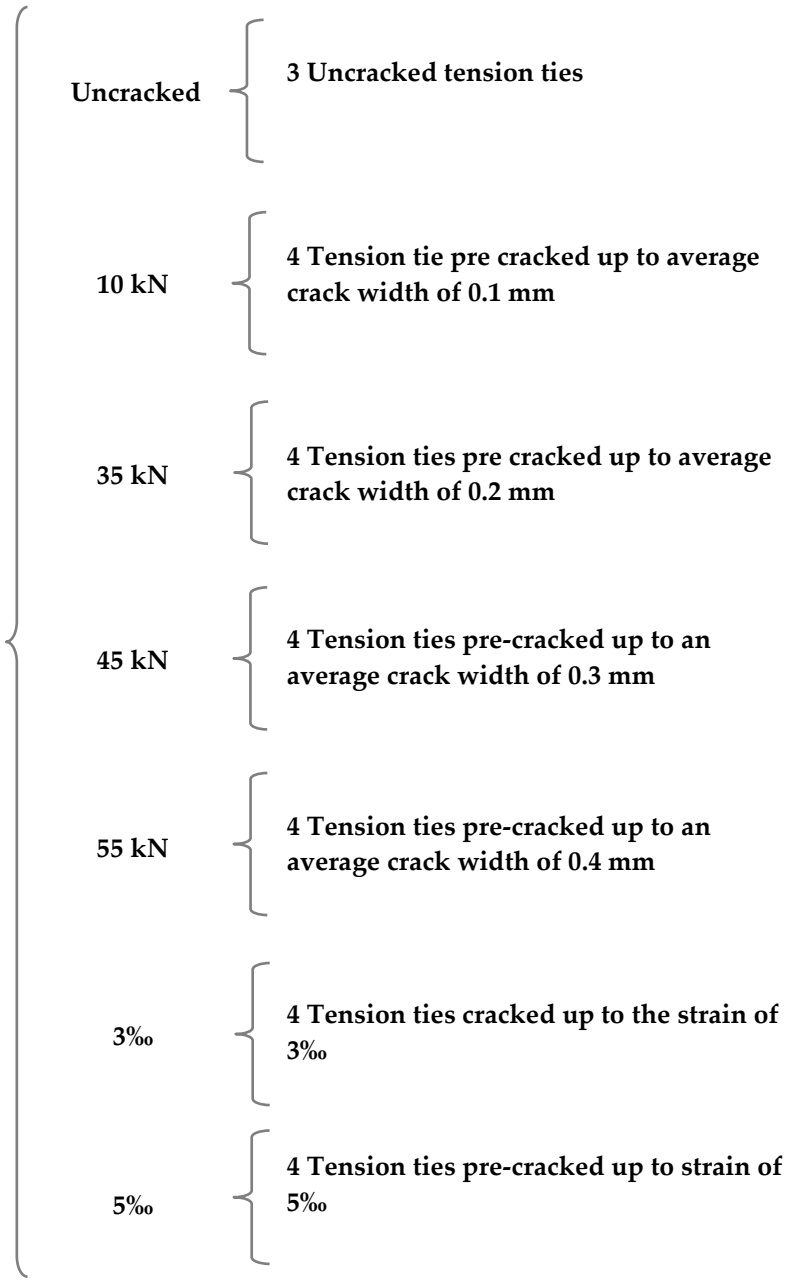


*Figure 3.3-3. Experimental campaign carried out on tension ties.*

## 3.4 Pre-cracking phase at different load levels

In this study, pre-cracking of the tension ties was carried out immediately after they were cured in a humidity chamber for 28 – 35 days. This pre-cracking was performed before applying the sustained loads, which were used to keep the crack open during the accelerated corrosion process exposed to chloride content in water tanks. The pre-cracking procedure was carefully controlled to ensure consistency and accurate results and to replicate real-life cracks in concrete structures.

### 3.4.1 Objective of pre-cracking

The primary objective of the pre-cracking phase was to induce controlled cracks in tension ties before subjecting them to wet and dry cycles. This approach ensured that the cracks remained open during exposure, replicating the conditions that cracks in concrete structures typically experience in a real-world environment.

The induced cracks created pathways for the ingress of sodium chloride, which is a common cause of corrosion in reinforced concrete structures. By establishing these cracks, the study aimed to investigate how varying crack width influences the rate of chloride penetration and the onset of corrosion. After placing the specimens in the wet tanks, the same amount of load was reapplied to ensure that the cracks remained open during the wet and dry cycles. This process allowed for continuous chloride penetration, fostering corrosion development over time. The goal was to assess how different crack widths impact both the initiation and propagation of corrosion in embedded reinforcement.

### 3.4.2 Methodology of inducing cracks

The pre-cracking procedure was carried out using an Instron machine, with the tension ties placed securely in the machine. Linear variable differential transducers (LVDTs) were applied on all four sides of the specimens *Figure 3.4-1* to monitor and record the elongation of tension tie [7].

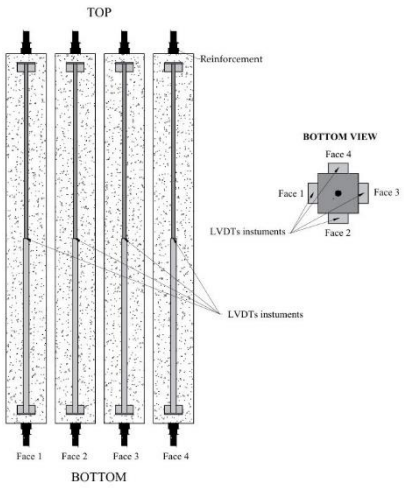


*Figure 3.4-1. Schematic diagram of tension ties with LVDT instruments*

The process began with four specimens, which were used to determine the amount of load required to induce specific crack widths on tension ties. A monotonic tensile load was gradually applied. the load was first increased to 35 kN; at this point, the average crack width was measured to be 0.2 mm. To achieve the average crack width of 0.1 mm, the load was released from 35 kN to 10 kN, and the average crack width was re-measured *Figure 3.4*. Subsequently, the load was incrementally increased to higher levels, with crack width measurements recorded at each stage. At 45 kN, the average crack width was found to be 0.3 mm, and at 55 kN, the average crack width reached 0.4 mm. The load was gradually increased to the total strain of 3‰ and 5‰, as shown in *Figure 3.4-2*.

This preliminary testing sequence allowed for precise calibration of the applied load to achieve target crack widths of 0.1 mm, 0.2 mm, 0.3 mm, and 0.4 mm. To ensure accuracy, the pre-cracking procedure was performed on four specimens for each target crack width. Specimens intended to achieve a 0.2 mm crack width were loaded to 35 kN, and subsequent specimens were subjected to the same incremental loading steps for 0.1 mm, 0.3 mm, and 0.4 mm crack widths, as outlined above. This controlled and sequential loading methodology ensured consistent crack width measurement across specimens and provided a standardized approach to inducing and documenting crack formation for subsequent experimental analysis.

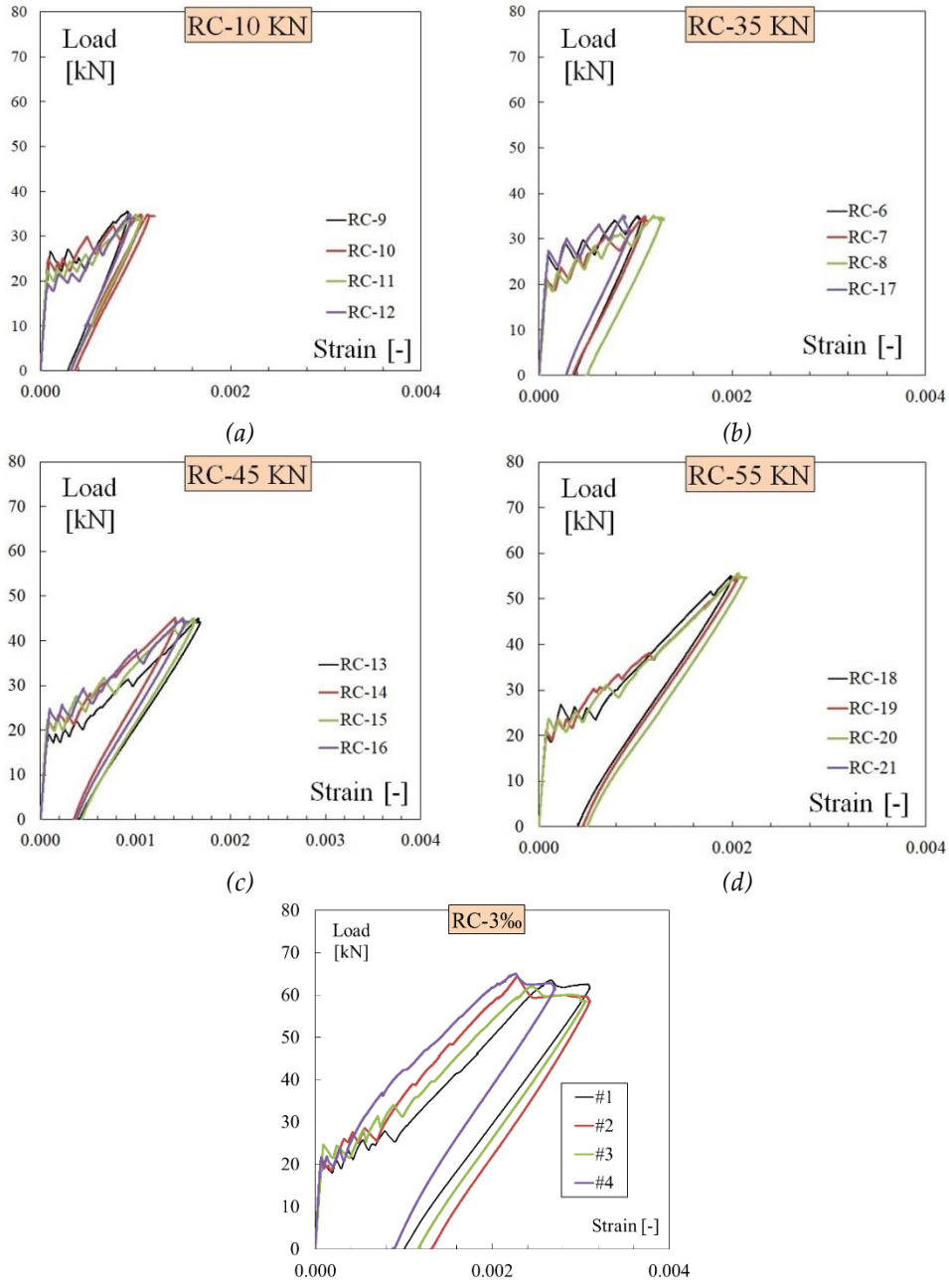


*Figure 3.4-2. Stress-strain diagram for; a) RC-10 kN; b) RC-35 kN; c) RC-45 kN; d) RC-55 kN; e) Up to total strain of 3‰.*

### *3.4.3* *Crack width measurement*

Crack measurements were carried out during the pre-cracking phase of specimens at various stages, including during the application of maximum loads and after the specimens were unloaded. Accurate measurement of crack width is essential to understanding the behaviour of concrete during both the corrosion initiation and propagation phases.

*Table 3.4-1. Average crack width calculated with digital microscope*

| Designation | Load | Average crack width (mm) |
|---|---|---|
| RC - 01 | 10 kN | 0.127 |
| RC - 02 | | 0.100 |
| RC - 03 | | 0.100 |
| RC - 04 | | 0.102 |
| RC - 01 | 35 kN | 0.290 |
| RC - 02 | | 0.288 |
| RC - 03 | | 0.203 |
| RC - 04 | | 0.252 |
| RC - 01 | 45 kN | 0.300 |
| RC - 02 | | 0.412 |
| RC - 03 | | 0.317 |
| RC - 04 | | 0.328 |
| RC - 01 | 55 kN | 0.414 |
| RC - 02 | | 0.328 |
| RC - 03 | | 0.448 |
| RC - 04 | | 0.446 |
| RC - 01 | 3‰ | 0.148 |
| RC - 02 | | 0.312 |
| RC - 03 | | 0.146 |
| RC - 04 | | 0.181 |
| RC - 01 | 5‰ | 0.130 |
| RC - 02 | | 0.351 |
| RC - 03 | | 0.439 |
| RC - 04 | | 0.485 |

To ensure precise crack width measurements, two different techniques were employed: Linear variable displacement transducers (LVDT) and a digital microscope. LVDTs were attached to all four sides of the tension ties to monitor the overall elongation during the loading process, as shown in *Figure 3.4-3*. In addition to LVDTs, a digital microscope was used to measure the crack width at specific points along the crack paths, as detailed in *Table 3.4-1*.

The use of the digital microscope allowed for higher-resolution imaging, providing accurate measurements at multiple locations along each crack. This technique facilitated precise measurements of each individual crack development during loading and after unloading. By combining the LVDT measurements for overall elongation with the digital microscope for detail crack width analysis, a comprehensive understanding of the relationship between crack width and corrosion progress was achieved. This dual approach enabled a deeper insight into the correlation between crack width and the rate of corrosion during both the initiation and propagation stages.

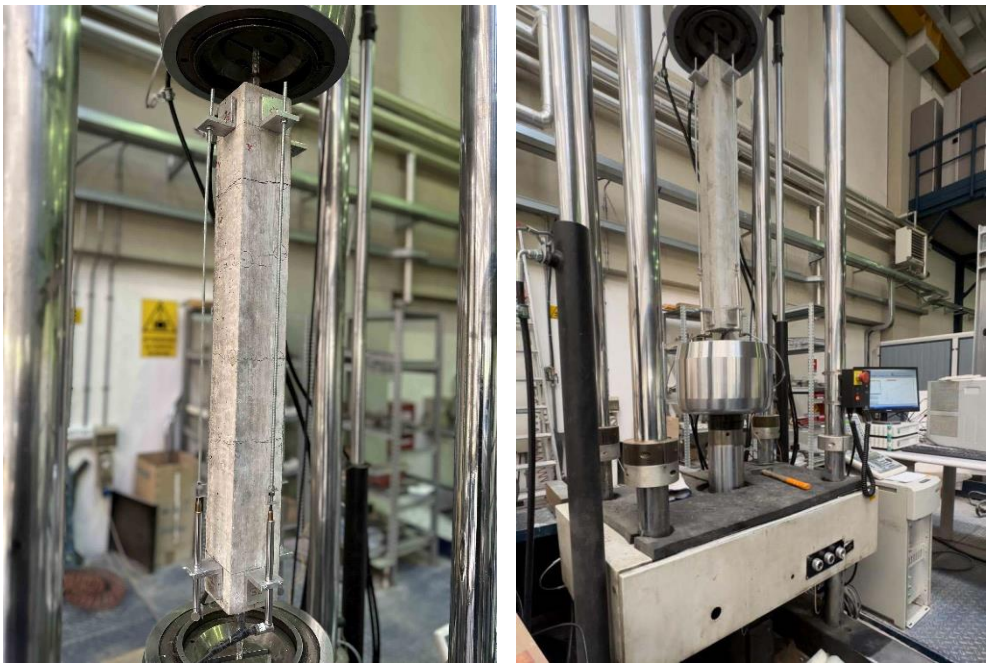

(a) (b)

*Figure 3.4-3. Tension tie in Instron machine; a) After pre cracking; b) before pre cracking.*

## 3.5 Corrosion Phase

In this phase of the study, after the pre-cracking of the specimens, several steps were taken to prepare the specimens for exposure to the sodium chloride solution and to ensure that they remained under the intended loading conditions throughout the experiment.

To protect the reinforcement from direct exposure to the corrosive sodium chloride solution, the rebars at the end of the tension ties were coated with a protective anti-corrosion paint. This protective layer was applied to prevent the chloride ions from

penetrating the rebar and initiating corrosion at the exposed ends of the tension ties. Additionally, a protective layer was applied at the ends of the rebars to prevent the sodium chloride solution from entering through the ends of the specimens, as shown in *Figure 3.5-1*. This ensured that the solution would only enter through the induced cracks, simulating realistic corrosion conditions where cracks in the concrete provide pathways for the ingress of aggressive agents.

*(a)* *(b)*

*Figure 3.5-1. a) Tension ties after waterproofing paint; b) Water storage tank after waterproofing paint.*

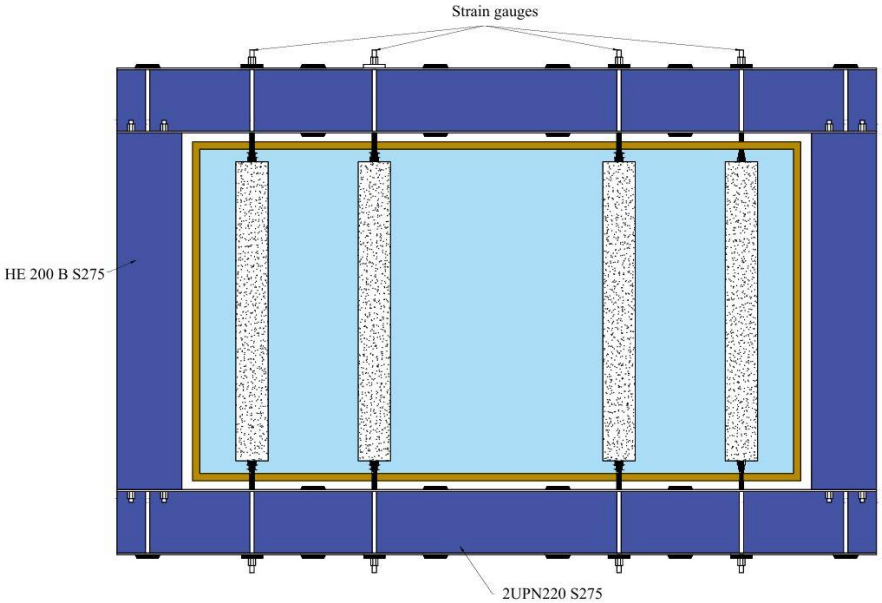


*Figure 3.5-2. Tension ties under loading in water tank*

The water tanks used to place tension ties during wet and dry cycles were made of plywood and placed inside self-equilibrating steel frames to ensure stability and prevent any deformation under loads. To make plywood tanks watertight and and prevent leakage, multiple layers of waterproofing paint were applied to the interior of the tanks. Once the waterproofing was completed, the specimens were placed in the tanks according to their respective crack widths. Specimens with crack widths of 0.1 mm were placed in one tank, those with 0.2 mm crack width in another tank, and so on. Additionally, separate tanks were used for specimens with larger total elongations. Specimens with strain up to 3‰ were placed in a separate set of tanks where no additional loading was applied, and similarly, specimens with strain up to 5‰ were stored under conditions where no load was applied.

A total of 28 tension tie specimens were prepared and divided into seven groups based on crack width and loading condition. For specimens where sustained tensile loads were required throughout the experimental phase, the tension ties were fixed in water tanks using screws at one end, while strain gauges and connectors were installed at the opposite end to monitor and control the applied loads. The strain gauges enabled real-time tracking of strain during the loading process *Figure 3.5-2*.

The loading process followed a systematic procedure. Pre-cracking of the specimens was performed using a universal testing machine (Instron), with target loads applied to induce specific crack widths. Following pre-cracking, the same load used to generate the crack was reapplied and maintained during the exposure phase.

- Uncracked: 4 specimens remained completely uncracked and were not subjected to any loading.
- Crack Width ≈ 0.1 mm (10 kN): 4 specimens were loaded to 10 kN and kept under sustained load in one exposure tank.
- Crack Width ≈ 0.2 mm (35 kN): 4 specimens were loaded to 35 kN and kept under sustained load in a separate tank.
- Crack Width ≈ 0.3 mm (45 kN): 4 specimens were loaded to 45 kN and exposed in another tank.
- Crack Width ≈ 0.4 mm (55 kN): 4 specimens were loaded to 55 kN and placed in a dedicated tank.

In addition, two sets of 4 pre-cracked specimens were exposed without any applied mechanical load:

- Strain = 3‰ (no load): 4 pre-cracked specimens (strain level of 3‰) were placed in a tank without sustained loading.
- Strain = 5‰ (no load): 4 pre-cracked specimens (strain level of 5‰) were placed in another tank without sustained loading.

Before beginning the wet-dry exposure cycles, all loaded specimens were kept in dry tanks to verify the stability of the applied forces. This ensured that the loading conditions remained consistent throughout the test duration. The distribution of specimens across crack widths and loading conditions allowed for a systematic

investigation of corrosion behaviour under different mechanical and environmental exposures, as shown in *Figure 3.5-3*.

*Figure 3.5-3. Tension ties placed in the water storage tank after applying waterproof paint.*

### *3.5.1 Wet and dry cycles*

Wet and dry cycles are a commonly used method to accelerate the corrosion process in experimental setups, simulating harsh environmental conditions that structures might face in real-life exposure [8], [9]. This process involves cycling between wet and dry phases using a sodium chloride solution, which promotes corrosion by subjecting the material to fluctuating moisture levels. The wet and dry cycles help to replicate the environmental stress that metals, especially steel reinforcements in concrete, are exposed to in various climates, thereby accelerating the development of corrosion.

#### *3.5.1.1 Objective of wet and dry cycles*

The primary objective of using wet and dry cycles in corrosion testing is to accelerate the corrosion process, allowing researchers to observe and evaluate the corrosion over a shorter period. These cycles simulate the exposure conditions of metals to natural environments, where the materials undergo periodic wetting and drying, similar to the periodic rainfall.

By controlling the cycle, researchers can simulate the effect of environmental factors on the material, providing a better understanding of its long-term performance under real-world conditions. The wet and dry cycles aim to accelerate corrosion under controlled conditions, replicating the moisture fluctuations common in natural environments. This technique offers insights into how corrosion begins and progresses in materials like rebar and enables a thorough assessment of the

effectiveness of corrosion protection strategies and the durability of materials in adverse conditions.

#### *3.5.1.2 Experimental procedure for wet and dry cycles*

After applying the loads to the tension tie places in the water tanks placed in self-equilibrium steel frames, a 35 g/l sodium chloride solution was used for wet and dry cycles, as shown in *Figure 3.5-4*. The wet and dry cycles consist of three days of wet

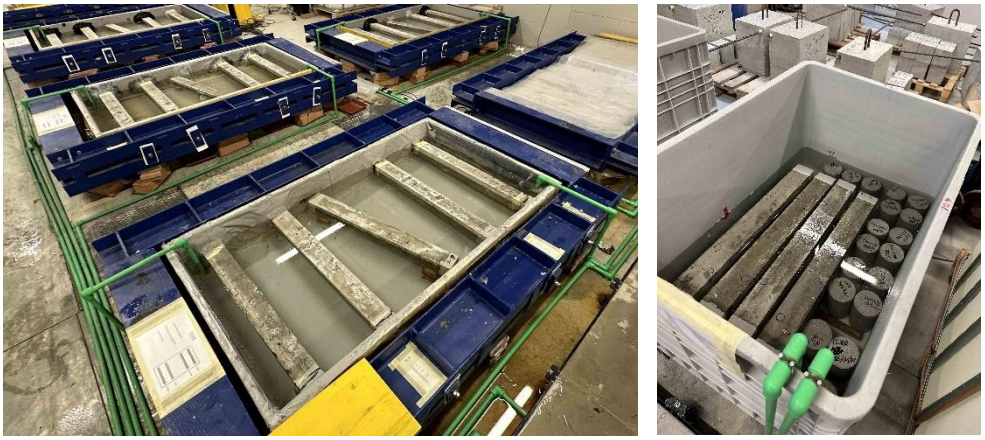

***1.1.1.1.1 (a)*** ***1.1.1.1.2 (b)***

*Figure 3.5-4. Tension ties during wet cycle; a) Under loading condition; b) Unloading condition.*

exposure followed by four days of drying, creating an environment that depicts conditions such as those near to marine environments or other areas with periodic moisture to exposure.

The experimental procedure was conducted over a total duration of 81 weeks. Each wet and dry cycle begins with three days of wetting, followed by four days of drying. The specimens were periodically evaluated during these cycles to monitor the onset and progression of corrosion. By maintaining these cycles for a long period, the experiment accelerated the corrosion process, replicating real-world exposure conditions.

#### *3.5.1.3 Corrosion initiation and propagation phase*

Corrosion initiation refers to the early stage of the corrosion process, during which environmental factors such as exposure to moisture, chlorides, and oxygen begin to degrade the protective oxide layer on the surface of the steel reinforcement. In reinforced concrete structures, for example, chloride ions from saltwater can penetrate the concrete and eventually reach the embedded steel. Once they do, these ions

compromise the passive film that normally protects the steel, thereby initiating the corrosion process.

To monitor the corrosion initiation phase, measurements of corrosion potential were performed using the COR-MAP system, which operates based on half-cell potential principles in accordance with ASTM C876-09. This method involves measuring the electrochemical potential difference between the embedded steel reinforcement and a stable reference electrode, providing insight into the likelihood of active corrosion at specific points on the specimen surface, as shown in *Figure 3.5-5* and *Figure 3.5-6* [10].

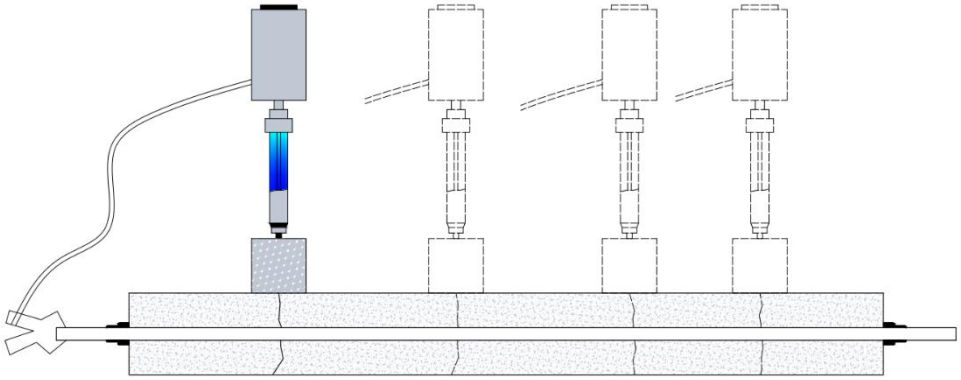

*Figure 3.5-5. Calculation of corrosion potential using Cor-map instrument on different cracks.*

The main components of the system included the COR-MAP voltmeter (James CM-4500), a portable $Cu/CuSO_4$ reference electrode (James CM-4400), a test lead wire reel, and alligator clips for establishing electrical connections. To ensure proper conductivity and accuracy, a direct connection was made to the reinforcement at exposed ends of the rebars, making sure that contact surfaces were clean and free from corrosion products or coatings.


*Figure 3.5-6. Corrosion potential measurement using Cor-map instrument.*

The $Cu/CuSO_4$ reference electrode was prepared by filling approximately one-third of the electrode tube with copper sulphate crystals and then topping it up with distilled water. The electrode was gently shaken to help dissolve the crystals, ensuring that some remained undissolved to maintain a saturated solution. To allow complete saturation of the porous plug, the electrode was typically prepared one day before measurements were conducted. New reference electrodes were prepared every two weeks to ensure measurement reliability, and the sponge covering the electrode tip was cleaned after each measurement session to maintain proper surface contact and accuracy. A sponge-covered bottle housed the tip of the electrode to ensure good surface contact during testing.

During measurement, one end of the test lead was connected to the reinforcement using an alligator clip, while the other end was connected to the voltmeter shown in *Figure 3.5-6*. The reference electrode was placed directly on the concrete surface above the crack area, which had been moistened slightly to improve ionic conductivity. The COR-MAP meter then recorded the half-cell potential.

Measurements were taken twice per week: once before the start of each wet cycle, and once before each dry cycle. This schedule enabled close tracking of corrosion development over time under cyclic exposure conditions. The recorded potentials served as an indicator of corrosion activity: readings more negative than -350 mV (with respect to the $Cu/CuSO_4$ reference) typically indicated a high probability (≥90%) of active corrosion at the time of testing.


*(a)* *(b)* *(c)*

*Figure 3.5-7. Cor-map items used to calculate corrosion potential; a) Bottle having copper sulphate crystals; b) Cor-map electrode with 1/3 filled with copper sulphate; c) Cor-map electrode filled with 3/4 of portable water.*

By applying this method consistently across all specimens and crack locations, the study was able to observe the electrochemical behaviour of the steel in response to different crack widths and exposure conditions, even though some data points were missing due to practical limitations during the testing period.
The assessment of the propagation phase included comparing the final weight of the rebars with the initial weight of the estimated mass loss due to corrosion. Additionally, parameters such as pitting depth (measured in relation to crack width), the area affected by pitting, and the overall length of the corrosion zone were evaluated. These metrics provide a quantitative understanding of the extent and severity of corrosion damage, which will be discussed in detail in the following chapter.

#### *3.5.1.4 Chloride penetration*

To assess the penetration of chloride ions in uncracked specimens, a thin layer of epoxy resin was applied to the sides and top surface of the concrete cylinders, as illustrated in *Figure 3.5-8*. The bottom surface was intentionally left uncoated to allow the sodium chloride solution to infiltrate the specimen solely from that direction. This selective sealing approach was implemented to simulate one-sided chloride exposure and to control the penetration path for more accurate measurement of ingress rates [11].

*Figure 3.5-8. Epoxy resin was applied to cylinders for the chloride penetration test.*

The treated cylinders were then placed in a water tank alongside unloaded specimens, ensuring they were subjected to the same alternating wet and dry cycles using sodium chloride solution. This setup mimicked the environmental conditions experienced by the main test specimens.

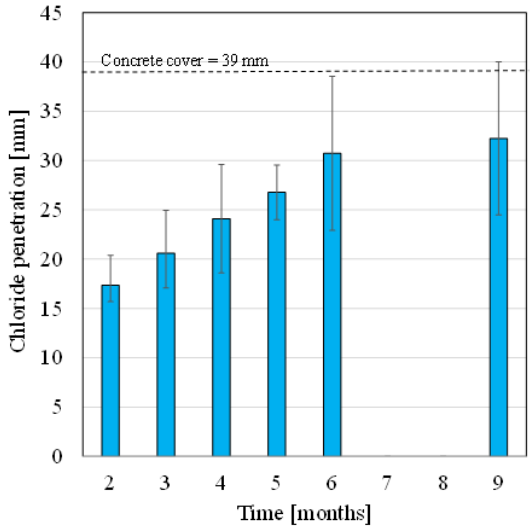


*Figure 3.5-9. Chloride penetration rate over nine months*

*Figure 3.5-9*. illustrates the progression of chloride penetration over a period of nine months. The data reveal a gradual but consistent increase in penetration depths, from approximately 15 mm after two months to around 30–35 mm at nine months. These findings provide insight into the rate of chloride ingress under cyclic exposure and were used as a comparative baseline for evaluating chloride penetration in the tension tie specimens exposed to similar conditions.

## 3.6 References


[1] A. Poursaee and B. Ross, "The Role of Cracks in Chloride-Induced Corrosion of Carbon Steel in Concrete—Review," *CMD*, vol. 3, no. 2, pp. 258–269, Jun. 2022, doi: 10.3390/cmd3020015.

[2] S. Robuschi, O. L. Ivanov, M. Geiker, I. Fernandez, and K. Lundgren, "Impact of cracks on distribution of chloride-induced reinforcement corrosion," *Mater Struct*, vol. 56, no. 1, p. 7, Feb. 2023, doi: 10.1617/s11527-022-02085-6.

[3] F. U. A. Shaikh, "Effect of Cracking on Corrosion of Steel in Concrete," *Int J Concr Struct Mater*, vol. 12, no. 1, p. 3, Dec. 2018, doi: 10.1186/s40069-018-0234-y.

[4] M. Ghanooni-bagha, M. A. Shayanfar, and M. H. Farnia, "Cracking effects on chloride diffusion and corrosion initiation in RC structures via finite element simulation," *Scientia Iranica*, vol. 0, no. 0, pp. 0–0, Dec. 2018, doi: 10.24200/sci.2018.50496.1725.

[5] G. Tiberti, F. Minelli, and G. Plizzari, "Cracking behavior in reinforced concrete members with steel fibers: A comprehensive experimental study," *Cement and Concrete Research*, vol. 68, pp. 24–34, Feb. 2015, doi: 10.1016/j.cemconres.2014.10.011.

[6] A. Amin, S. J. Foster, and M. Watts, "Modelling the tension stiffening effect in SFR-RC," *Magazine of Concrete Research*, vol. 68, no. 7, pp. 339–352, Apr. 2016, doi: 10.1680/macr.15.00188.

[7] B. Leporace-Guimil, A. Conforti, R. Zerbino, and G. A. Plizzari, "Chloride-induced corrosion in reinforced concrete and fiber reinforced concrete elements under tensile service loads," *Cement and Concrete Composites*, vol. 124, p. 104245, Nov. 2021, doi: 10.1016/j.cemconcomp.2021.104245.

[8] J. Wei, J. H. Dong, and W. Ke, "Corrosion Evolution of Scaled Rebar in Concrete under Dry/wet Cyclic Condition in 3.5% NaCl Solution," *International Journal of Electrochemical Science*, vol. 8, no. 2, pp. 2536–2550, Feb. 2013, doi: 10.1016/S1452-3981(23)14330-6.

[9] F. Qu, J. Zhang, G. Liu, and S. Zhao, "Experimental Study on Chloride Ion Diffusion in Concrete Affected by Exposure Conditions," *Materials*, vol. 15, no. 8, p. 2917, Apr. 2022, doi: 10.3390/ma15082917.

[10] L. Tang and Y. Fu, "A Rapid Technique Using Handheld Instrument for Mapping Corrosion of Steel in Reinforced Concrete / Eine Schnellmethode zur Bestimmung der örtlichen Verteilung der Korrosion des Stahles in bewehrtem Beton

mit Hilfe eines Handgerätes," *Restoration of Buildings and Monuments*, vol. 12, no. 5–6, pp. 27–40, Dec. 2006, doi: 10.1515/rbm-2006-6078.

[11] J. Liao, Y. Wang, X. Sun, and Y. Wang, "Chloride Penetration of Surface-Coated Concrete: Review and Outlook," *Materials*, vol. 17, no. 16, p. 4121, Aug. 2024, doi: 10.3390/ma17164121

# 4 EXPERIMENTAL RESULTS AND DISCUSSION

## 4.1 Introduction

This chapter summarizes the findings from the experimental campaign of corrosion initiation and propagation in reinforced concrete structures. The primary objective of this study was to evaluate the effect of varying crack width on both corrosion initiation and propagation under sustained loading conditions in an aggressive environment.
The first section addresses corrosion initiation, including corrosion monitoring techniques employed and the influence of crack width on time required for corrosion to begin. This stage provides crucial insights into the early phase of degradation processes affecting reinforced concrete.
Following the initiation phase, the chapter further investigates the corrosion propagation phase, which is a localized type of degradation. This section is further divided into sub-sections that analyse rebar weight loss and explore the relationship between crack width, corrosion rate, pitting depth, and length of corrosion zone.
Finally, this chapter examines the mechanical performance of corroded rebar, focusing on changes in yield strength and ultimate strength. This analysis is essential for understanding the extent to which corrosion affects the load-bearing capacity and overall structural integrity of reinforcement steel.

## 4.2 Overall response of tension ties strains up to 5‰

To assess the overall response of tension ties under applied loading, four specimens were tested, as shown in *Figure 4.2-1*. At the initial stage of the loading, the specimen exhibits an uncracked response, characterized by a linear load strain relationship. During this phase, the composite materials comprising both concrete and reinforcement behaved elastically. The applied tensile load was shared by both constituents, and the system's stiffness was governed by the elastic modulus of the materials. This phase is critical for evaluating the inherent material properties before any structural damage occurs. During the uncrack stage, the tensile forces are uniformly distributed across the specimen cross section [1], [2]. The absence of the crack indicates that the tensile stress inside the materials is lower than the tensile strength of the matrix.
Cracking initiates when the tensile strength of the matrix is exceeded at its weakest point, which may arise from pores, pre-existing micro-defects, or stress concentration within concrete. Cracks typically form perpendicular to the direction of the applied

load. Upon crack formation, the tensile stress near the crack location drops by redistributing the tensile forces to the nearby uncracked region and embedded steel reinforcement [3], [4].

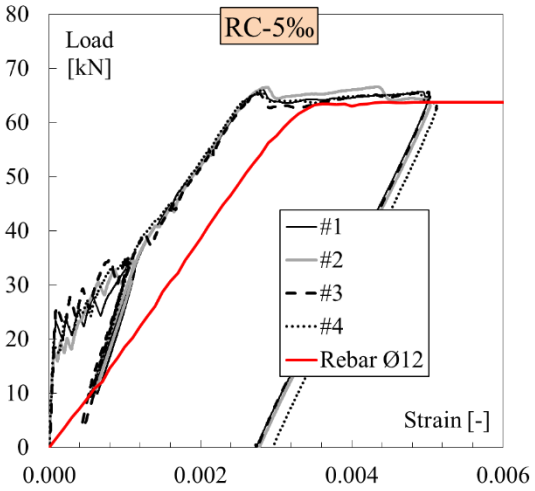


*Figure 4.2-1. Overall response of tension ties up to total elongation of 3.75 mm*

After the formation of multiple cracks, the stabilized crack stage begins. In this phase, the embedded reinforcement plays an important role by resisting the majority applied load. Crack spacing tends to become constant, and crack width increases in a relatively uniform manner. The reinforcement, in conjunction with the bond between steel and concrete, contributes to the uniform distribution of cracks along the length of the member, preventing the development of isolated, wide cracks. The bond strength plays a crucial role in controlling the crack spacing and preserving the overall stiffness of the system. Experimentally, this phase offers valuable insights into the structural behaviours under sustain loading conditions.

The final phase observed during the tension tie tests is the yielding stage. Here, the steel reinforcement reaches its yield strength, initiating plastic deformation. At this point, the load-bearing capacity of the system either stabilizes or shows only a marginal increase while strain continues to accumulate. The onset of yielding marks the end of elastic behaviour in the reinforcement.

Throughout the tensile loading process, the evolution of crack width is closely linked to the structural response. During the uncracked stage, no visible cracks are present, and the crack width is effectively zero. Once cracking begins, crack width increases progressively as the crack propagates. In the stabilized cracking phase, the crack width continues to grow but in a more consistent and uniform manner. The average crack width at this stage is significantly influenced by the reinforcement's ability to

bridge cracks and redistribute stress [5], [6]. Finally, in the yield phase, the crack width significantly increases as the reinforcement elongates under plastic deformation.

## *4.3 Corrosion initiation*

The degradation process in reinforced concrete typically begins with the corrosion initiation phase. In this study, corrosion initiation was monitored using the COR-MAP instrument, which recorded half-cell potential measurements at each visible crack on the surface of the tension tie specimen.

Corrosion was induced through alternating wet and dry cycles, comprising 3-day wet cycles and 4-day dry cycles. As shown in *Figure 4.3-1*, corrosion potential measurements were taken during both phases of the cycle. For the first 10 weeks, measurements were taken weekly both during wet and dry cycles. From weeks 11 to 26, measurements were taken every two weeks, and from weeks 27 to 40, monthly readings were conducted as the corrosion potential began to stabilize.

Under the given exposure conditions, specimens appear to be rapidly prone to corrosion, indicated by the early dip in the corrosion potential value observed during the first week, likely due to immediate exposure to aggressive environments. These early shifts indicate that the initiation of corrosion occurred rapidly, particularly during the wet cycle when moisture facilitated the electrochemical reaction. In contrast, partial re-passivation was observed during the dry cycle, when reduced electrolyte availability temporarily slowed down corrosion processes.

Corrosion initiation begins from the first cycle in all specimens except for the specimens having a 0.1 mm crack width. The corrosion potential values of specimens having a 0.1 mm crack width are closer to those of uncracked specimens, implying that corrosion initiation is slow due to less aggressive agents' penetration because of the smaller crack width.

The difference in corrosion potential between cracked and uncracked specimens increased with crack width. This trend indicates that wider cracks permit greater penetration of corrosion agents such as chloride, oxygen, and moisture, thus accelerating corrosion initiation. The specimen with the widest crack exhibited the greatest deviation in corrosion potential, reflecting the highest degree of exposure to aggressive substances.

Furthermore, specimens subjected to higher applied loads (e.g., 55 kN) demonstrated more negative corrosion potentials. This can be attributed to increased microcracking or the propagation of existing cracks under stress, which facilitates further ingress of corrosive agents. Additionally, the elevated stress may impair the material's ability to maintain or regenerate a passive oxide layer, leading to more severe corrosion initiation.

After the initial decline, corrosion potential across all specimens tends to stabilize, indicating a transition to a steady-state corrosion process. This phase is characterized

by a balance between the ingress of chlorides and moisture and the ongoing corrosion activity. The periodic fluctuation in potential observed throughout the study reflects the cyclic nature of the exposure conditions.

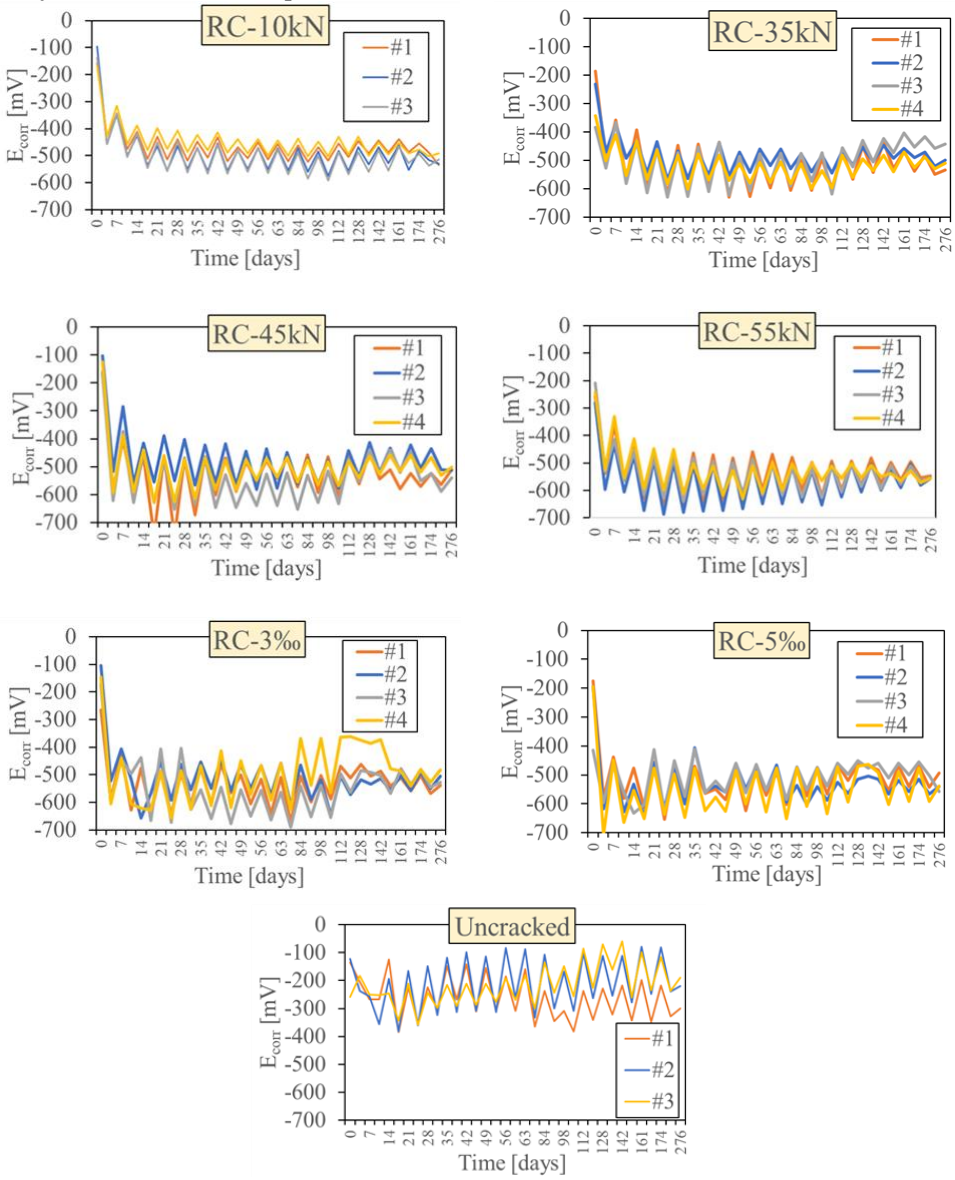


*Figure 4.3-1. corrosion potential of cracked and uncracked samples.*

During the wet cycles, the corrosion potential tends to decrease (i.e., becomes more negative), indicating an increase in electrochemical activity at the surface of the material. This behaviour is primarily due to elevated moisture levels, which enhance

iconic conductivity and promote the migration of chloride ions into concrete. The presence of moisture accelerates the oxidation reaction, thereby intensifying the corrosion process and reducing the material's corrosion resistance.
In contrast, during dry cycles, the corrosion potential typically shifts toward less negative values, reflecting a temporary reduction in corrosion activity. This occurs due to the reduced availability of moisture, which limits iconic movement and slows the electrochemical reactions responsible for corrosion.
In our study, we encountered challenges in determining the critical chloride content of our sample, primarily due to two factors. First, the corrosion initiation time was relatively short, at just three days, making it difficult to assess the chloride threshold before significant corrosion activity began. Second, given the need to focus on corrosion propagation rather than initiation, destructive chloride analysis was not feasible as it would interfere with the progression of the study. Furthermore, we recognize the limitations of relying solely on Fick's law to estimate chloride diffusion as this model assumes an intact concrete matrix. In practice, however, cracks in the concrete significantly reduce the diffusion resistance, allowing chloride ions to bypass the intact concrete and reach the rebar more quickly. As a result, the chloride penetration rate is faster than predicted by traditional diffusion models, and this dynamic needs to be considered in the context of our research.

## *4.4 Corrosion propagation*

A thorough investigation of corrosion propagation is presented in this section, beginning with the removal and assessment of corroded rebar, followed by the measurement and analysis of pitting corrosion. The study also investigates the corrosion-induced degradation in tension ties and evaluates how different crack widths influence the extent of pitting. Finally, the effects of pitting corrosion on the mechanical properties of reinforcement bars are analysed to understand the degree of ductility and strength loss. These findings provide essential insights into how corrosion affects the long-term durability of reinforced concrete structures.

### *4.4.1 Extraction of rebar*

Following the 40-week exposure period, the next step was to release the applied load on the tension ties and remove them from the water tanks to assess the corrosion propagation phase. One of the initial observations, as shown in *Figure 4.4-1* was absence of visible corrosion on the specimen surface. The lack of corrosion-induced longitudinal cracks suggests that both concrete quality and the cover thickness played a significant role in protecting the reinforcement. The limited exposure period, combined with the absence of any external acceleration methods (e.g., electric current), likely explains the minimal surface-level corrosion observed.

*Figure 4.4-1. Specimens after corrosion test.*

The extraction of the rebar was carried out using saw-cutting, as shown in *Figure 4.4-2*. The tension tie was cut to a depth of approximately a couple of millimetres from the rebars to allow mechanical opening of the specimen without damaging the surrounding concrete. The tension ties were then carefully separated into two halves using a hammer and a concrete chisel *Figure 4.4-3* to avoid damaging rebar.

It is worth noting that although some cracks were present in the specimens, no corrosion was visibly evident within these cracks. This can be attributed to the formation of a microcell between the surrounding concrete and the anodic zones, areas most susceptible to corrosion. In such conditions, the uncracked concrete region serves as the cathode (the region where there is no corrosion), while the exposed rebar near the cracks acts as an anode (the part where corrosion occurs). The electrochemical interaction between the anodic and cathodic areas confines the corrosion process near the cracks. Since electron flow from anode to cathode is essential for corrosion to progress, the surrounding intact concrete may act as a protective barrier, limiting corrosion to a region adjacent to the cracks.

To put it another way, although cracks may have developed, the electrochemical environment likely restricted corrosion to the immediate vicinity of those cracks, while the rest of the rebar remained protected by the concrete. This explains the absence of corrosion signs in regions away from visible cracks.

After extraction, the rebars were cleaned with a metallic bristle brush to remove the debris dust. The cleaned rebars were then weighed and compared to their original recorded weights, taken before casting the tension tie specimen. The purpose of cleaning was to obtain a clear measurement of the metal mass loss, free from concrete product and corrosion layers. This method provides a balance between thorough cleaning and maintaining the integrity of the rebar surface. Any minimal loss of material during cleaning is assumed to be negligible to the overall mass loss during the corrosion process.

*Figure 4.4-2. Saw-cutting of tension ties after corrosion propagation.*

Weight loss of rebar is a reliable indicator to measure the uniform corrosion, where material deteriorates evenly across its surface. Weight loss can also serve as a metric for localized corrosion, despite the fact that it is often more difficult to measure.
Pitting corrosion generally takes longer to result in noticeable weight loss because it is confined to small areas and may not affect the entire surface of the rebar immediately.
*Table 4.4-1* presents the weight loss of rebars, calculated after the specimens were opened and the reinforcement bar were cleaned using a metallic bristle brush.
The mass-loss rate refers to the amount of materials lost due to corrosion over a specific period, typically expressed relative to the surface area (e.g., in grams per square meter per year). It's a dimensionless measure that accounts for both the surface area of the material and its exposure duration, providing a standardized way to evaluate the severity of corrosion over time.

*Figure 4.4-3. Extraction of rebar after saw cutting.*

However, since this study focused on localized (pitting) corrosion, it's more appropriate to use the penetration rate than the general corrosion rate. This is due to the fact that pitting corrosion does not corrode the entire surface area uniformly.

The corrosion rate (CR) can be calculated by dividing the mass loss by the metal's density, and it's typically expressed in micrometers per year (μm/year). This value represents the reduction in metal thickness due to corrosion over a given period. For instance, if the mass loss for reinforcing steel is 1 gram per square meter per year (1 $g/m^2$ x year), this corresponds to a corrosion rate of approximately 0.127 μm/year. This means that over the course of one year, the steel's thickness would decrease by decrease by 0.127 micrometers due to corrosion.

### *4.4.2* *Measurement of pitting*

The next stage in assessing the corrosion propagation, to measure the pitting depth and pit area on the rebar's surface, as shown in *Figure 4.4-4*. A digital indicator *Figure 4.4-5*a *with a* precision of 1 x $10^{-3}$ was used to measure the pitting depth, enabling precise measurements of the depth of each corrosion pit. Additionally, a digital microscope *Figure 4.4-5b* was used to measure the length of each pit in addition to its depth, providing comprehensive analysis of both depth and morphology of the corrosion. High-resolution images of the pit were obtained using the digital microscope, allowing precise assessments of their size and a comprehensive evaluation of the degree of corrosion.

*Figure 4.4-4. Rebar showing pitting corrosion on all four sides.*

The digital microscope further allowed for a thorough analysis of the pit morphology. The level of localized corrosion, which is frequently the main reason for structural failure in corroded tension ties, was determined by measuring the area of each pit. Pit length and pitting depth studies together gave a complete picture of the corrosion process and how it affects the rebar's structural integrity.

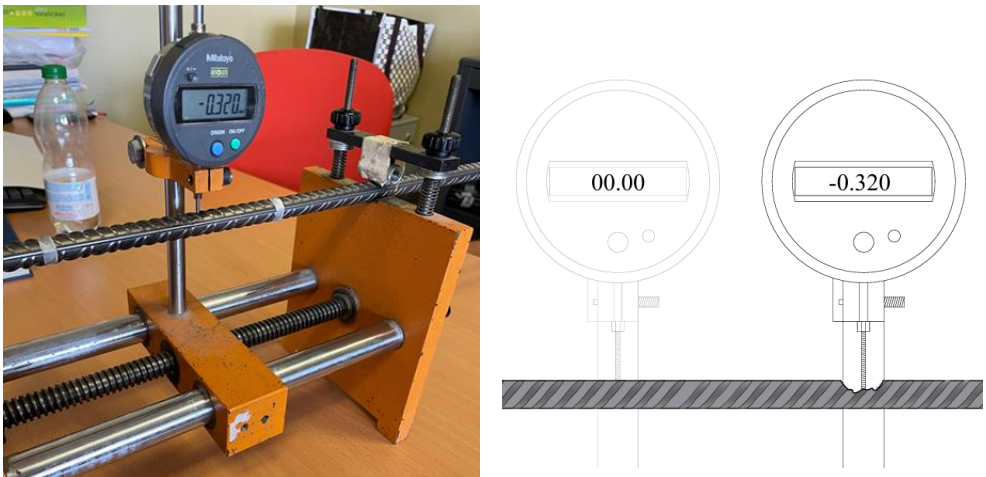


*a)*

*b)*

*Figure 4.4-5. a) Measuring pitting depth by using a digital dial indicator b) Measuring pitting using a digital microscope*

### *4.4.3* *Analysis of tension tie degradation and pitting measurement*

The specimen's crack patterns and the corrosion damage caused by the corrosion test were drawn in *Figure 4.4-7*, *Figure 4.4-8*, *Figure 4.4-9*, *Figure 4.4-10*, *Figure 4.4-11*, *Figure 4.4-12*, *Figure 4.4-13* and *Figure 4.4-17*, which provides a clear picture of reinforcing bar's level of damage in relation to the crack that developed during the pre-cracking phase of the test. The black irregular patterns show the appearance of cracks, along with their numbering, while the red marking shows the precise length (in millimetres)

of the corroded zones where localized pits were found on the reinforcement bar. In the table, *dpit* refers to the maximum depth of the pit measured on the rebar surface, while *lpit* indicates the corresponding length of the pit along the reinforcement. These measurements provide insight into how corrosion develops along the bar's length.
The "side" designation is used to indicate the location of the corrosion pits relative to the tension tie shown in *Figure 4.4-6*. There are four sides of the tension tie, each numbered for clarity:

- Side one refers to the left side of the tension tie (as positioned in the Instron machine),
- Side two refers to the front side,
- Side three refers to the right side,
- Side four refers to the back side of the tension tie.

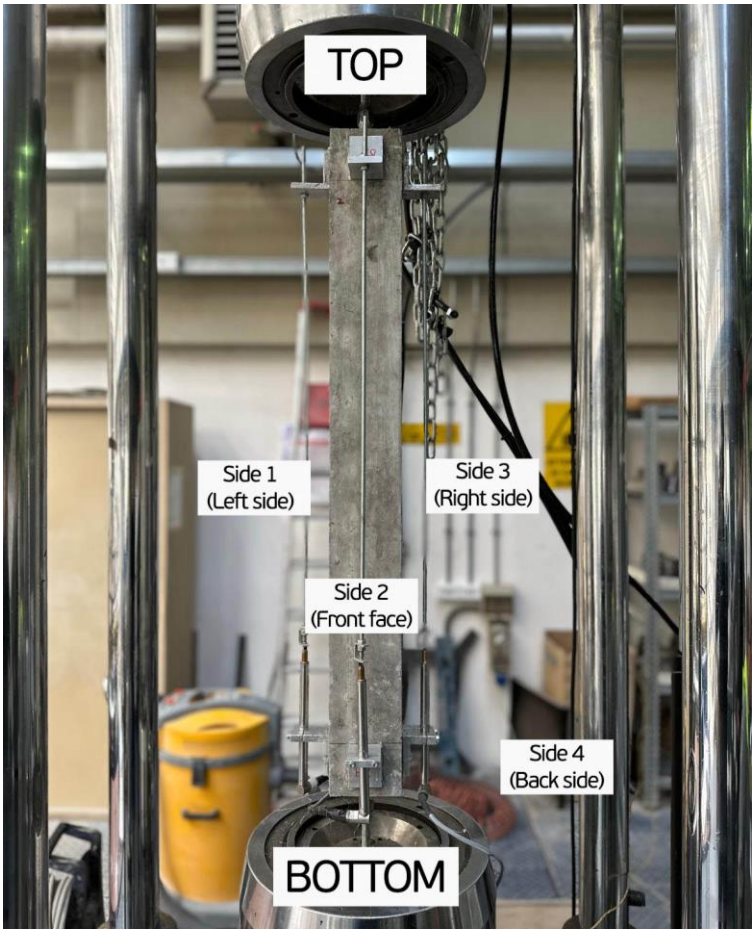


*Figure 4.4-6. tension tie side identification during testing.*


| Crack Number | Pit number | side | $d_{pit}$ (mm) | $l_{pit}$ (mm) |
|---|---|---|---|---|
| - | 1 | 2 | 0.148 | 0.85 |
| - | 2 | 3 | 0.174 | 0.598 |
| - | 3 | 1 | 0.031 | 1.786 |
| - | 4 | 4 | 0.064 | 0.567 |

Uncracked tension tie - 1


| Crack Number | Pit number | side | $d_{pit}$ (mm) | $l_{pit}$ (mm) |
|---|---|---|---|---|
| - | | | | |
| - | | No Corrosion | | |
| - | | | | |
| - | | | | |

Uncracked tension tie - 2


| Crack Number | Pit number | side | $d_{pit}$ (mm) | $l_{pit}$ (mm) |
|---|---|---|---|---|
| - | 1 | 1 | 0.130 | 1.198 |
| - | 2 | 1 | 0.063 | 0.835 |
| - | 3 | 1 | 0.151 | 0.611 |
| - | 4 | 4 | 0.169 | 1.789 |

Uncracked tension tie - 3

*Figure 4.4-7 Crack pattern and affected zone in uncracked samples.*

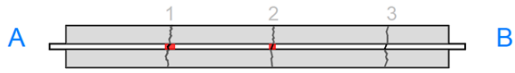


| Crack Number | Pit number | Side | $d_{pit}$ (mm) | $l_{pit}$ (mm) |
|---|---|---|---|---|
| 1 | 1 | 3 | 0.192 | 0.475 |
| 1 | 2 | 3 | 0.033 | 0.58 |
| 2 | 1 | 1 | 0.280 | 0.795 |
| 2 | 2 | 1 | 0.172 | 0.448 |
| 2 | 3 | 1 | 0.147 | 3.106 |
| 2 | 4 | 1 | 0.201 | 1.991 |
| 2 | 5 | 1 | 0.213 | 0.678 |
| 2 | 6 | 4 | 0.198 | 3.358 |
| 2 | 7 | 3 | 0.240 | 0.524 |
| 2 | 8 | 1 | 0.123 | 0.786 |
| 2 | 9 | side 1 | 0.124 | 0.724 |
| 2 | 10 | side 1 | 0.183 | 2.621 |
| 2 | 11 | side 2 | 0.174 | 4.125 |
| 3 | | No corrosion | | |

10 kN tension tie - 1

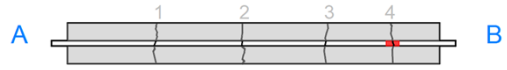


| Crack Number | Pit number | side | $d_{pit}$ (mm) | $l_{pit}$ (mm) |
|---|---|---|---|---|
| 1 | | | | |
| 2 | | No corrosion | | |
| 3 | | | | |
| 4 | 1 | 3 | 0.142 | 0.97 |
| 4 | 2 | 3 | 0.191 | 1.248 |
| 4 | 3 | 3 | 0.085 | 1.952 |
| 4 | 4 | 2 | 0.253 | 0.58 |

10 kN tension tie - 2

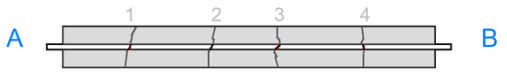


| Crack Number | Pit number | side | $d_{pit}$ (mm) | $l_{pit}$ (mm) |
|---|---|---|---|---|
| 1 | 1 | 1 | 0.220 | 1.024 |
| 2 | | No corrosion | | |
| 3 | 1 | 1 | 0.182 | 2.019 |
| 3 | 2 | 1 | 0.157 | 0.841 |
| 4 | 1 | 1 | 0.123 | 0.848 |
| 4 | 2 | 2 | 0.154 | 1.82 |

10 kN tension tie - 3

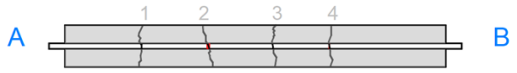


| Crack Number | Pit number | side | $d_{pit}$ (mm) | $l_{pit}$ (mm) |
|---|---|---|---|---|
| 1 | | | | |
| 2 | 1 | side 2 | 0.222 | 4.389 |
| 2 | 2 | side 2 | 0.218 | 2.734 |
| 2 | 3 | side 2 | 0.08 | 2.076 |
| 2 | 4 | side 2 | 0.096 | 2.743 |
| 2 | 5 | side 2 | 0.118 | 2.561 |
| 3 | | No corrosion | | |
| 4 | 3 | side 3 | 0.240 | 2.51 |

10 kN tension tie - 4

*Figure 4.4-8 Crack pattern and affected zone in 10 kN tension tie samples.*

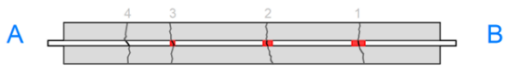


| Crack Number | Pit number | side | $d_{pit}$ (mm) | $l_{pit}$ (mm) |
|---|---|---|---|---|
| 1 | 1 | 1 | 0.072 | 0.703 |
| 1 | 2 | 1 | 0.123 | 0.598 |
| 1 | 3 | 2 | 0.142 | 2.632 |
| 2 | 1 | 1 | 0.119 | 1.057 |
| 2 | 2 | 4 | 0.117 | 1.145 |
| 2 | 3 | 1 | 0.111 | 0.434 |
| 3 | 1 | 1 | 0.199 | 0.756 |

| | | | | |
|---|---|---|---|---|
| 3 | 2 | 2 | 0.101 | 1.757 |
| 3 | 3 | 3 | 0.065 | 2.213 |
| 4 | | No corrosion | | |

35 kN tension tie - 1

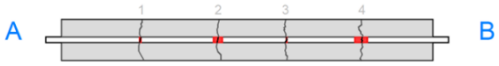


| Crack Number | Pit number | side | $d_{pit}$ (mm) | $l_{pit}$ (mm) |
|---|---|---|---|---|
| 1 | 1 | 3 | 0.137 | 3.724 |
| 1 | 2 | 3 | 0.254 | 2.501 |
| 1 | 3 | 4 | 0.222 | 0.959 |
| 1 | 4 | 4 | 0.101 | 2.663 |
| 2 | 1 | 1 | 0.140 | 0.598 |
| 2 | 2 | 4 | 0.218 | 0.722 |
| 2 | 3 | 1 | 0.091 | 0.809 |
| 2 | 4 | 1 | 0.123 | 2.46 |
| 2 | 5 | 4 | 0.203 | 3.90 |
| 3 | 1 | 2 | 0.232 | 1.188 |
| 4 | 1 | 2 | 0.205 | 2.235 |
| 4 | 2 | 1 | 0.08 | 0.576 |

35 kN tension tie - 2

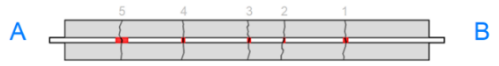


| Crack Number | Pit number | side | $d_{pit}$ (mm) | $l_{pit}$ (mm) |
|---|---|---|---|---|
| 1 | 1 | 3 | 0.136 | 2.28 |
| 1 | 2 | 2 | 0.114 | 0.633 |
| 1 | 3 | 1 | 0.142 | 0.78 |
| 2 | 1 | 3 | 0.132 | 1.6 |
| 3 | 1 | 2 | 0.110 | 2.146 |
| 3 | 2 | 2 | 0.119 | 0.648 |
| 3 | 3 | 2 | 0.104 | 1.297 |
| 4 | 1 | 1 | 0.117 | 0.671 |
| 4 | 2 | 4 | 0.084 | 0.567 |
| 4 | 3 | 3 | 0.137 | 1.4 |
| 5 | 1 | 1 | 0.183 | 0.92 |
| 5 | 2 | 1 | 0.133 | 2.838 |
| 5 | 3 | 1 | 0.126 | 2 |
| 5 | 4 | 3 | 0.06 | 0.5 |
| 5 | 5 | 3 | 0.082 | 2.35 |

35 kN tension tie - 3

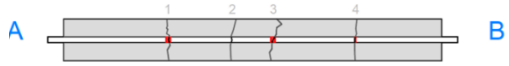


| Crack Number | Pit number | side | $d_{pit}$ (mm) | $l_{pit}$ (mm) |
|---|---|---|---|---|
| 1 | 1 | 3 | 0.074 | 0.572 |
| 1 | 2 | 3 | 0.082 | 1.172 |
| 1 | 3 | 3 | 0.084 | 0.512 |
| 2 | No corrosion | | | |
| 3 | 1 | 2 | 0.144 | 2.32 |
| 3 | 2 | 1 | 0.030 | 0.512 |
| 3 | 3 | 4 | 0.053 | 0.621 |
| 4 | 1 | 1 | 0.039 | 1.7 |
| 4 | 2 | 4 | 0.099 | 0.826 |
| 4 | 3 | 4 | 0.128 | 2.4 |

35 kN tension tie - 4

*Figure 4.4-9 Crack pattern and affected zone in 35 kN tension tie samples.*

When the specimen was opened for further examination, the corroded areas along the rebars, indicated by the red zone in the diagram, were clearly visible. This specific region of corrosion is known as the length of corrosion. It represents the portion of rebar that experienced significant material loss as a result of corrosion. This area also indicates the zone where mechanical loading conditions used during testing likely caused the deterioration of the bond between the concrete and steel interface.
In the drawing, a tension tie is represented with two reference points: point A and point B. Point A corresponds to the top part of the tension tie, while point B refers to the bottom, as defined during the pre-cracking phase of the experiment. In the


| Crack Number | Pit number | side | $d_{pit}$ (mm) | $l_{pit}$ (mm) |
|---|---|---|---|---|
| 1 | No corrosion | | | |
| 2 | | | | |
| 3 | 1 | 1 | 0.231 | 2.123 |
| 3 | 2 | 1 | 0.093 | 2.67 |
| 3 | 3 | 1 | 0.153 | 4.99 |
| 4 | 1 | 1 | 0.306 | 3 |
| 4 | 2 | 1 | 0.152 | 1.964 |
| 4 | 3 | 1 | 0.192 | 1.966 |
| 5 | 1 | 1 | 0.127 | 3.2 |
| 5 | 2 | 1 | 0.042 | 1.179 |
| 5 | 3 | 1 | 0.032 | 2.44 |

45 kN tension tie - 1


| Crack Number | Pit number | side | $d_{pit}$ (mm) | $l_{pit}$ (mm) |
|---|---|---|---|---|
| 1 | No corrosion | | | |
| 2 | | | | |
| 3 | 1 | 3 | 0.107 | 2.39 |
| 3 | 2 | 3 | 0.186 | 1.618 |
| 3 | 3 | 3 | 0.133 | 1.407 |

45 kN tension tie - 2


| Crack Number | Pit number | side | $d_{pit}$ (mm) | $l_{pit}$ (mm) |
|---|---|---|---|---|
| 1 | 1 | 3 | 0.284 | 3.335 |
| 1 | 2 | 3 | 0.304 | 2.88 |
| 2 | 1 | 1 | 0.144 | 2.364 |
| 2 | 2 | 2 | 0.110 | 3.68 |
| 2 | 3 | 3 | 0.045 | 1.945 |
| 2 | 4 | 3 | 0.104 | 2.908 |
| 2 | 5 | 3 | 0.263 | 3.818 |
| 3 | 1 | 1 | 0.139 | 3.145 |
| 3 | 2 | 1 | 0.139 | 2.334 |
| 3 | 3 | 1 | 0.102 | 2.621 |
| 3 | 4 | 3 | 0.062 | 0.747 |
| 4 | 1 | 3 | 0.117 | 1.726 |
| 5 | No corrosion | | | |

45 kN tension tie - 3

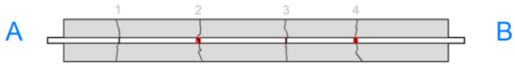


| Crack Number | Pit number | side | $d_{pit}$ (mm) | $l_{pit}$ (mm) |
|---|---|---|---|---|
| 1 | No corrosion | | | |
| 2 | 1 | 1 | 0.190 | 2.39 |
| 2 | 2 | 1 | 0.064 | 2.35 |
| 2 | 3 | 3 | 0.122 | 1.82 |
| 3 | 1 | 2 | 0.066 | 2.065 |
| 4 | 1 | 3 | 0.100 | 2.188 |
| 4 | 2 | 2 | 0.411 | 3.3 |
| 4 | 3 | 3 | 0.243 | 2.228 |
| 4 | 4 | 2 | 0.557 | 3.223 |
| 4 | 5 | 2 | 0.345 | 2.587 |

45 kN tension tie - 4

*Figure 4.4-10 Crack pattern and affected zone in 45 kN tension tie samples.*

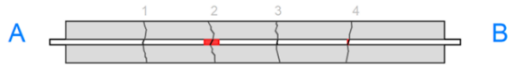


| Crack Number | Pit number | side | $d_{pit}$ (mm) | $l_{pit}$ (mm) |
|---|---|---|---|---|
| 1 | | No corrosion | | |
| 2 | 1 | side 3 | 0.207 | 1.591 |
| 2 | 2 | side 4 | 0.186 | 2.056 |
| 2 | 3 | side 3 | 0.420 | 2.3 |
| 3 | | No corrosion | | |
| 4 | 1 | side 1 | 0.140 | 3.068 |

55 kN tension tie - 1


| Crack Number | Pit number | side | $d_{pit}$ (mm) | $l_{pit}$ (mm) |
|---|---|---|---|---|
| 1 | | No corrosion | | |
| 2 | 1 | 3 | 0.180 | 1.526 |
| 2 | 2 | 4 | 0.176 | 2.103 |
| 2 | 3 | 4 | 0.144 | 1 |
| 3 | | No corrosion | | |
| 4 | 1 | 2 | 0.251 | 2.787 |
| 4 | 2 | 2 | 0.084 | 1.841 |
| 5 | 1 | 1 | 0.07 | 1.69 |
| 5 | 2 | 3/4 | 0.247 | 1.952 |

55 kN tension tie – 2

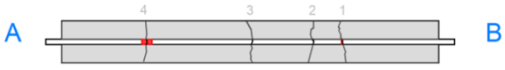


| Crack Number | Pit number | side | $d_{pit}$ (mm) | $l_{pit}$ (mm) |
|---|---|---|---|---|
| 1 | 1 | 3/4 | 0.091 | 4.755 |
| 2 | 2 | No corrosion | | |
| 3 | 3 | | | |
| 4 | 1 | 1/2 | 0.096 | 1.786 |
| 4 | 2 | 4 | 0.246 | 2.456 |

55 kN tension tie - 3


| Crack Number | Pit number | side | $d_{pit}$ (mm) | $l_{pit}$ (mm) |
|---|---|---|---|---|
| 1 | 1 | 2/3 | 0.247 | 6.822 |
| 2 | | No corrosion | | |
| 3 | 1 | 1 | 0.154 | 1.42 |
| 3 | 2 | 1 | 0.198 | 1.89 |
| 3 | 3 | 1 | 0.147 | 1.496 |
| 3 | 4 | 2 | 0.169 | 2.687 |
| 3 | 5 | 3 | 0.175 | 2.321 |
| 3 | 6 | 4 | 0.587 | 2.949 |
| 4 | 1 | 2 | 0.252 | 1.557 |

55 kN tension tie - 4

*Figure 4.4-11 Crack pattern and affected zone in 55 kN tension tie samples.*


| Crack Number | Pit number | side | $d_{pit}$ (mm) | $l_{pit}$ (mm) |
|---|---|---|---|---|
| 1 | 1 | 1 | 0.611 | 2.75 |
| 1 | 2 | 1 | 0.224 | 3.38 |
| 1 | 3 | 2 | 0.129 | 0.696 |
| 1 | 4 | 1 | 0.152 | 0.946 |
| 1 | 5 | 3 | 0.192 | 2.405 |
| 1 | 6 | 3 | 0.505 | 6.287 |
| 2 | No corrosion | | | |
| 3 | | | | |
| 4 | 1 | 4 | 0.416 | 1.21 |
| 5 | No corrosion | | | |

3‰ tension tie – 1

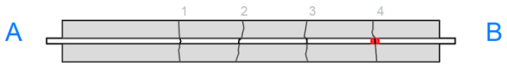


| Crack Number | Pit number | side | $d_{pit}$ (mm) | $l_{pit}$ (mm) |
|---|---|---|---|---|
| 1 | | | | |
| 2 | No corrosion | | | |
| 3 | | | | |
| 4 | 1 | 1 | 0.602 | 1.227 |
| 4 | 2 | 1 | 0.076 | 2.539 |
| 4 | 3 | 1 | 0.190 | 0.591 |
| 4 | 4 | 2 | 0.446 | 5.17 |
| 4 | 5 | 2 | 0.242 | 0.878 |
| 4 | 6 | 2 | 0.551 | 3.633 |
| 4 | 7 | 2 | 0.539 | 3.66 |

3‰ tension tie - 2


| Crack Number | Pit number | side | $d_{pit}$ (mm) | $l_{pit}$ (mm) |
|---|---|---|---|---|
| 1 | 1 | 1 | 0.238 | 4.234 |
| 1 | 2 | 1 | 0.171 | 0.669 |
| 1 | 3 | 3 | 1.643 | 5.485 |
| 1 | 4 | 2 | 0.574 | 1.069 |
| 2 | | | | |
| 3 | No corrosion | | | |
| 4 | | | | |
| 5 | | | | |

3‰ tension tie – 3

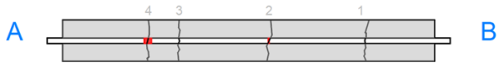


| Crack Number | Pit number | side | $d_{pit}$ (mm) | $l_{pit}$ (mm) |
|---|---|---|---|---|
| 1 | | No corrosion | | |
| 2 | 1 | 1 | 0.055 | 1.167 |
| 3 | | No corrosion | | |
| 4 | 1 | 1 | 0.315 | 1.618 |
| 4 | 2 | 1 | 0.148 | 1.267 |
| 4 | 3 | 3 | 0.940 | 3.922 |
| 4 | 4 | 3 | 0.343 | 1.057 |
| 4 | 5 | 3 | 0.145 | 0.633 |
| 4 | 6 | 3 | 0.648 | 1.125 |
| 4 | 7 | 4 | 0.506 | 7.346 |

3‰ tension tie - 4

*Figure 4.4-12 Crack pattern and affected zone in 3‰ tension tie samples.*


| Crack Number | Pit number | Face | $d_{pit}$ (mm) | $l_{pit}$ (mm) |
|---|---|---|---|---|
| 1 | | No corrosion | | |
| 2 | | | | |
| 3 | 1 | 1 | 0.358 | 0.835 |
| 3 | 2 | 1 | 0.105 | 1.124 |
| 3 | 3 | 1 | 0.608 | 9.5 |
| 3 | 4 | 2 | 0.895 | 9.5 |
| 3 | 5 | 3 | 0.678 | 9.4 |
| 3 | 6 | 4 | 0.603 | 9.5 |
| 4 | 1 | 4 | 0.126 | 0.478 |

5‰ tension tie - 1


| Crack Number | Pit number | side | $d_{pit}$ (mm) | $l_{pit}$ (mm) |
|---|---|---|---|---|
| 1 | 1 | 3 | 0.350 | 1.23 |
| 1 | 2 | 1 | 0.920 | 3.762 |
| 1 | 3 | 2 | 0.616 | 1.863 |
| 1 | 4 | 3 | 0.786 | 5 |
| 1 | 5 | 4 | 1.06 | 7 |
| 2 | | | | |
| 3 | | No corrosion | | |
| 4 | | | | |
| 5 | 1 | 1 | 0.554 | 3.869 |
| 5 | 2 | 4 | 0.426 | 3.584 |
| 5 | 3 | 3 | 0.534 | 1.5 |

5‰ tension tie - 2


| Crack Number | Pit number | Face | $d_{pit}$ (mm) | $l_{pit}$ (mm) |
|---|---|---|---|---|
| 1 | 1 | 1 | 0.322 | 0.567 |
| 1 | 2 | 1 | 0.855 | 2.082 |
| 1 | 3 | 4 | 0.704 | 0.835 |
| 1 | 4 | 4 | 0.534 | 0.835 |
| 1 | 5 | 1 | 0.712 | 5 |
| 1 | 6 | 2 | 0.804 | 5 |
| 1 | 7 | 3 | 0.628 | 5 |
| 1 | 8 | 4 | 0.724 | 9.5 |
| 2 | | No corrosion | | |
| 3 | | | | |
| 4 | 1 | 1 | 0.094 | 0.667 |
| 4 | 3 | 3 | 0.023 | 0.393 |
| 5 | | No corrosion | | |

5‰ tension tie - 3

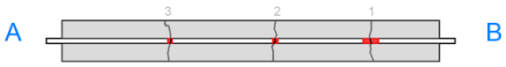


| Crack Number | Pit number | Side | $d_{pit}$ (mm) | $l_{pit}$ (mm) |
|---|---|---|---|---|
| 1 | 1 | 3 | 0.083 | 0.65 |
| 1 | 2 | 4 | 0.087 | 0.633 |
| 2 | 1 | 1 | 0.354 | 1.038 |
| 2 | 2 | 2 | 0.187 | 0.724 |
| 2 | 3 | 2 | 0.616 | 4.816 |
| 2 | 4 | 4 | 0.102 | 2.412 |
| 2 | 5 | 1 | 0.309 | 5 |
| 2 | 6 | 3 | 0.312 | 7 |
| 3 | 1 | 1 | 0.215 | 0.891 |
| 3 | 2 | 1 | 0.175 | 0.994 |

5‰ tension tie - 4

*Figure 4.4-13 Crack pattern and affected zone in 5‰ tension tie samples.*

column, each crack formed on the tension ties is assigned a unique crack number for identification purposes. These crack numbers are important for tracking the progress of damage and corrosion within the tension tie.

Additionally, multiple pits can appear within a single crack. To ensure proper documentation, each corrosion pit is also given a specific pit number, allowing for the precise identification and organization of the corrosion damage.

This system ensures that each corrosion pit is accurately referenced according to its position on the specimen.

For each identified pit, the pit depth is measured. The pit depth refers to the depth of the corrosion pit at a specific crack and its corresponding location.

Finally, the length of the pitting zone is calculated. This refers to the total length of the area affected by corrosion along the rebar. This measurement represents the extent of corrosion along the rebar, offering insight into the degree of deterioration in the reinforcement.

### *4.4.4 Influence of crack width on pitting corrosion*

Corrosion damage in the specimen was generally shallow, with attacks localized mostly along the cracks. This shows that the corrosion process was restricted to the areas surrounding the cracks, leaving the uncracked parts of the specimen largely undamaged. Cracks facilitated chloride ingress, creating a suitable environment for corrosion to initiate. On the other hand, no corrosion was observed in the uncracked concrete regions, which remained resistant to corrosion.

One important factor that may have prevented corrosion from spreading beyond the cracks is the presence of a microcell between the anodic region (at the cracks) and the surrounding concrete. Corrosion predominantly occurs in the anodic zones, where the rebar is exposed to chlorides. Meanwhile, the surrounding uncracked concrete may act as cathodic region, producing limited electrochemical reaction. This anodic cathode microcell effect might have restricted overall corrosion by confining it to the vicinity of the cracks and protecting the uncracked regions.

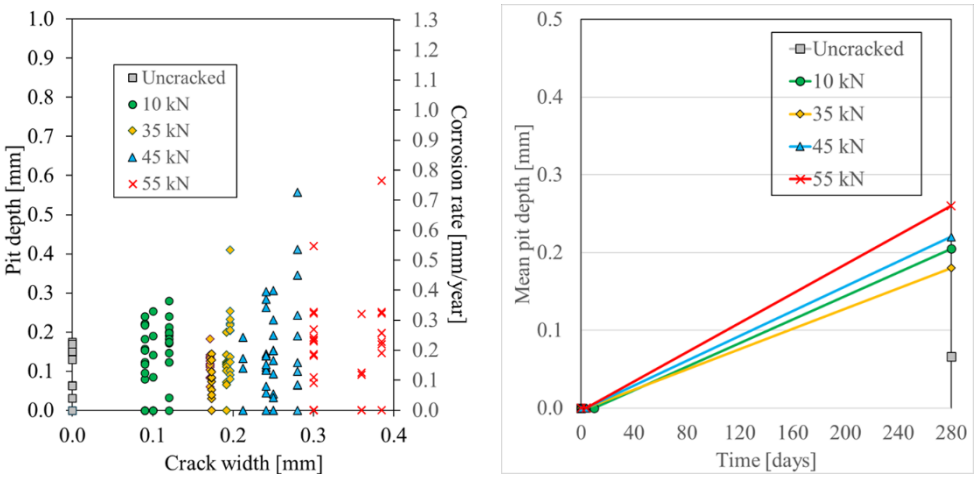


*Figure 4.4-14. Crack width vs pitting depth b) show time in days vs mean pit depth*

When analyzing the average corrosion damage, it was found that crack widths ranging from 0.1 mm to 0.3 mm had very little effect on corrosion propagation. Within this range, crack width did not significantly increase the corrosion rate. However, when the crack width exceeded 0.3 mm, its impact became much more pronounced,

resulting in a noticeable increase in corrosion activity. This suggests that larger cracks offer chloride a more direct path to the rebar.

As shown in *Figure 4.4-14* Specimens subjected to higher loads (e.g., 55 kN) displayed greater mean pit depths compared to those subjected to lower loads (e.g., 10 kN). These findings indicate that higher loads have a substantial effect on corrosion damage, primarily by inducing wider cracks that enable deeper penetration of aggressive agents. The deeper the crack, the more susceptible the rebar becomes to severe corrosion attack.

A comparison between cracked and uncracked specimens showed that uncracked samples had significantly less pitting corrosion. In uncracked specimens, the concrete matrix serves as a protective barrier that limits the ingress of chloride and other aggressive agents. Conversely, cracks provide a direct pathway for these agents to reach reinforcement, leading to localized pitting corrosion.

The corrosion rates were also found to be higher in specimens with yielded rebar compared to those without yielding. Yielding may make the rebar more prone to corrosion, likely due to internal tension, microstructural changes, or increased surface exposure. The study revealed that higher strain levels over time resulted in deeper pitting. In particular, specimens under 5‰ strain exhibited a mean pit depth of 0.77 mm after 280 days, whereas those 3‰ strain had a slightly lower mean pit deoth of 0.6 mm. This implies that higher strain levels place additional stress on the reinforcement, making it more vulnerable to corrosion. The increased deformation may also lead to wider cracks, further exposing the rebar to corrosive agents.

Therefore, it is crucial to consider both mechanical and environmental factors when assessing the durability of reinforced concrete structures subjected to sustained or heavy loading.

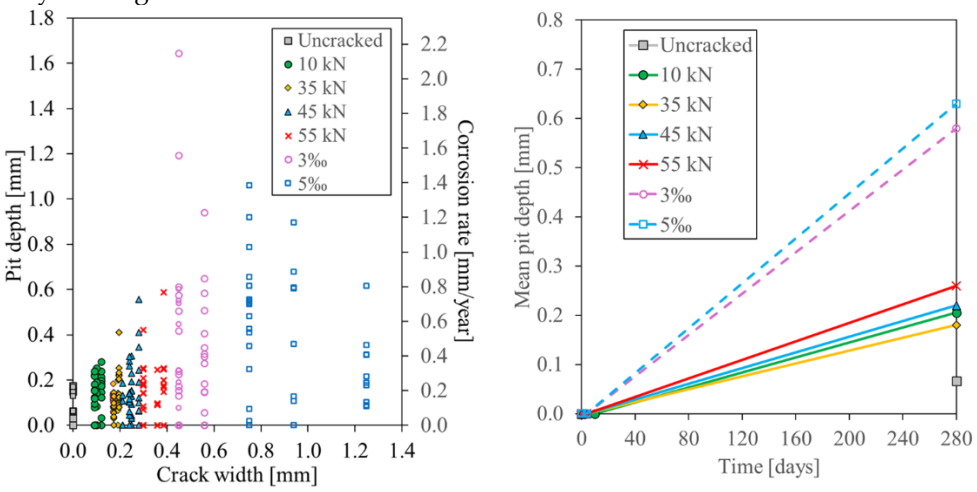


*a)* *b)*

*Figure 4.4-15. Crack width vs pit depth b) Time in days vs mean pit depth.*

Restricting the crack width to less than 0.3 mm may have a significant positive impact on the structural durability of concrete exposed to harsh environments. When the crack width is below this threshold, corrosion initiation is delayed, and the total extent of the corrosion is reduced.
Controlling crack width can be an effective and practical strategy to improve the durability and performance of reinforced concrete structures. It may help to reduce the negative impacts of corrosion and enhance the long-term durability of reinforced concrete in aggressive environmental conditions.

### *4.4.5 Influence of pitting corrosion on the mechanical properties of rebar*

*Table 4.4-1*. provides a comprehensive overview of the mechanical properties of rebars, including crack width, corrosion initiation time (in days), weight loss, mass loss rate, critical crack location where rebars breaks during the tensile test, strain and elasticity of rebars that were exposed to chloride-rich environment under different loading conditions during corrosion process.
Rebars corroded under sustained loading exhibit a progressive increase in weight loss and mass loss, with higher loads (e.g., 45 kN and 55 kN) resulting in more significant deterioration. This suggests that mechanical loading accelerates the corrosion process.

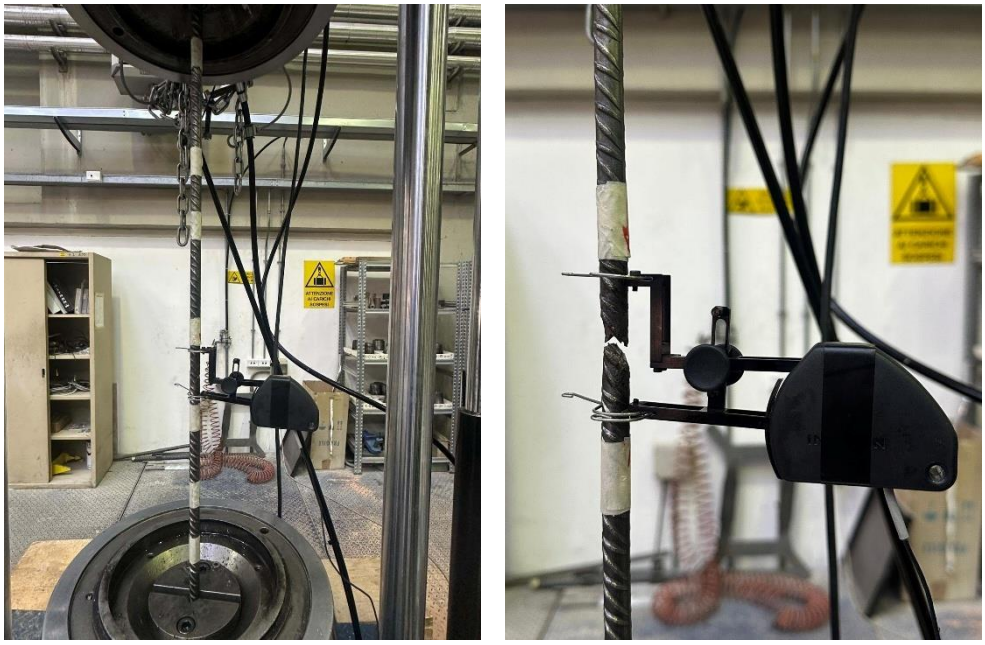

*(a)* *(b)*

*Figure 4.4-16. a) tensile test on corroded rebar; b) rebar failure at the pit location.*

The column $F_{uD}/F_u$ represents the ratio of the ultimate load capacity of the corroded rebar ($F_{uD}$) to the ultimate load capacity of the uncorroded rebar ($F_u$). A value close to 1.0 indicates that the rebar has lost most of its tensile strength despite corrosion. A lower value, however, indicates that corrosion has weakened the rebar, reducing its ability to carry load. In specimens with extensive corrosion, this ratio slightly decreases, confirming that corrosion can lead to some strength loss, especially in severely corroded rebars.

In a similar trend, there is a significant decline in strain, particularly under higher loads. For reinforced concrete structures, ductility is an essential characteristic that permits stress redistribution and prevents abrupt failure. The strain capacity noticeably decreases, particularly in specimens with (e.g., 5‰ strain). This shows that corroded rebar may still support large loads, but their reduced deformation capacity makes them more vulnerable to sudden failure.

The results indicate that corrosion leads to gradual materials deterioration, particularly a reduction in the ductility in reinforcement bars. Although the ultimate strength remains relatively consistent under moderate corrosion conditions, the notable drop in strain capacity highlights an increased risk of brittle failure.

Following the pit morphology analysis, all the rebars were extracted from tension ties to assess their mechanical properties of corroded rebar compared to uncorroded rebars. The graphs presented in this analysis illustrate the relation between load (kN) and strain, where corroded rebar are shown with a red line and uncorroded rebar as referance.

*Table 4.4-1. Mechanical characteristics of corroded rebar.*

| Specimen Designation | $w$ [mm] | $t_{in}$ [days] | Weight loss [%] | Mass loss rate [g / m²y] | Critical crack | $F_{uD}/F_u$ [-] | $\varepsilon_{uD}/\varepsilon_u$ [-] |
|---|---|---|---|---|---|---|---|
| Uncracked | | | | | | | |
| #1 | - | No data | 0.12 | 41 | - | 0.96 | 0.89 |
| #2 | - | - | 0.00 | 0 | - | 1.02 | 1.09 |
| #3 | - | No data | 0.10 | 33 | - | 0.99 | 1.05 |
| **Mean** | **-** | **-** | **0.08** | **25** | **-** | **0.99** | **1.01** |
| CV | - | - | 0.88 | 0.88 | - | 0.03 | 0.10 |
| RC - 10 kN | | | | | | | |
| #1 | 0.12 | 4 | 0.19 | 62 | 2 | 1.01 | 0.93 |
| #2 | 0.10 | 4 | 0.12 | 40 | 4 | 0.96 | 1.08 |
| #3 | 0.09 | 4 | 0.15 | 50 | 3 | 1.02 | 0.86 |
| #4 | 0.09 | 4 | 0.17 | 54 | 2 | 1.01 | 0.76 |
| **Mean** | **0.10** | **4** | **0.16** | **52** | **-** | **1.00** | **0.91** |

| | | | | | | | |
|---|---|---|---|---|---|---|---|
| CV | 0.14 | - | 0.22 | 0.22 | - | 0.03 | 0.15 |
| RC - 35 kN | | | | | | | |
| #1 | 0.19 | 4 | 0.11 | 35 | 2 | 0.99 | 0.95 |
| #2 | 0.20 | 4 | 0.10 | 33 | 2 | 0.98 | 0.70 |
| #3 | 0.17 | 4 | 0.13 | 42 | 1 | 1.00 | 0.89 |
| #4 | 0.18 | 4 | 0.26 | 83 | 3 | 0.98 | 0.90 |
| **Mean** | **0.19** | **4** | **0.15** | **48** | **-** | **0.99** | **0.86** |
| CV | 0.07 | - | 0.49 | 0.49 | - | 0.01 | 0.12 |
| RC - 45 kN | | | | | | | |
| #1 | 0.25 | 4 | 0.26 | 83 | 4 | 0.98 | 0.89 |
| #2 | 0.21 | 4 | 0.27 | 87 | 3 | 0.95 | 0.96 |
| #3 | 0.24 | 4 | 0.40 | 129 | 2 | 1.00 | 0.94 |
| #4 | 0.28 | 4 | 0.38 | 125 | 4 | 0.99 | 0.75 |
| **Mean** | **0.25** | **4** | **0.33** | **106** | **-** | **0.98** | **0.88** |
| CV | 0.12 | - | 0.23 | 0.23 | - | 0.02 | 0.10 |
| RC - 55 kN | | | | | | | |
| #1 | 0.30 | 4 | 0.36 | 117 | 2 | 0.93 | 0.92 |
| #2 | 0.30 | 4 | 0.28 | 92 | 2 | 1.00 | 0.75 |
| #3 | 0.36 | 4 | 0.31 | 100 | 4 | 1.00 | 0.74 |
| #4 | 0.38 | 4 | 0.25 | 81 | 3 | 0.95 | 0.93 |
| **Mean** | **0.34** | **4** | **0.30** | **97** | **-** | **0.97** | **0.84** |
| CV | 0.12 | - | 0.15 | 0.23 | - | 0.04 | 0.12 |
| RC - 3‰ | | | | | | | |
| #1 | 0.45 | 4 | 0.25 | 80 | 1 | 0.96 | 0.75 |
| #2 | 0.46 | 4 | 0.23 | 74 | 4 | 0.93 | 0.69 |
| #3 | 0.56 | 4 | 0.27 | 90 | 1 | 0.92 | 0.66 |
| #4 | 0.55 | 4 | 0.24 | 79 | 4 | 0.92 | 0.76 |
| **Mean** | **0.51** | **4** | **0.25** | **83** | **-** | **0.93** | **0.72** |
| CV | 0.11 | - | 0.09 | 0.09 | - | 0.02 | 0.07 |
| RC - 5‰ | | | | | | | |
| #1 | 0.94 | 4 | 0.40 | 130 | 3 | 0.91 | 0.29 |
| #2 | 0.75 | 4 | 0.33 | 108 | 1 | 0.92 | 0.21 |
| #3 | 0.76 | 4 | 0.31 | 102 | 1 | 0.89 | 0.24 |
| #4 | 1.25 | 4 | 0.34 | 112 | 2 | 0.95 | 0.31 |
| **Mean** | **0.93** | **4** | **0.35** | **113** | **-** | **0.92** | **0.26** |
| CV | 0.25 | - | 0.11 | 0.11 | - | 0.03 | 0.18 |

In the uncracked condition, the uncorroded rebars *Figure 4.4-17a*, shows a similar trend to the uncorroded rebars. When analysing cracked specimens, the results demonstrate that as crack width increases, there is a gradual decline in the ductility of the rebar, while strength is minimally affected. For example, in rebars subjected to a 10 kN cracking load, there is no significant reduction in strength but a 9% drop in ductility. This indicates that while cracking does not impact the peak load capacity, it leads to localized strain concentrations, reducing the rebar's ability to undergo plastic deformation.

This pattern becomes more noticeable at 35 kN, where ductility drops by 14% and strength by 1%.

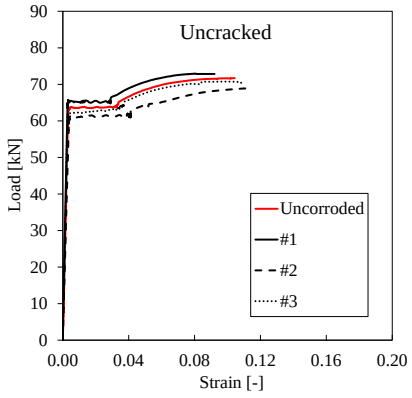


(a)

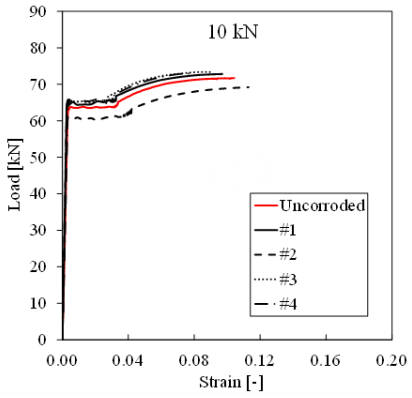


(b)

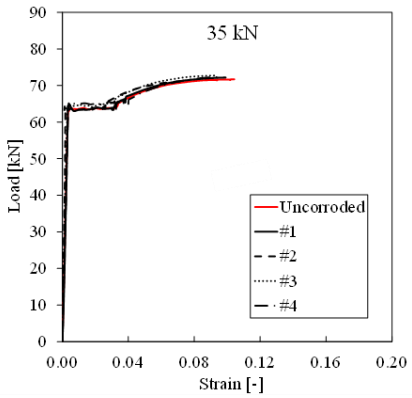


(c)

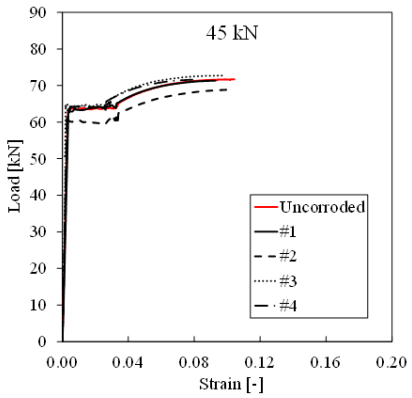


(d)

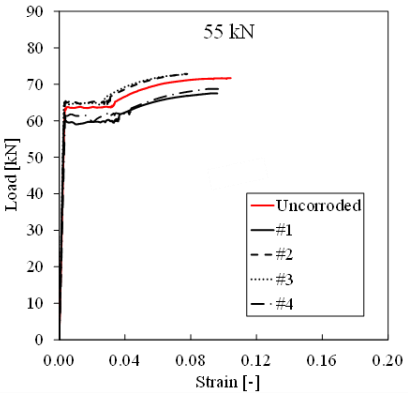


(e)

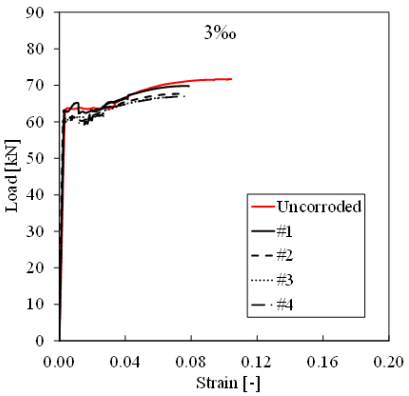


(f)

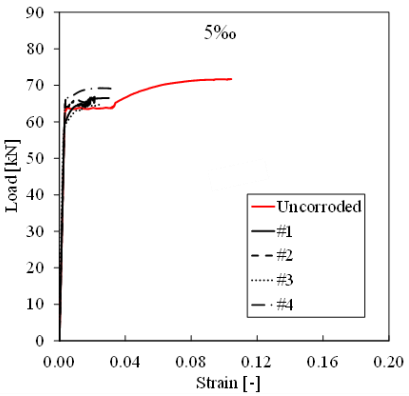


(g)

*Figure 4.4-17. load strain relationship of rebar: comparison between damaged and corroded rebar.*

Rebars extracted from 45 kN loading show a 2% reduction in strength and 12% loss in ductility. A more considerable decline is observed in rebars from specimens subjected to 55 kN, with a 3% strength drop and 16% ductility loss. This pattern among the cracked specimens indicates that cracking considerably reduces ductility but does not lead to a rapid loss in strength. Mechanical loading conditions significantly influence corrosion progression and its impact on mechanical performance.

The effect of strain become especially noticeable in the samples with 3‰ and 5‰ strain *Figure 4.4-17e*, and *Figure 4.4-17f.* At these higher strain levels, corrosion significantly weakens the ductility of the rebars, making them more brittle and less capable of withstanding further elongation.

At 3‰ , strength is reduced 7%, and ductility by 28%, while for specimens at 5‰ strain experience an 8% strength loss and an extreme 74% ductility loss, which is the most severe deterioration among all specimens. As corrosion progresses, the rebar loses its ability to elongate, and its capacity to absorb stresses diminishes, making it more vulnerable to sudden, brittle failure, as they are less able to undergo plastic deformation before failure.

The severe impact of corrosion on the rebar's mechanical properties, especially in terms of its ability to endure higher strain without failing highlights this increased brittleness in corroded reinforcement. This is concerning, as brittle failure under strain can be catastrophic in structural situations, where some level of ductility is needed for safety and performance.

Overall, the results highlight that crack width has a moderate effect on strength reduction, and corrosion significantly amplifies ductility loss, weakening the materials' ability to deform under stress, a condition that can lead to premature failure in structures.

In summary, the experimental findings in this chapter provide insight into the critical role of crack width in the development of corrosion initiation and propagation in tension ties exposed to wet and dry cycles. The majority of specimens exhibited abrupt corrosion initiation during the first cycle (4 days), with exception of one specimen with a crack width of 0.1 mm, which showed delayed in corrosion initiation until the tenth day of wet and dry cycle.

Considering the average corrosion damage, the propagation of corrosion appears to be only mildly influenced by crack widths ranging from 0.1 mm to 0.3 mm. However, beyond 0.3 mm, this influence becomes considerably more pronounced, indicating that wider cracks facilitate more aggressive corrosion progression. Additionally, in specimens that had undergone yielding, the corrosion rate was significantly higher compared to non-yielded samples, suggesting that prior mechanical deformation exacerbates corrosion susceptibility.

For the tested specimens, the maximum pitting depth was also found to be influenced by crack width within the studied range. This highlights the critical role of crack size in accelerating localized corrosion, which can further weaken the structural integrity of reinforcement over time.

Moreover, testing specimens with yielded rebar's revealed a substantial impact on corrosion damage, reinforcing the importance of evaluating corrosion behaviour under realistic loading conditions. As a result, conducting tests under sustained loads should be generally adopted to better simulate real-world structural performance and deterioration mechanisms.

Regarding corrosion propagation, it was observed that as the crack width increases, both strength and ductility decrease. However, the findings indicate that corrosion primarily affects the ductility of the rebar rather than its ultimate strength.

## *4.5 Reference*

[1] G. Tiberti, F. Minelli, and G. Plizzari, "Cracking behavior in reinforced concrete members with steel fibers: A comprehensive experimental study," *Cement and Concrete Research*, vol. 68, pp. 24–34, Feb. 2015, doi: 10.1016/j.cemconres.2014.10.011.

[2] U. M. Angst, "Predicting the time to corrosion initiation in reinforced concrete structures exposed to chlorides," *Cement and Concrete Research*, vol. 115, pp. 559–567, Jan. 2019, doi: 10.1016/j.cemconres.2018.08.007.

[3] G. Tiberti, F. Minelli, G. A. Plizzari, and F. J. Vecchio, "Influence of concrete strength on crack development in SFRC members," *Cement and Concrete Composites*, vol. 45, pp. 176–185, Jan. 2014, doi: 10.1016/j.cemconcomp.2013.10.004.

[4] M. Słowik, P. Stroeven, and A. Akram, "Crack mechanisms in concrete – from micro to macro scale," *Bud-Arch*, vol. 19, no. 4, pp. 053–066, Nov. 2020, doi: 10.35784/bud-arch.2147.

[5] J. Cramer, S. Javidmehr, and M. Empelmann, "Simulation of Crack Propagation in Reinforced Concrete Elements," *Applied Sciences*, vol. 11, no. 2, p. 785, Jan. 2021, doi: 10.3390/app11020785.

[6] F. Leonhardt, "Cracks and Crack Control in Concrete Structures," *pcij*, vol. 33, no. 4, pp. 124–145, Jul. 1988, doi: 10.15554/pcij.07011988.124.145.

# 5 CONCLUSIONS

This PhD thesis presents a detailed experimental study on the corrosion of reinforced concrete structures exposed to aggressive environments, such as marine environments or de-icing salts. Corrosion of reinforcement remains a significant concern in the durability of RC structures, and this research investigates how crack width influences both the initiation and propagation phases of corrosion, as well as its effect on the mechanical properties of reinforcement bars.
Despite extensive research on the corrosion of RC structures, the relationship between crack width and corrosion rate remains inadequately understood, particularly in the context of chloride-induced corrosion. The primary objective of this study was to explore how crack width affects corrosion initiation, corrosion propagation, and the mechanical performance of rebar in RC structures exposed to accelerated laboratory conditions. This study also examines the influence of corrosion on the ductility and strength of reinforcement bars.

To achieve this, 31 tension tie specimens (90 x 90 x 830 mm) were cast using grade C30/37 concrete, with Ø12 mm hot-rolled ribbed reinforcement rebar. The specimens were pre-cracked using an Instron machine to induce different crack widths and then subjected to controlled accelerated corrosion process. The accelerated testing involved applying sustained tensile loads to the specimens to keep the crack open, followed by exposure to chloride-rich environments under wet and dry cycles, simulating real-world service conditions.

The main conclusions of this research are as follows:

1. The procedure involving sustained tensile loading and alternating wet-dry cycles was highly efficient for accelerating the corrosion process. The cracks remained open under load, allowing chloride ions to penetrate and initiate corrosion. The 3-day wet and 4-day dry cycle realistically mimicked environmental exposure in marine or de-icing conditions.

2. Corrosion initiation occurred during the first cycle in all specimens, regardless of the crack width. This indicates that the presence of cracks, even as narrow as 0.1 mm, was sufficient to facilitate the immediate penetration of chloride ions, leading to early corrosion initiation.

3. The effect of crack width on corrosion propagation became significantly more evident once the crack exceeded 0.3 mm. While propagation was stable for crack widths between 0.1 mm and 0.3 mm, rates increased significantly

beyond this threshold. Controlling crack width to under 0.3 mm can substantially reduce corrosion propagation.

4. Specimens with cracks exhibited greater corrosion rates than uncracked ones. Although a direct correlation between pitting depth and crack width was not always consistent, maximum pit depth increased as crack width increased. Therefore, crack width is a critical factor in reducing localized corrosion in RC.

5. Corrosion led to a notable loss in the ductility of reinforcement bars, especially in specimens with crack width > 0.3 mm. While ultimate strength remained relatively unaffected under moderate corrosion, the reduction in ductility increased the risk of brittle failure. This highlights the importance of crack control in preserving the ductility of reinforcement and preventing structural failure.

6. Corrosion progressively degrades reinforcement, reducing its ductility. As a result, even flexural members typically expected to fail in a ductile manner can exhibit brittle, sudden failure. Preserving the steel's deformability is therefore essential to prevent premature and catastrophic collapse.

7. These findings have critical implications for the design and maintenance of RC structures in aggressive environments. Limiting crack width to below 0.3 mm can reduce corrosion propagation, extending the service life of reinforced concrete structures.

8. This study highlights the relevance of crack width control provisions in existing design standards (e.g., Eurocode 2, ACI 318) with respect to corrosion-related deterioration. Further investigation could help clarify how these limits perform under chloride-induced corrosion conditions.

9. While this research offers valuable experimental insights, future work could include numerical modelling to study corrosion impacts on structural members using the constitutive law derived here. It is also recommended to test flexural elements (e.g., beams) under chloride-induced corrosion to understand long-term effects more comprehensively.

In conclusion, this thesis highlights the critical influence of crack width on the corrosion behaviour in RC structures exposed to harsh environments. The experimental procedure using sustained tensile loading and wet-dry cycles

accelerated corrosion, providing key data on crack width and corrosion relationship. The findings clearly show that limiting crack width is essential for reducing corrosion, preserving ductility, and maintaining the structural integrity and durability of RC elements. This work contributes meaningful guidance toward improving the service life, safety, and reliability of reinforced concrete infrastructure in chloride-rich environments.